de Wit, M., Furnes, H., MacLennan, S., Doucouré, M., Schoene, B., Weckmann, U., Martinez, U., Bowring, S. (2018): Paleoarchean bedrock lithologies across the Makhonjwa Mountains of South Africa and Swaziland linked to geochemical, magnetic and tectonic data reveal early plate tectonic genes flanking subduction margins. - *Geoscience Frontiers*, *9*, 3, pp. 603—665.

DOI: http://doi.org/10.1016/j.gsf.2017.10.005

Geoscience Frontiers 9 (2018) 603–665

HOSTED BY

Contents lists available at ScienceDirect

China University of Geosciences (Beijing)

Geoscience Frontiers

journal homepage: www.elsevier.com/locate/gsf

Research Paper

Paleoarchean bedrock lithologies across the Makhonjwa Mountains of South Africa and Swaziland linked to geochemical, magnetic and tectonic data reveal early plate tectonic genes flanking subduction margins

Maarten de Wit [a,*], Harald Furnes [b], Scott MacLennan [a,c], Moctar Doucouré [a,d], Blair Schoene [c], Ute Weckmann [e], Uma Martinez [a,f], Sam Bowring [g]

[a] AEON-ESSRI (Africa Earth Observatory Network-Earth Stewardship Science Research Institute), Nelson Mandela University, Port Elizabeth, South Africa
[b] Department of Earth Science & Centre for Geobiology, University of Bergen, Norway
[c] Department of Geosciences, Princeton University, Guyot Hall, Princeton, NJ, USA
[d] Department of Geosciences, Nelson Mandela University, Port Elizabeth, South Africa
[e] Department Geophysics, GFZ - German Research Centre for Geosciences, Helmholtz Centre, Telegrafenberg, 14473 Potsdam, Germany
[f] GISCAPETOWN, Cape Town, South Africa
[g] Earth, Atmosphere and Planetary Sciences, Massachusetts Institute of Technology, Cambridge, MA, USA

ARTICLE INFO

Article history:
Received 12 June 2017
Received in revised form
2 October 2017
Accepted 5 October 2017
Available online 31 October 2017

Keywords:
Paleoarchean
Barberton Greenstone Belt
Onverwacht Suite
Geologic bedrock and structural maps
Geochemistry and geophysics
Plate tectonics

ABSTRACT

The Makhonjwa Mountains, traditionally referred to as the Barberton Greenstone Belt, retain an iconic Paleoarchean archive against which numerical models of early earth geodynamics can be tested. We present new geologic and structural maps, geochemical plots, geo- and thermo-chronology, and geophysical data from seven silicic, mafic to ultramafic complexes separated by major shear systems across the southern Makhonjwa Mountains. All reveal signs of modern oceanic back-arc crust and subduction-related processes. We compare the rates of processes determined from this data and balance these against plate tectonic and plume related models. Robust rates of both horizontal and vertical tectonic processes derived from the Makhonjwa Mountain complexes are similar, well within an order of magnitude, to those encountered across modern oceanic and orogenic terrains flanking Western Pacific-like subduction zones. We conclude that plate tectonics and linked plate-boundary processes were well established by 3.2–3.6 Ga. Our work provides new constraints for modellers with rates of a 'basket' of processes against which to test Paleoarchean geodynamic models over a time period close to the length of the Phanerozoic.

1. Introduction

There is fierce controversy about how Paleoarchean geology may be interpreted to reveal the nature and pace of global geodynamics that far back in time (3.2–3.6 Ga). Central to the present geologic disputes are whether or not present-day style plate tectonics and linked orogeny with a dominance of horizontal forces operated during the Paleoarchean or even earlier (e.g., De Ronde and Kamo, 2000; Diener et al., 2005, 2006; Dziggel et al., 2006; Moyen et al., 2006, 2007; Stevens and Moyen, 2007; Kusky et al., 2013; Turner et al., 2014; Komiya et al., 2015; Maruyama et al., 2016; Greber et al., 2017; Maruyama and Ebisuzaki, 2017), or if vertical tectonics and linked epeirogeny driven by plume-dynamics and crustal delamination dominated the planet during that time (e.g., Hamilton, 1998, 2011; Zegers and Van Keeken, 2001; Van Kranendonk, 2011a, b; François et al., 2014; Van Kranendonk et al., 2014, 2015; Kröner et al., 2016; Chowdhury et al., 2017). This controversy about the nature of early Archean tectonics has been extensively debated over the last two decades without reaching consensus (de Wit, 1998; Witze, 2006; Hynes, 2014). There is agreement that better modelling of tectonic, igneous and sedimentary processes will provide fundamental keys to unravel

* Corresponding author.
E-mail address: maarten.dewit@mandela.ac.za (M. de Wit).
Peer-review under responsibility of China University of Geosciences (Beijing).

https://doi.org/10.1016/j.gsf.2017.10.005

the origin and formation of Earth's earliest continental crust (3.5–4.0 Ga) in addition to understanding their linked paleo-environments and ecosystems. However, such models must be tested against robust empirical field and laboratory data in order to unravel the geodynamic evolution of Earth (e.g., St-Onge et al., 2006; Hawkesworth and Kemp, 2006; Keller and Schoene, 2012; Korenaga, 2013; Ernst et al., 2016; Hawkesworth et al., 2016; Weller and St-Onge, 2017).

Recent field, rock and mineral analyses have provided some evidence for modern-like plate tectonics by 3.0–3.2 Ga (e.g., Smithies et al., 2007; Polat et al., 2008; Mints et al., 2010; Shirey and Richardson, 2011; Van Kranendonk, 2011a, b; Dhuime et al., 2015; Smart et al., 2016; Halla et al., 2017) and possibly as early as 3.8–4.0 Ga (Komiya et al., 1999, 2002, 2004, 2015; Furnes et al., 2007, 2009, 2014, 2015; Maruyama and Komiya, 2011; Adam et al., 2012; Turner et al., 2014; Maruyama et al., 2016; Greber et al., 2017). However, these data are not generally accepted as conclusive before ca. 3.2 Ga, and have been interpreted to reflect mantle plume magmatism or subduction processes (Bédard, 2006; Cawood et al., 2006; Ernst et al., 2016; Johnson et al., 2017).

Numerical modelling based on elevated mantle temperatures and crustal geotherms, as are generally assumed for the Archean, is consistent with mantle plume activity driven by dry mantle convection (Davies, 2007; Arndt et al., 2013; Fischer and Gerya, 2016). Similar modelling and experimental petrology assuming a more hydrous mantle, shows that plate tectonics is also capable of removing excess heat produced in the Archean at rates comparable to, and possibly even lower than its current rate at mid-ocean ridges (de Wit and Hynes, 1996; Korenaga, 2013); and that under wetter mantle conditions, subduction-related processes can also account for high-magnesium basalts and komatiites at significantly lower temperatures than under dry mantle conditions (e.g., Parman et al., 1997, 2001, 2004; Grove and Parman, 2004; Parman and Grove, 2004a, b; Arndt, 2013; Blichert-Toft et al., 2015; Sobolev et al., 2016).

Field observations linked to thermochronology and metamorphic petrology have questioned the existence of ubiquitous higher geothermal gradients everywhere during the Paleoarchean, and argued for subduction-like processes to account for these findings (e.g., Diener et al., 2005, 2006; Dziggel et al., 2006; Moyen et al., 2006, 2007; Stevens and Moyen, 2007; Schoene and Bowring, 2010; Grosch et al., 2012). These interpretations have been disputed on the basis, for example, of rheological processes in subduction zones (e.g., Van Kranendonk et al., 2014, 2015). However, recent metamorphic modelling has pointed to a lack of detailed knowledge about variability of rock rheologies at subduction margins (Hodges, 2017; Yamato and Brun, 2017). Resolving these issues concerning modern systems will no doubt influence diverse interpretations concerning the (albeit rare) relatively high pressure/low temperature metamorphic assemblages at ca. 3.2 Ga discovered by Moyen et al. (2006) and linked to subduction-like processes; in addition to Archean diamonds with subduction-like carbon signatures (Smart et al., 2016), and titanium isotopes of shales linked to subduction processes at 3.5 Ga (Greber et al., 2017).

But none of these findings have provided convincing evidence to distinguish between dominance of different geodynamic regimes (e.g., Adam et al., 2012; Martin et al., 2014). Whilst there is no compelling theoretical argument against efficient subduction processes at that time (Hynes, 2014), most modellers insist that tectonics during the early Archean was radically different and was driven by plume-lid tectonics (e.g., Fischer and Gerya, 2016). Sufficient deterministic field observations linked to geochemistry are crucially lacking to resolve these controversies.

A fundamental distinction between plate tectonics and plume- or delamination-driven Archean tectonics, for example, could be made with evidence for, or absence of, relatively large horizontal lithosphere motions, respectively, based on paleomagnetism. Todate, quantifying large-scale horizontal motions and rates using paleomagnetism have been convincing only in Mesoarchean terranes (2.7–3.0 Ga; Strik et al., 2007; de Kock et al., 2009). Yet results from two Paleoarchean regions have produced similar paleo-latitude estimates: (1) A short episode of large scale motion (12–673 cm/yr) has been obtained between 3.46 and 3.48 Ga from the Pilbara craton in Australia (Suganuma et al., 2006); and (2) About 1100 km motion, averaged over 9 million years at 3445 Ma, yield an equivalent to a latitudinal velocity of ca. 12 cm/yr from the Makhonjwa Mountain (MMt) sequences (Biggin et al., 2011). Whilst this is fast by today's standards, the lower numbers are well within the range of plate velocities observed in the Phanerozoic. The reliability of the data emerging from these studies is far from certain, but there are no grounds for their outright dismissal.

By contrast, geological field observations have revealed significant local Paleoarchean horizontal crustal motions of up to 10 km. For example, large-scale tectonic extension during formation of volcano-sedimentary listric basins as early as 3.45 Ga (e.g., Nijman and de Vries, 2004), as well as significant horizontal shortening episodes linked to foreland basin evolution during regional thrusting at ca. 3.4 Ga and 3.2 Ga (de Wit, 1982; Lamb, 1984a, b; Paris, 1987; De Ronde and de Wit, 1994; Lowe, 1994; De Ronde and Kamo, 2000; Grosch et al., 2011) suggest horizontal tectonic processes that possibly, but not definitively, link to plate tectonic motions (e.g., see Van Kranendonk et al., 2009, 2014 for counter arguments). Thus a first order tectonic model for the early Archean Earth remains elusive and malleable. The interpretations and models remain controversial in part because of a lack of field geology systematically linked to modern chemical and magneto-stratigraphy, and a lack of high resolution geophysics of tectonic structures linked to precise geochronology. In this context both the timing and mechanism of onset of unambiguous subduction processes remain important to establish.

Here, we summarize recent advances in linked field and laboratory studies across the world's best well-preserved Paleoarchean crustal blocks that flank the escarpment along the eastern margin of southern African Highlands (Fig. 1). This region, known geologically as the Barberton Greenstone Belt and geographically as the Barberton Mountain Land, was recently renamed the Makhonjwa Mountains (de Wit, 2010; following Hall's original terminology, 1918). We use the name Makhonjwa Mountains (MMts) because the term 'greenstone belt', and the definition it generally carries, is restrictive, anachronistic and no longer conducive to developing a deeper understanding of Earth history (de Wit and Ashwal, 1995). We therefore appropriately apply terminology used for modern orogenic belts to what have, until recently, been collectively and uncritically categorized as 'greenstone belts'.

Collectively, our results provide new rates of a 'basket' of processes against which to test Paleoarchean geodynamic models over a time period close to the length of the Phanerozoic. We show that paleo-oceanic components (basalts and komatiites and their linked intrusive complexes) of this region formed predominantly in oceanic environments at water depths of ca. 2–4 km; and that for more than 300 million-years these environments were generated in a variety of back-arc type environments. We find that absolutely none of the geochemical analyses presently available from this region plot in plume domains, no matter what sort of discriminant diagrams are used. We consolidate structural field evidence that reveals the region contains three separate terranes comprising at least seven litho-tectonic complexes, all with chemical signatures indistinguishable from modern rocks found in and around subduction systems. Based on high-resolution aeromagnetic and electrical conductivity surveys across the major shear systems

within the MMts, and Sm-Nd and Lu-Hf isotopic data from surrounding granitoids and orthogneisses, we evaluate the merging of these three terranes through subduction processes. We find that two major, relatively short orogenic episodes separated by about 200 million years (ca. 3.4 Ga and 3.2 Ga), both resemble accretion and collision processes that are operative along the margin of the western Pacific, and which transformed the Makhonjwa region into a stable continental terrain between 3.1 Ga and 3.0 Ga.

The signatures of the first tectonic episode are dominated by normal listric faults and layer parallel shear systems, followed by thrusting and large scale overturning of sequences within a period of about 30 million years, between 3.46 Ga and 3.43 Ga (Armstrong et al., 1990; Grosch et al., 2011). The structures of the second major tectonic episode formed within less than 10 million years, between 3223 Ma and 3214 Ma (De Ronde and de Wit, 1994; De Ronde and Kamo, 2000), dominating late folding and thrusting along the two outer flanks of the greenstone belt (the Weltevreden and Malalotsha Domains), and molasse-like sedimentation covering the internal sector (the Songimvelo Domain) of the MMts (e.g., Lamb, 1984a, b; Paris, 1984; Heubeck and Lowe, 1994; Lowe and Byerly, 2007; Heubeck et al., 2016; Drabon et al., 2017; see Fig. 2 for Domains). During this period younger subduction related complexes were assembled through accretionary orogenesis, and older complexes were re-worked and uplifted (Moyen et al., 2007; Lana et al., 2010a, b). We use the high resolution magnetic data to trace one of the shallow to steep plunging paleo-subduction zones down to depth of 6–7 km. Oblique convergence ended in collision and strike-slip displacements, followed by regional extension/exhumation between 3.0 Ga and 3.1 Ga, at rates comparable to those measured in modern orogenic zones flanking transcurrent plate boundaries.

We show that episodes of vertical tectonism (e.g., epeirogeny, c.f., de Wit, 2007) were also prevalent throughout the evolution of the greenstone belt. During the first tectonic episode, local vertical uplift in the order of 2–5 km, from deep-water to subaerial conditions, created a regional unconformity. Following shortly after the second major episode of convergent tectonism (orogeny), regional exhumation with up to 10–20 km erosion, as determined from thermochronology and extensional listric faults mapped along all the margins of the Makhonjwa Mountains, exposing numerous TTG gneiss domes flanking the external margins of the belt, and large scale granite batholiths that dominated final stabilization of the area by 3.0 Ga (Kisters and Anhaeusser, 1995; Schoene et al., 2008, 2009; Lana et al., 2010a, b). During this period significant gold-bearing fluids were injected over ca. 70 million years, and regularly spaced major gold deposits of the greenstone belt generated within 12 million years (e.g., De Ronde et al., 1992; Dirks et al., 2009, 2013; Dziggel et al., 2010 and references therein).

Subsequently, the region was covered by sub-horizontal terrestrial and shallow marine Neoarchean and Paleoproterozoic sequences until rapid Late Cretaceous uplift and exhumation re-exposed the greenstone belt and shaped the Makhonjwa Mountains (de Wit, 2007). Presently erosion rates of this granite-greenstone basement are low (<1–5 m/Myr), due to the physical and chemical resistant quartzites and cherts (e.g., Scharf et al., 2012) that form the backbones of the Makhonjwa Mountain Ranges.

Below, we first summarize geologic field data collected over more than 40 years, in the form of a lithology (bedrock) and a structural map (Maps 1 and 2), and then link this to a synthesis of our geochemical data gathered since 2004 with a focus on the tectonic environments of the silicic, mafic to ultramafic volcanics and intrusives of the Onverwacht Suite. We also present a magneto-telluric (MT) section across the study area and, using data from a high-resolution magnetic survey in 2011, we present a 3-D magnetic image across one of the circa 3.2 Ga accretion-collision margins to reveal a possible fossil subduction zone. Thereafter we

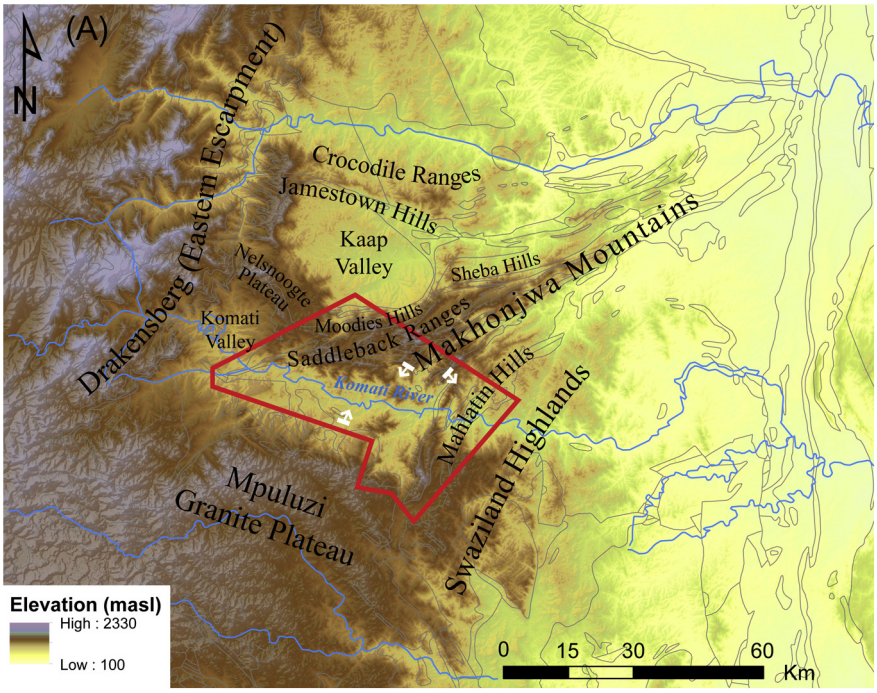

Figure 1. **(A)** Topography the Makhonjwa Mountains and surroundings overlain with the shapes of its major geologic units. ALOS Global Digital Surface Model (AW3D330) http://www.eorc.jaxa.jp/ALOS/en/aw3d30/index.htm. Polygons from 1:1 Million GIS Geology Map, Council for Geoscience, South Africa. White arrows locations and directions of panoramic views, shown in (Fig. 1B1–B4). (B) Panoramic views from the southern Makhonjwa Mountains. (B1) Looking south towards the Mpuluzi Plateau; (B2) looking north from the Komati Valley towards the Makhonjwa Mountains with parts of Tjakastad townships in the foreground; (B3) looking east towards the Swaziland Highlands in the far distance, with Komati River below; (B4) within the mountains, with typical chert layer in the foreground and overturned, steeply dipping lower sequence of Noisy Complex in distance looking east.

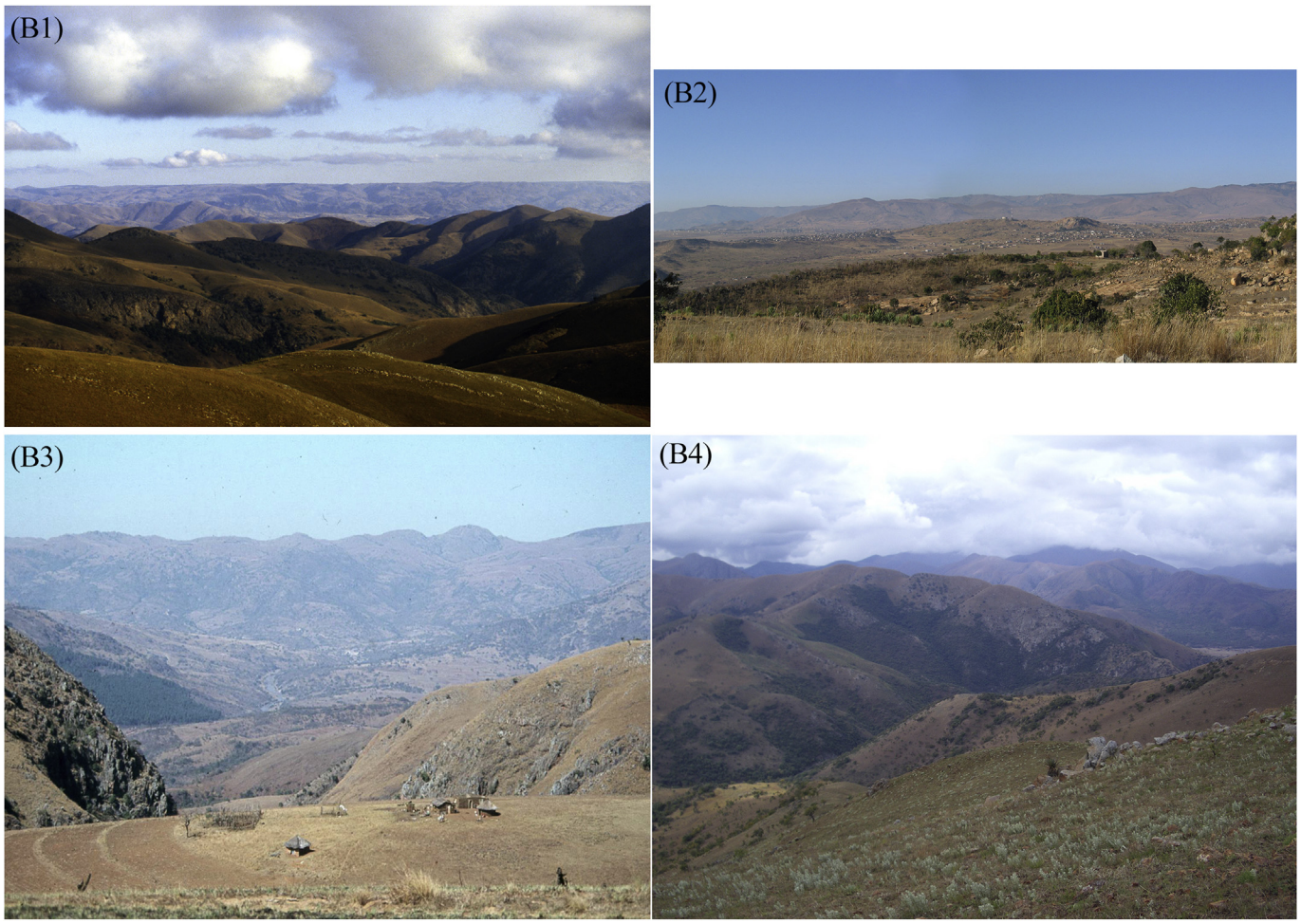

Figure 1. (*continued*).

summarize the rates of processes determined from this and earlier published data, and balance these against plate tectonic and plume related models.

2. General geology of the southern Makhonjwa Mountain ranges

The literature about the geology of the Makhonjwa Mountains is vast, and goes back to the late 19th Century when gold was first discovered there. We refer readers interested in the earlier work to Hall (1918) and Visser et al. (1956; and references therein), and reports of Anhaeusser (1976, 1986, 1987, 1997) that collate the bibliography of the region prior to 1996. Our work is confined to the southern sector of the greenstone belt within these mountain ranges because it contains the best preservation and exposures of all sequences. The general geology of this study area is summarized in Figs. 2–4, and the detailed bedrock geology on Map 1 and its inset.

The lithologies of the MMts (ca. 120 km × 60 km) are surrounded on all sides by granitoid gneiss domes and plutons that span about 500 million years (e.g., Moyen et al., 2007; Schoene et al., 2008; and references therein). Across the Swaziland Highlands, the Ancient Gneiss Complex (AGC) that flanks the southeast margin of the MMts contain the oldest rocks yet identified in Africa (Schoene et al., 2008; Schoene and Bowring, 2010; Kröner et al., 2013, 2016; and references therein).

The oldest dated sequences within the belt (in the Theespruit Complex) overlap with ages determined for the younger gneisses of the AGC (Kröner et al., 2013, 2016). The youngest sequences within the MMts comprise molasse-like sandstone-conglomerate sequences (Moodies Group, subsequently referred to as MG) deposited during and after a second tectonic period ending just before and during the onset of emplacement of regional-scale granite batholiths at 3.14 Ga that widely surround the belt (Inset Map 1 and Fig. 2; Lamb, 1984a, b; Schoene et al., 2008; Heubeck et al., 2016 and references therein).

Along the northwest margin of the MMts, TTG granitoid orthogneisses and shear zones separate mafic-ultramafic rocks of the Weltevreden sequences (Anhaeusser, 2006; and here referred to as the Weltevreden Domain, Figs. 2 and 3; and see below) from adjacent TTG core-complexes and GGM (Granite-Granodiorite-Monzonite) plutons bounding the Stentor (e.g., Honeybird Shear Zone flanking the 3258 Ma Stentor banded tonalite and the 3106 Ma Stentor granitic orthogneiss); the Nelspruit (3105 Ma), Nelshoogte (3236 Ma), and Kaap Valley (3227 Ma) batholiths (Inset, Map 1). These older granitic gneiss zones are dated between ca. 3350 and 3100 Ma (Anhaeusser, 2006; Moyen et al., 2007; Stevens and Moyen, 2007; Schoene et al., 2008). Visser et al. (1956) predicted the presences of these flanking gneisses on the basis of deformed granitoid pebbles derived from the northwest that they discovered in the MG. Later analyses found some pebbles to be as old as ca. 3570–3520 Ma, and interpreted to be derived from the AGC to the east (Compston and Kröner, 1988). These granitoid clasts were sourced and deposited within 10 million years (Heubeck et al., 2016) from widely dispersed *external* terrains of mixed ages during

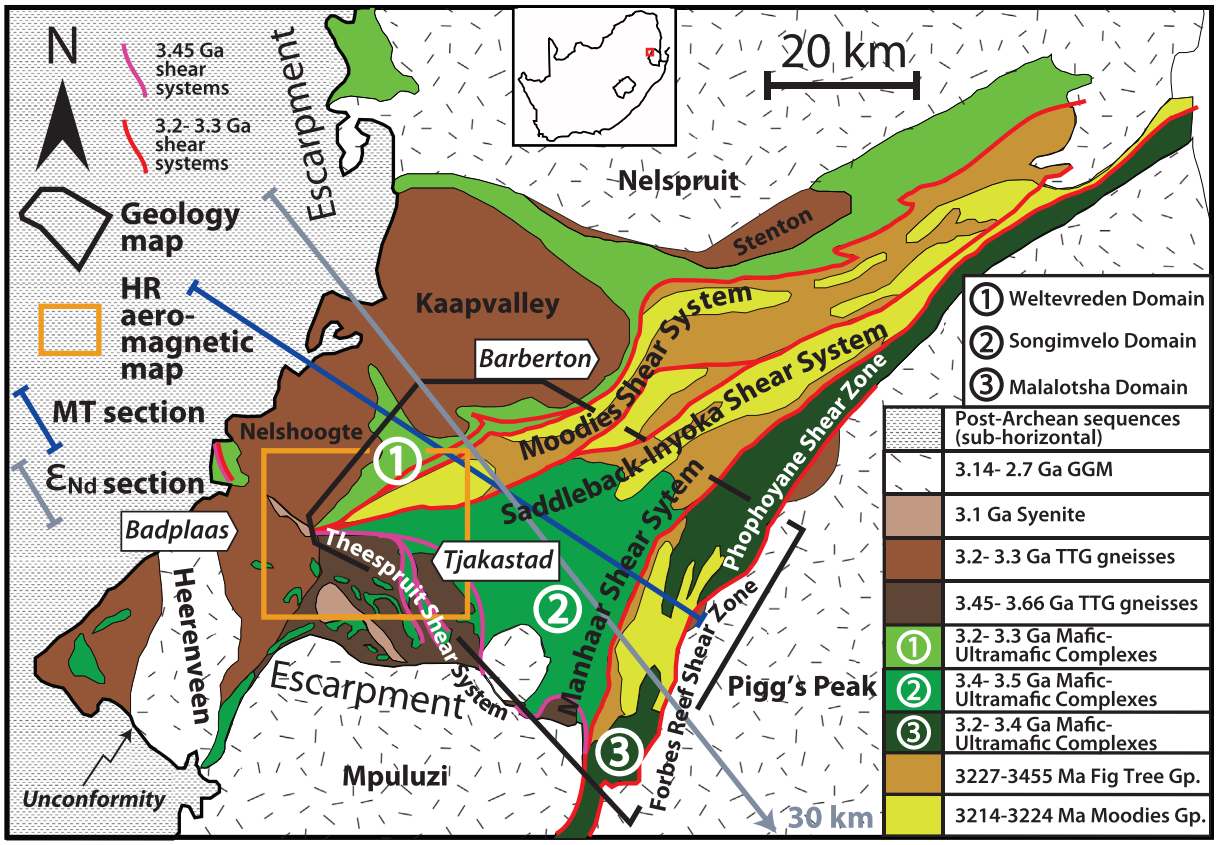

Figure 2. Outline of the Makhonjwa Mountains and its flanking granitoids. Highlighted are the major shear systems separating the three internal Tectonic Domains of mafic-ultramafic complexes and their overlying sedimentary sequences (Fig Tree and Moodies Groups). Location of the detailed bedrock and structural Maps 1 and 2 are shown as black rectangle. Also shown are locations of the High-Resolution Magnetic Map, the Magneto-Telluric and Nd-isotope sections described in the text.

emplacement, uplift and erosion of the granitoid batholiths and TTG core-complexes, following the main deformation episode in this region between ca. 3227 Ma and 3229 Ma (de Ronde and Kamo, 2000; Drabon et al., 2017).

The boundary of the Weltevreden Domain with the central Songimvelo Domain of the MMts (Fig. 2) coincides with a major fault system with both thrust and strike-slip components (Moodies-Sheba-Inyoka-Saddleback) active during the deposition of both deep water Fig Tree Group (shales and turbidites) and shallow marine-terrestrial siliciclastic arkoses and wackes (in places molasse-like) of the MG, deposited between 3223–3224 Ma and 3214 Ma (De Ronde and Kamo, 2000; Heubeck et al., 2016).

There is a progressive chemical change in the composition of the Fig Tree Group (FTG) to the MG (Toulkeridis et al., 2015), as also noted in southern region of the Swaziland side of the MMts (Malalotsha Domain; Fig. 2), where the MG lithologic equivalent is known as the Malalotsha Group and the FTG as the Diepgezet Group (Lamb, 1984a, b). The FTG sediments were derived predominantly from mafic and ultramafic (and rare felsic) sources *internal* to the greenstone belt, whilst the MG sediments were sources from felsic and highly feldspathic granitoid plutons. The Moodies sequences are varied over relatively short distances and were likely deposited during rapid burial in separate fault controlled, isolated basins close to marine shorelines, from both internal and external sources (Sanchez-Garrido et al., 2011; Heubeck et al., 2016; Drabon et al., 2017). In Swaziland they were deposited syn-tectonically as molasse-like sequences during complex east-directed thrusting likely within a period of less than 10 million years (Map 2; Lamb, 1984a,b, 1987). It is not known if these sequences on opposite sides of the greenstone belt are precise age-equivalents; accurate geochronology is missing in the Songimvelo and Malalotsha Domains.

Thus, in general the bed rock of the MMts is dominated by a siliciclastic cover in the north that has been increasingly removed towards the southern part of the mountain belt covered by our Maps. Thermochronology indicates that up to 5–10 km rock cover has been removed here (Schoene et al., 2008), exposing the predominantly magmatic sequences that comprise the underlying mafic-ultramafic 'basement' to the sedimentary archives of the FG and MG.

The southern part of the MMts can be simply divided into three tectonic domains; regional allochthons of crustal fragments here informally referred from west to east as the Weltevreden Domain, the central Songimvelo Domain (following Lowe, 1994; Lowe and Byerly, 2007), and the eastern Malalotsha Domain (Fig. 2). The latter is predominantly in Swaziland. The eastern and western domains strike roughly NNE–SSW, whilst sequences in the Songimvelo Domain strike roughly E–W and, NNE–SSW in the east across the Onverwacht Bend (Map 2). The Weltevreden and Malalotsha Domains are separated from the central domain by major tectonic breaks, respectively the Saddleback-Inyoka Shear System (SISS) and the Manhaar-Msauli Shear System (MMSS – Figs. 2–4; Map 2). The structures in the marginal domains are dominated by late fold, thrust and strike-slip structures (D2/D3 dated between 3227 Ma and 3240 Ma) that overlap with deposition of molasse-like sequences (MG). The central domain best preserves a long history of early listric extensional faults (D0, 3.47–3.3 Ga) and a relatively short fold and thrust belt (D1), dated between 3.45 Ga and 3.43 Ga, with back-trusting possibly lasting until 3.33 Ga (e.g., Kamo, 1992), and

emplacement of a major nappe (de Wit, 1982; here renamed the Pylon Nappe) during deposition of the Fig Tree Group (Map 2 and Fig. 3b; de Wit et al., 2011).

2.1. Songimvelo Domain

The lowermost sequences of the Onverwacht Suite are the Sandspruit and Theespruit Complexes that form parts of subvertical mafic-felsic schist belts along the southern margin of the Songimvelo Domain. They are isoclinally folded and deformed at higher grades of metamorphism (upper amphibolite facies) than all the other overlying internal complexes at greenschist-facies (Dziggel et al., 2002, 2006; Kisters et al., 2003; Diener et al., 2005, 2006; Stevens and Moyen, 2007). Within internal imbricate tectonic slices, pillow structures, felsic volcanic and volcaniclastic sequences, conglomerates and sedimentary successions with graded lapilli are still well-preserved (de Wit et al., 1983; de Wit et al., 2011). The Theespruit Complex has been dated between 3538 Ma and 3521 Ma (Armstrong et al., 1990; Kröner et al., 2016), but there is dispute since detrital zircon from a felsic volcaniclastic horizon in the Theespruit sequence has also yielded ages as young as 3453 Ma (Fig. 3b; and see below). These sequences, herewith collectively referred to as the Theespruit Shear System (Fig. 2; inset Map 1) were thrust to the south across the older adjacent TTG cores, and in places back-thrust, around 3445 Ma, and later exhumed by up to 18 km during extensional faulting and formation of core complexes at circa 3.2 Ga (Kisters et al., 2003; Stevens and Moyen, 2007; Lana et al., 2010a, b).

The type section of the Onverwacht Suite includes the Komati Complex from which komatiites were originally discovered flanking the Komati River (Viljoen and Viljoen, 1969a, b). The geology of the Komati Complex has been re-mapped by numerous geologists, but most recently in detail (1:500 to 1:5000) by J. Dann (Dann, 2000, 2001 and references therein). Field observations are incorporated on Map 1, but this does not do justice to Dann's superb maps to which the reader is referred for further details.

Field observations and petrology across the Komati Complex have been widely published. The findings are not discussed here further, other than to mention that there are still significant controversies about the percentages of volcanic lavas versus shallow intrusions (published ratios of volcanic versus intrusive components range from 100% versus ca. 50%–70%); and on the magma sources of the komatiites, and about the origin of their olivine and pyroxene spinifex textures (e.g., Viljoen and Viljoen, 1969a; de Wit et al., 1987a; Grove et al., 1997; Dann, 2000, 2001; Dann and Grove, 2007; Robin-Popieul et al., 2012). The Komati Complex rocks are metamorphic, and very little original olivine (<1%) or pyroxene is preserved.

In 2014, an ICDP drill site (BARB 1-1; http://barberton.icdp-online.org/) was completed through a section of an inflated flow (tumulus) or very shallow intrusive, described in detail by Dann (2008) and Robin-Popieul et al. (2012).

The most accepted igneous age of the mafic-ultramafic Komati Complex has been derived from its central sector (3482 ± 5 Ma, and 3481 ± 2 Ma; Fig. 3b), but its precise age range is unconstrained. The complex is cut by silicic dykes dated between 3470 Ma and 3458 Ma by Armstrong et al. (1990) and at ca. 3467 Ma by Kamo (1992). The age of its greenschist facies metamorphism is best bracketed between 3.45 Ga and 3.49 Ga ($^{40}Ar/^{39}Ar$) and 3.43 Ga (Rb/Sr) dated from the same central sector (de Wit et al., 1987a, b, and references therein).

We focus here further only on the geochemical signatures from a number of studies on the komatiites and related basalts (see section 5).

The mafic-ultramafic sequences of the overlying Hooggenoeg Complex have not been dated directly. However, zircons isolated from two of the ten interlayered chert horizons (HC on Fig. 3b) have provided U–Pb dates of 3472 Ma (Middle Marker) and 3470 Ma (HC4). Its litho-stratigraphy and volcanic/intrusive complexities (including the massive Rozentuin Ultramafic Complex) have been described in detail elsewhere (de Wit et al., 2011; Furnes et al., 2011, 2012; Robins et al., 2011; Sandstå et al., 2011). In the glassy margins of pillow lavas and the interpillow hyaloclastites just below the highest preserved chert horizon (HC10; Fig. 3b) the oldest trace fossils of the MMts have been recorded (Furnes et al., 2004; Banerjee et al., 2006; Staudigel et al., 2008). Recently these have been critically re-examined (Grosch and McLoughlin, 2015; Staudigel et al., 2015).

The Hooggenoeg Complex is unconformably and tectonically overlain by the Noisy Complex and intruded by its felsic sills. The most complete sections are best preserved along its E–W trending sector (Map 1) where it has been mapped in detail by de Vries (2004), de Vries et al. (2006, 2010), Nijman and de Vries (2009). Here conglomerates with boulders including silicified spinifex and quartz-carbonate-fuchsite gneiss that directly overlie mafic pillows of the Hooggenoeg Complex are interbedded with felsic volcanic and volcanoclastic rocks (3448–3452 Ma) that are intruded by felsic sills (Nijman and de Vries, 2009) dated between 3451 Ma and 3445 Ma (Fig. 3b; de Wit et al., 2011; Kröner et al., 2013; and references therein). These sequences were deposited in shallow water to subaerial environments during active regional extension along listric faults that merge with layer parallel shear zones within the underlying Hooggenoeg Complex (Nijman and de Vries, 2009; Map 2).

A similar but reduced sequence of shallow water to subaerial diamictites, conglomerates and sandstones overlie the Hooggenoeg Complex along its N–S trending sector, which are described in detail from the Etimambeni section along the Komati River and from drill core (de Wit et al., 2011; Grosch et al., 2011; de Wit and Furnes, 2016). This section has yielded detrital zircons ranging in age between ca. 3455 ± 8 Ma and 3432 ± 10 to 3437 ± 14 Ma (Grosch et al., 2011, 2012; Grosch and Slama, 2017), which implies that this condensed section (less than 200 m) represents the youngest part of the Noisy siliciclastic units. 5 km farther north, this section cuts 1–1.5 km into the upper part of the Hooggenoeg Complex (Map 1), and elsewhere its lower section is overlain by felsic volcanic and volcaniclastic rocks (Nijman and de Vries, 2009; de Wit et al., 2011; Fig. 3b). Whilst it has been argued that the two sections (E–W and N–S) are not equivalents (Grosch et al., 2011), the units have been traced all the way across the Onverwacht Bend (Map 1, and see below).

Both sections are disconformably overlain by Banded Iron Formation (BIF) and thick gray-white layered cherts known as the Buck Ridge cherts and in the E–W type section reach more than 500 m in thickness (de Vries, 2004; de Vries et al., 2006, 2010; Nijman and de Vries, 2009, and references therein). Recent ICDP drilling has penetrated a thickness of more than 1000 m in the western part of this type section (BARB-2; http://barberton.icdp-online.org/; Map 2). Along the Etimambeni section these are tectonically reduced in thickness to less than 50 m (de Wit et al., 2011). Along the section, the Noisy Complex is separated from the overlying Kromberg Complex by a carbonate-fuchsite-serpentinite shear zone (the Etimambeni thrust System, Map 2; Fig. 3b), which is generally poorly exposed along the N–S section, except in parts of the Dunbar region (Paris, 1984, 1987).

In the central part of the Songimvelo Domain, the E–W striking lithologies and structures merge with those of the Weltevreden Domain along the NNE–SSW faults of the Inyoka-Saddleback Shear System (ISSS) and from there extend southwestward into the Stolzburg Schist Belt (Maps 1 and 2; Fig. 5). The general geology of the Stolzburg Schist Belt is discussed further below. In the east, the E–W structures merge over a broad zone with the NNE–SSW trending D2

Transect Across the Paleoarchean Sequences of the Southern Makhonjwa Mountains and Adjacent Granitoids of South Africa and Swaziland.

Bed Rock Lithologies

Regional location of the Map across the southern Makhonjwa Mountains

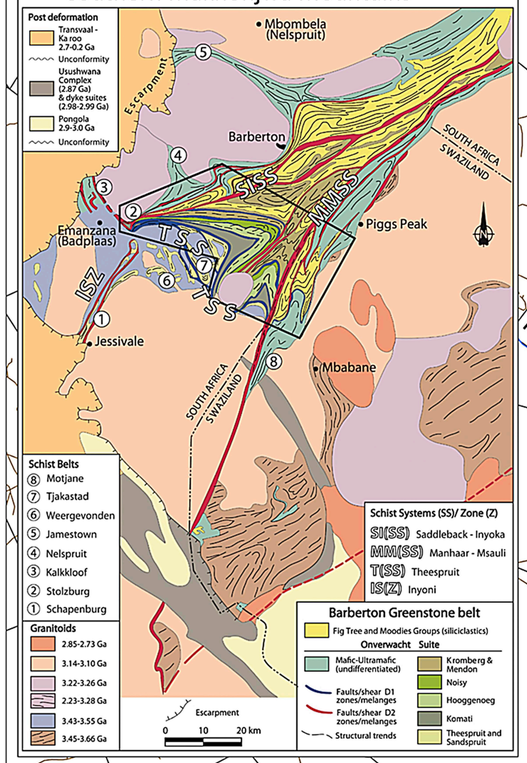

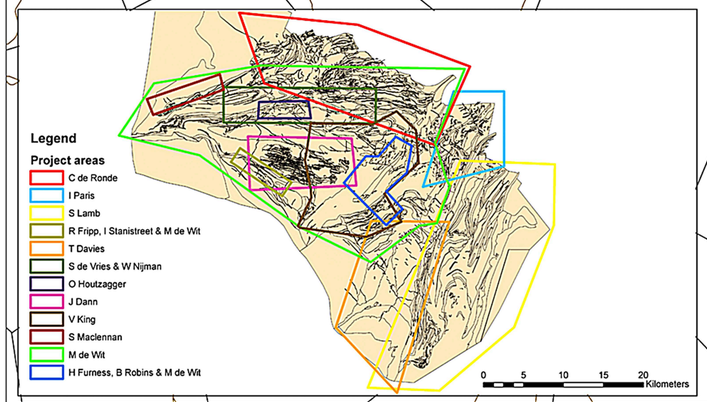

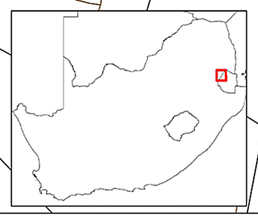

LEGEND

Alluvium cover

Igneous

- Mafic (Dolerite - Gabbro - Diorite) Dykes
- Felsic Dykes
- Granite
- Granite gneiss
- Tonalite (TTG)
- Tonalite gneiss
- Quartz - feldspar porphyry
- Mafic - Felsic gneisses, undifferentiated
- Tholeiitic pillow and massive basalt with minor basaltic komatiite (H)
- Mafic - ultramafic volcanics and sills undifferentiated (K,H)
- Tholeiitic pillow basalt and basaltic komatiite (K)
- Massive basalt and basaltic komatiite (K)
- Massive wehrlite/gabbro/diabase (K)
- Wehrlite (K)
- Olivine komatiite sometimes with olivine spinifex (K)
- Olivine komatiite, vesicular (K)
- Pyroxene spinifex komatiite (K)

Serpentinized

- Tholeiitic pillow basalt and basaltic komatiite (H, Kr)
- Komatiite and basaltic komatiite, undifferentiated (K, Kr)
- Tholeiitic pillow and massive basalt (Kr)
- Tholeiitic pillowed and massive tholeiitic basalt, undifferentiated (Kr + M)
- Mafic-ultramafic rocks, undifferentiated (K)
- Mafic - ultramafic tephra; phlogopite - calcsilicate - carbonate - serpentine matrix (often schist-gneiss) (Kr, M)
- Mafic - ultramafic intrusives, undifferentiated (Kr)
- Massive and pillowed tholeiite with undifferentiated ultramafic rock (Kr)
- Tholeiitic pillowed and massive basalts (Kr)
- Mafic - ultramafic volcanics and intrusives, undifferentiated (M)
- Mafic - ultramafic volcanics and intrusives, undifferentiated (W)
- Felsic - mafic - ultramafic rocks, often schist, undifferentiated (T)
- Mafic - ultramafic rock (often amphibolites), undifferentiated (T)
- Felsic volcanics and quartz sericite-chlorite-schist, undifferentiated (Sw)
- Felsic volcanics, volcanoclastics, and hypabyssal sills, undifferentiated (N)

Sedimentary

- Chert - Silicified tuff and sediments
- Breccia, undifferentiated
- Banded Iron Formation (BIF) - Jaspilite - Chert
- Ironstone
- Slagg/ironstone pods
- Ferruginous chert and / or shale
- Ferruginous tuff
- Zones impregnated with iron
- Conglomerate
- Sandstone and conglomerate
- Sandstone (fine - coarse), often quartzite, sometimes schistose
- Siltstone and shale
- Siltstone/Shale/Sandstone/Conglomerates, undifferentiated
- Thinly bedded siltstone and sandstone

Metamorphic

- Sheared, silicified or ferruginous sandstone/siltstone
- Quartz-chlorite-sericite-muscovite-feldspar schist
- Serpentinite (dunite) and talc schist (W)
- Serpentinite (dunite) and talc, sometimes schist (Sw)
- Serpentinite (M,W)
- Serpentinite (Kr)
- Meta - dunite with rare rhodingites (W)
- Meta - orthopyroxenite (W)
- Sheared varieties of ultramafic rock (talc - chlorite - magnesite sericite - carbonate fuchsite schists); Quartz - magnesite schist
- Banded and foliated fuchsite - quartz - carbonate - chlorite - gneiss

Cadastral data

- Farm boundary
- River
- National border
- Road
- Border Post
- Survey beacon
- Towns and villages

Complexes: T = Theespruit; K = Komatiite; H = Hoogenoeg; N = Noisy; Kr = Kromberg; M = Mendon; W = Weltevreden; Sw = Swaziland

M J de Wit 2017

Mapped at various scales between 1978 - 2014 by

Maarten de Wit, Simon Lamb, Isabelle Paris, Cornel de Ronde, Tim Davies, Jesse Dann, Vic King, Rod Fripp, Ian Stanistreet, Hielke Jelsma, Sjoukje de Vries, Wouter Nijman, Ono Houtzager, Blair Schoene, Scott McLennan, Harold Furness, Brian Robins

Cartography and GIS by Laura Middelmann an Iuma Martinez

Topographic and cadastral data from Peter Bowerman, Chief Directorate, Surveys and Mapping, Mowbray, RSA

Earth Stewardship Science Research Institute
NELSON MANDELA UNIVERSITY

Barberton_2017_09_29_Final_MAP

Map 1: Bed Rock Lithologies of the Southern Makhonjwa Mountains and adjacent granitoids. Insets show: 1 (lower left) the locations of detailed maps and their authors; and 2 (upper left) the regional distribution of the granite-greenstone lithologies, with major shear systems and linked internal/external schist belts, and the general distribution of tectono-stratigraphic complexes of the Onverwacht Suite (GIS database available on request).

Transect Across the Paleoarchean Sequences of the southern Makhonjwa Mountains and Adjacent Granitoids, Mpumalanga, South Africa and Swaziland.

Folds and Faults

Vygeboom Dam
Komati River
KALKKLOOF SCHIST BELT
Badplaas
Seekoeispruit
STOLZBURG SCHIST BELT
Tjakastad
Josefsdal
Steynsdorp
South Africa
Swaziland
N
M. J. de Wit, 2017
Earth Stewardship Science Research Institute
AEON
NELSON MANDELA UNIVERSITY
0 2 4 8 12 16 Km

- Fold axis/ Fold System (FS) with plunge direction
- Faults (F) and Shear System (SS)
- Downward facing
- Unconformity
- Normal (symbol on upper plate)
- Thrust (symbol on upper plate)
- Main transport direction D1/D2
- Homogenous deformation D2 80% minimal shortening Tectonic shortening

WELTEVREDEN

1. Mawelawela F
2. a Stolzburg F-Moodies F; b Bellvue F
3. Queens River SS
4. Saddleback F
5. Morgan F
6. Sheba F
7. Inyoka SS

(1) Weltevreden synform
(2) Stolzburg syncline

THEESPRUIT

1. Tjakastad SS
2. a Dalmein SS; b Steynsdorp SS
3. Theespruit SS

KOMATI

1. Komati SS
2. Steambell shear
3. Mbjega SS

HOOGGENOEG - NOISY

1. Geluk SS
2. Noisy listric system
3. Etimambeni thrust system

(1) Onverwacht bend/SS

KROMBERG - MENDON - MALALOTSHA

NORTH

1. Power Line Nappe

(1-4) Synclines/forms (unnamed)

1. Granville Grove SS
2. Aubervilliers SS
3. Schulzenhorst SS

EAST

2. Malalotsha thrust sheet
1. Emlembe SS
2. Msauli SS
3. Havelock SS
4. Phophoyane SS
5. Forbes Reef SS
6. Manhaar-Msauli SS

EAST

1. Kromberg antiformal syncline
1. Makonhjwa bend
2. Sigadeni synform
3. Waterfall antiformal synclinorium
4. Xecacatu synform
5. a Simbubule syncline; b Kranskop syncline
6. Masali syncline
7. Malalotsha antiform
8. Malalotsha synform
9. Ngwenya syncline
10. Steynsdorp FS
11. Ekulindini bend

- Towns
- Roads
- Rivers
- Farm boundaries
- Scientific Drillholes

Map 2: Faults and Folds and related tectonic features across the Southern Makhonjwa Mountains . The major folds and thrusts are named, and discussed further in the text. Also shown is the location of the Stolzburg Schist Belt detailed further in Fig. 5.

structures of the Malalotsha Domain that farther south merge into the Motjane Schist Belt (Inset Map 1). Detailed structural and strain analyses of Motjane and Stolzburg schist belts are reported elsewhere (de Wit, 1983; Jackson and Robertson, 1983; MacLennan, 2012).

Similar subvertical schist belts flank the southern margin of the Komati and Theespruit Complexes (e.g., the Tjakastad and the Stolzburg Schist Belts; Kisters et al., 2003, 2010; Diener et al., 2005) and possibly also link to other schist belts that are separated from the main MMt ranges and whose relationships are therefore not obvious (e.g., the Schapenburg and Weergevonden Schist Belts within the southern Stolzburg TTG cores to the south; and the Kalkkloof Schist Belt (KSB) to the NW of the Weltevreden Domain, flanking the Nelspruit TTG). The geology of the two southern external schist belts are not further discussed here; they are described elsewhere (Van Kranendonk et al., 2014, and references therein). Potential links to the external Kalkkloof and Schapenburg Schist Belts are discussed below.

There is significant tectonic debate about if and how the Stolzburg Schist Belt, and specifically its Saddleback-Inyoka Shear System (SISS), links up to the south with an external schist belt and its related shear system known as the Inyoni Shear Zone (ISZ), or to the west with an external system that links to the Kalkkloof Shear System (KSS; Fig. 2, and inset Map 1).

Previous investigations identified relatively high pressure metamorphic assemblages in folded mafic-ultramafic assemblages within the foliated contact between the Badplaas and Stolzburg tonalite terrains (Dziggel et al., 2002; Moyen et al., 2006; Nédélec et al., 2012; Cutts et al., 2014). This shear zone, the Inyoni Shear Zone (ISZ), was subsequently interpreted as a southern extension to the SISZ, and thought to represent a Mesoarchean paleo-subduction zone, with metamorphic mineral assemblages indicative of relatively high pressure (1.2–1.5 GPa) and moderate temperature (600–650 °C) during a low geothermal gradients (12–15 °C/km) across a large area of the Stolzburg terrain (Dziggel et al., 2002; Diener et al., 2005; Moyen et al., 2006, 2007; Stevens and Moyen, 2007; Kisters et al., 2010). These pressures are the highest crustal pressures reported in Paleoarchean rocks at the lowest apparent geothermal gradients. Slightly higher geothermal gradients (20–30 °C/km) reported from related mineral assemblages (e.g., Nédélec et al., 2012) are likely associated with retrograde metamorphic reactions under increasing temperatures during exhumation. Presently the only tectonic environments where such P–T conditions occur are in subduction zones. Metamorphic and structural analyses yielding lower pressure (0.5 GPa) some 15 km farther south of the HP assemblages, have placed doubts on this interpretation as a subduction zone (Van Kranendonk et al., 2014). We will address these potential links below using new high resolution magnetic data.

2.2. Weltevreden Domain

The western margin of the MMts comprises the Weltevreden Domain, mapped in details in the study area by C.E.J. De Ronde, and dated by De Ronde and Kamo (2000). This region contains structurally separated sections of komatiite and tholeiite as well, as the well-known tectonically bound Stolzburg Layered Ultramafic Complex (SLUC, ca. 1–2 km thick), which is composed of serpentinized dunites and orthopyroxenites, with lesser amounts of internal gabbro and rodingite, and flanked to the NW by a large gabbro unit (de Wit et al., 1987a, and recently re-assessed by; MacLennan, 2012). These sequences were originally defined as the Jamestown Series (Hall, 1918), but are here collectively re-named the Weltevreden Domain (Map 1 and Fig. 5). No dates have been obtained from the mafic and ultramafic sequences, but a date of ca. 3210 Ma has been obtained from a titanite in a rodingite dike in the SLUG (S.A. MacLennan, unpublished data).

The mafic-ultramafic rocks N of the SLUC are poorly outcropping, but along strike to the NE they contain well-preserved spinifex-bearing komatiites and related ultramafic complexes, often deeply carbonatized and serpentinized, and dislodged by a number of complex and refolded shear zones/faults that are well known for their association with the largest gold mines near Barberton (Visser et al., 1956; Anhaeusser, 1986; De Ronde et al., 1991, 1992; Ward, 1999; Dziggel et al., 2007; Munyai et al., 2011; Dirks et al., 2013).

The Weltevreden Domain is cut by a number of major subvertical faults that separate the mafic and ultramafic sequences from the younger FTG and MG sedimentary sequences that are best preserved within a large syncline (the Stolzburg syncline; Map 2). Only along the hinge of this fold, and occasionally along its subvertical limbs, are disrupted sections of unconformities preserved. Some of the faults (e.g., the Mawelawele and parts of the Moodies faults) are presently SE directed back-thrusts (Map 2; De Ronde and de Wit, 1994; De Ronde and Kamo, 2000). The mafic-ultramafic sequences of the Weltevreden Domain merge along the southeastern tectonic margin of the Stolzburg syncline with the E–W striking mafic-ultramafic sequences of the Kromberg and Mendon Complexes of the Songimvelo Domain. The original boundary between the mafic-ultramafic sequences of these two domains are arbitrarily defined (Map 1) for lack of outcrop and sufficient geochemical data.

Within the hinge of the Stolzburg syncline is a sequence of felsic ignimbrites and tuffs dated between 3227 Ma and 3223 Ma (Kamo, 1992) that separates the FTG and MG (Map 1), and thus predates MG deposition; the onset of tectonic activity of the SISS faults; and the formation of the Stolzburg syncline in this region.

Farther west, the Weltevreden Domain merges systematically with the Noisy, Hooggenoeg, Komati and Theespruit Complexes of the Songimvelo Domain. All these complexes and the FTG/MG coalesce westward to form the subvertical Stolzburg Schist Belt (Fig. 5), reducing the total thickness of all the complexes from near 23 km to less than 3 km, a decrease in thickness of some 20 km over a similar strike distance (Map 2); including a homogeneous ductile flattening of about 75–80% within the mafic schists, as measured from deformed ocelli (Map 2; de Wit et al., 1983; De Ronde and Kamo, 2000). More than 95% of the original litho-stratigraphy must have been tectonically dismembered within the Stolzburg Schist Belt along faults of the SISS.

Anhaeusser et al. (2006) interpreted the Weltevreden block to be part of a complex 'suture zone', separated by a tectonic break from the central Songimvelo Domain. We concur with that general interpretation (see below).

2.3. Malalotsha Domain

This domain is tectonically complex (Map 2), comprising many D2 thrust packages of the Onverwacht Suite rocks and the well-preserved Fig Tree/Moodies like lithologies, especially flanking the borders in the northern sector. Little is known however about the stratigraphy and original thickness of the mafic and ultramafic rocks, including massive tholeiitic pillow lavas and occasional spinifex bearing units. Viljoen and Viljoen (1969a, b) correlated these sequences with the uppermost Onverwacht Suite (here the Kromberg and Mendon Complexes), but this correlation has been disputed (Barton, 1982).

The mafic sequences, commonly with significant layered iron deposits, are associated with three major ultramafic complexes, at Msauli, Havelock and Motjane, which comprise a number of steep, southwest inclined allochthonous serpentinite bodies up to 1 km thick, tectonically emplaced along major shear zones with west

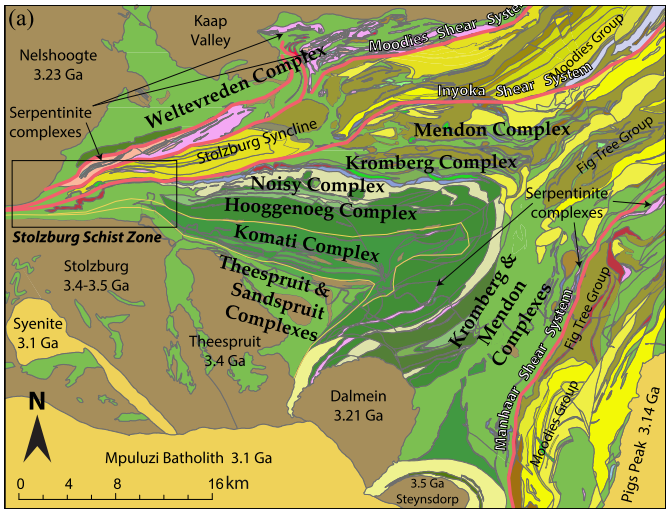

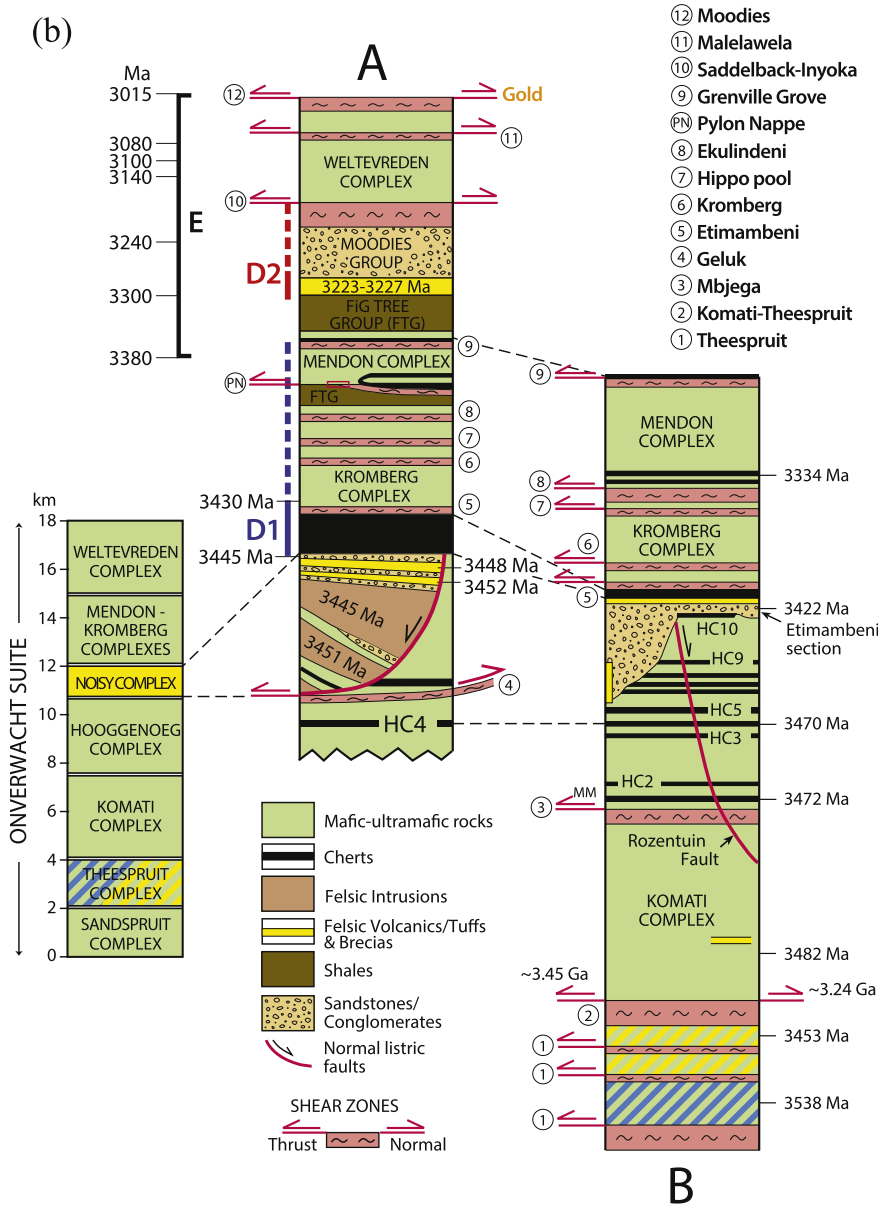

Figure 3. (a) Simplified map showing the location and distribution of the litho-tectonic complexes and major fault systems across the Maps 1 and 2, as detailed in the text. (b) Generalised tectono-stratigraphic column of the Onverwacht Suite, as representative across the map area, showing tectonic contacts between the respective complexes of the

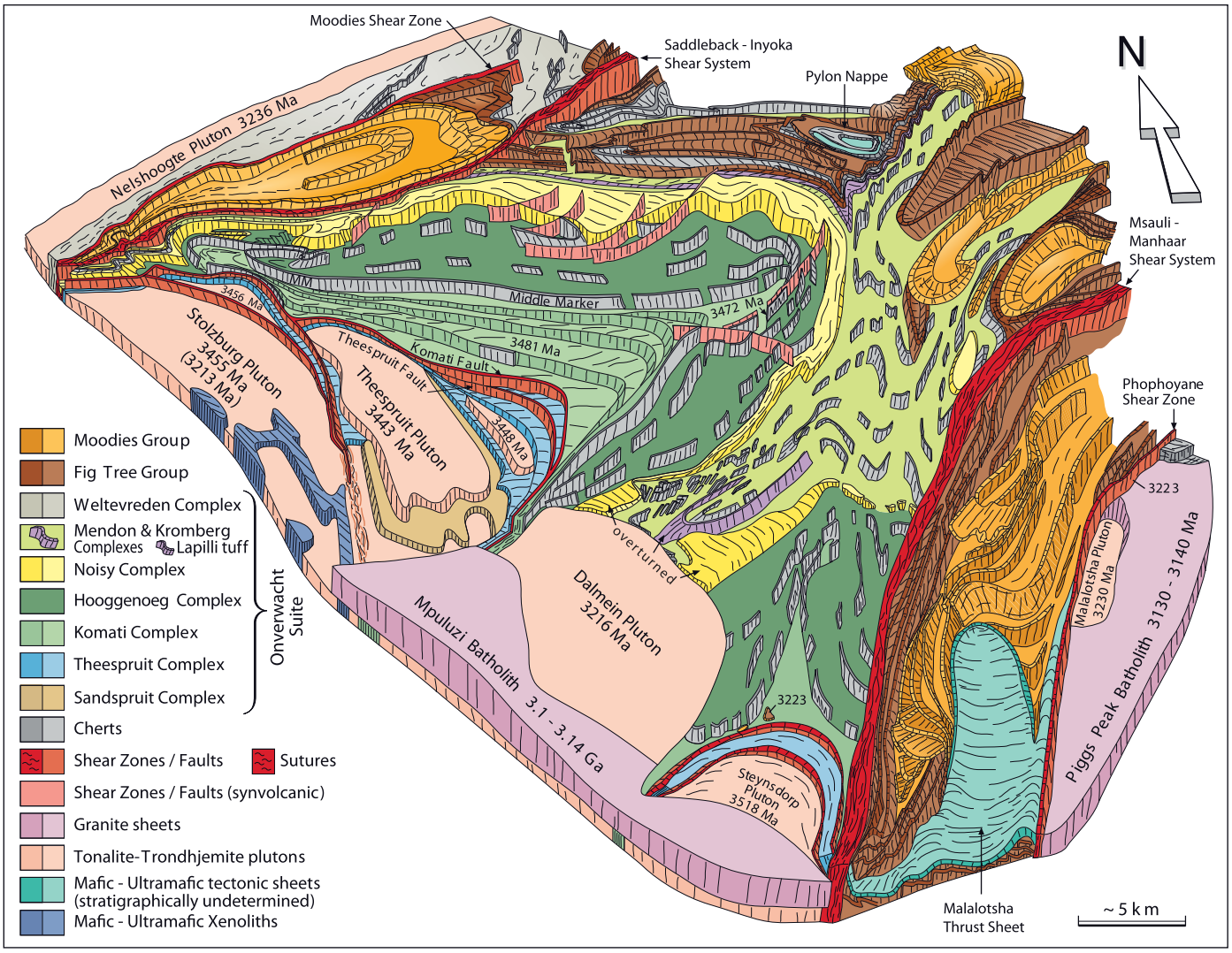

Figure 4. Simplified 2.5-D map illustrating the general geologic and tectonic relationships of the study area. The two major NE–SW striking shear systems (Inyoka-Saddleback and Manhaar-Msauli) and post Moodies Group related synclines and anticlines, are the surface expression of inferred 3.2 Ga suture zones dipping to the NW and SE, respectively (e.g., Schoene et al., 2009; Schoene and Bowring, 2010; de Wit et al., 2011), whilst the WNW–ESE striking shear zones are connected to a 3.4 Ga suture zone (e.g., de Wit et al., 2011), overprinted by 3.2 Ga extensional exhumation along these same shear zones (e.g., Kisters and Anhaeusser, 1995; Diener et al., 2006). Note that most of the Onverwacht Suite (as expressed by the grey cherts) is subvertical, and unconformably overlain by the Fig Tree and Moodies Groups *before* the 3.2 Ga deformation events (D2; Map 2). Along the southernmost margin flanking the granitoid terrain, parts of the Onverwacht Suite are overturned in places prior to D2 folding and thrusting and crosscut by granitoids (e.g., just northeast of the Dalmein pluton; de Ronde and de Wit, 1994; de Wit et al., 2011). For clarity, not all structures and shear zones are shown (modified from de Wit et al., 2011).

facing leading edge thrust zones (e.g., Barton, 1982). These shears are part of the Msauli-Manhaar Shear System (Map 2) along which the serpentinites are extensively replaced by talc (e.g., Visser, 1956). The Msauli and Havelock bodies consist predominantly of discontinuous bodies of serpentinized dunite and harzburgite, with local gabbros and rodingites, and a stockwork of abundant cross-fibre chrysotile veins that were extensively mined as far back as the 1930s (Barton, 1982; Büttner, 1984; Maps 1 and 2). In the Havelock deposits, the chrysotile formed by hydrous fluids in dilation cracks at temperatures below dehydration of lizardite serpentine, whilst farther south, lizardite occurs extensively along the bounding shear zones of the Msauli bodies with estimated formation temperatures between 315 and 500 °C (Barton, 1982; Büttner, 1984). The asbestos zones of the Havelock complex formed predominantly near the leading edge of a west-directed thrust sheet in a broad zone where the décollement was not a simple planer sheet, but comprised a number of west-verging stacked duplexes, which were subsequently flattened and rotated to near vertical (Barton, 1982). Modern geochemical data is lacking, but from detailed mineral chemistry and limited whole rock geochemistry of major elements and deep underground mine geology, Büttner (1984) suggested that the Msauli complex is similar to that of Alpine peridotites and similar ultramafic bodies in Phanerozoic ophiolites. Serpentinized and carbonatized ultramafic lenses, locally with listvenite, of this Archean ophiolite (Barton, 1982) occur

Onverwacht Suite, with age dates and names of shear zones shown. Movement directions across tectonic contacts are based on kinematic indicators observed in the field or inferred from the regional geology, but are not always well-established, as discussed in the text. The age ranges of all of the tectonically juxtaposed complexes, as well as their original spatial relationships remain unresolved. Section A = across the upper section of the E-W trending northern Songimvelo Domain and linked to the NE-SW Weltevreden Domain; Section B = across the N-S trending Songimvelo Domain and the EW trending lower section of this Domain. Also shown are the age-ranges of major tectonic events: D = episodes of the two main compressional deformations as referred to in the text (1 = early; 2 = late; solid lines are well-dated; broken lines are less well defined); E = episodes of exhumation of the greenstone belt and surrounding core complexes. Note the columns are not to scale; and the thicknesses indicated along the left hand column are only rough estimates. Small red rectangle in column A (at the bottom of Mendon Complex) indicates the location of pictures shown in Fig. 29 (modified from de Wit et al. (2011)).

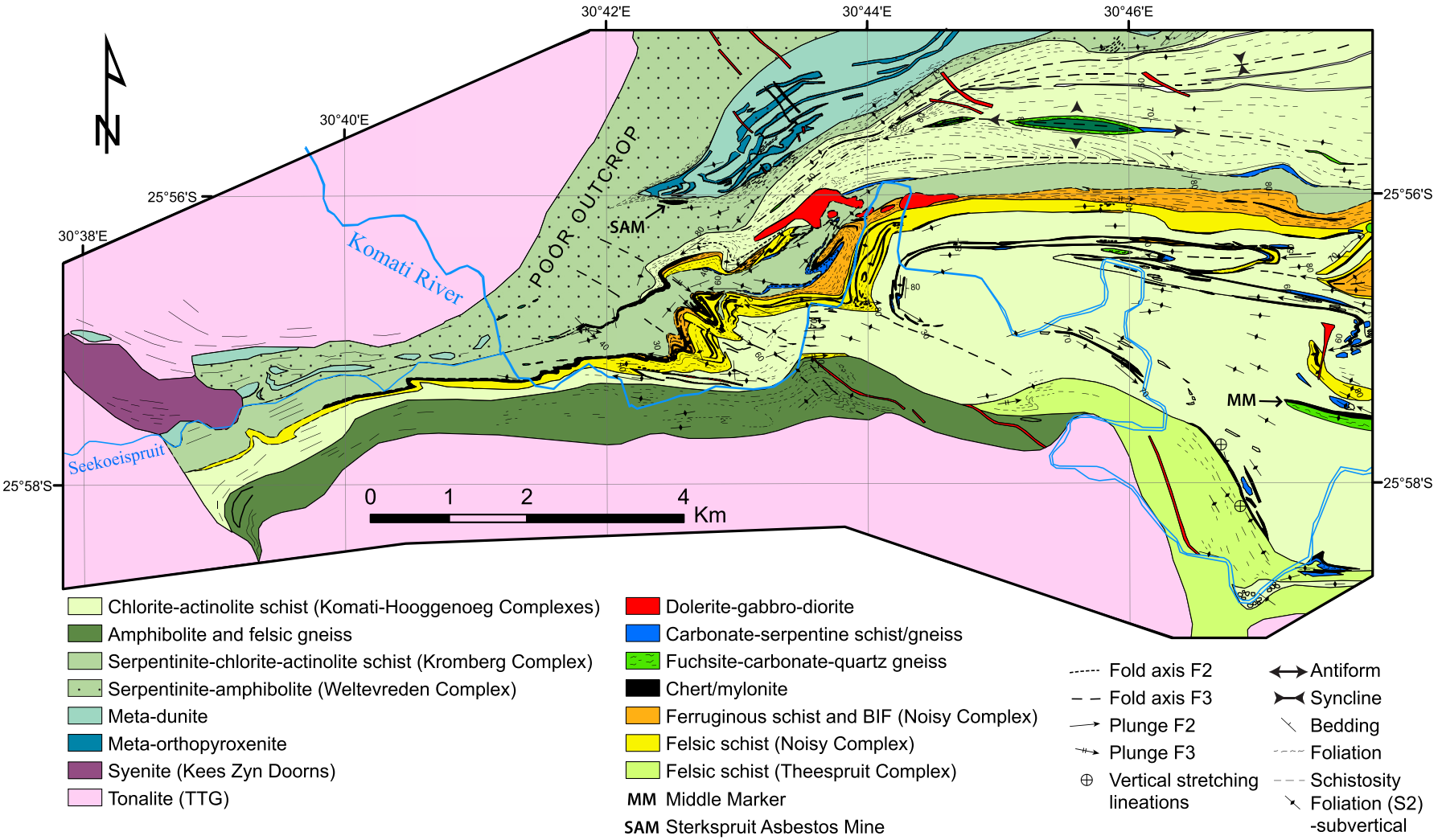

Figure 5. Geologic map of the Stolzburg Schist Belt (see inset Map 1 for location), within which all regional lithologies of the west-central Onverwacht Suite and the Fig Tree and Moodies Groups have merged and been intensely deformed, often isoclinally folded and refolded. Sections of the basaltic rocks in this area are chlorite-actinolite schists that have been shortened by more than 80%, as quantified by strain analyses of ocelli. The ca. 1800 m total thickness of the subvertical sequence to the west of the Komati River, where all the shear systems have merged, represents at least a near 90% decrease in thickness of the total stratigraphy Onverwacht Suite. It is likely that large sections of the original sequences were therefore tectonically dislocated through extensive thrusting and strike slip deformation (Map 2; and see text). A High Resolution magnetic survey further suggests the origin for this reduction is related to accretion-wedge dislocations. Modified from unpublished maps of M.J. de Wit; merged in the west to a simplified map modified from Kisters et al. (2003, 2010).

along the entire length of the Manhaar-Msauli fault (Map 1). Occasional spinifex zones occur in the Msauli area.

Along the southeastern margin of the Malalotsha Domain, Lamb (1984a, b, 1987; Map 1 inset) was the first to definitively show that Moodies-like siliciclastics were deposited during major fold and thrust processes. Farther inland to the NW, Paris (1984, 1987; Map 1 inset) recorded similar data showing major folding and thrusting during the deposition of the Moodies siliciclastics derived from the east. In the SE, Lamb (1984a, b) further confirmed that the central part of the Malalotsha synform (Map 2) comprises a unit of ultramafic-mafic sequences, with local disrupted cherts, up to 1 km thick (now chlorite-talc-serpentinites with a sub-horizontal schistosity) that tectonically overlie the Moodies-Fig Tree Groups. Although no age has been assigned to this mafic-ultramafic sheet, it is generally assumed to be part of the older Onverwacht Suite. We have assigned a slightly darker green color to this Malalotsha allochthon to reflect this uncertainty (Map 1). This large tectonic thrust-nappe was emplaced towards the west to northwest (Map 2), with horizontal movement exceeding 10 km (Lamb, 1984a, b, 1987). Gravity data is consistent with an average tectonostratigraphic thickness across this domain in the order of 3 km (Barton, 1982).

3. Bed rock lithologies (Map 1)

Map 1 documents all lithologies mapped across the area without any undue interpretations but mindful of the fact that bedrock outcrop is relatively poor. The map, built on a preliminary map at 1: 25,000 published 34 years ago (de Wit, 1983), represents a compilation of fieldwork as part of a long-term project since then by the authors and a number of MSc, PhD and postdoctoral researchers as well as collaborators from Utrecht University in the Netherlands (S. de Vries and W. Nijman), across various sectors of the region at a range of scales between 1: 500 and 1:10,000 (see inset). Some individual maps have been published elsewhere (de Wit, 1982; de Wit et al., 1983, 2011; De Ronde and de Wit, 1994; De Ronde et al., 1994; Dann, 2000; De Ronde and Kamo, 2000; Nijman and de Vries, 2009), or are available in theses (Lamb, 1984a, b; Paris, 1984; De Ronde et al., 1991; de Vries, 2004; MacLennan, 2012). Others are available in AEON's archives (T. Davies; V. King), and in particular a detailed map of C. E. J. De Ronde across a large area of the north part of the map covering the Weltevreden-Kromberg-Mendon Complexes (see inset), completed during a postdoctoral research period (1992–1995) from which only small parts are published (De Ronde et al., 1991, 1994; de Ronde and Kamo, 2000).

Most of the igneous rock complexes below the sedimentary Fig Tree and Moodies Groups are presently in a subvertical position and in places are downward facing (e.g., just north of the Dalmein Pluton, Map 2, Fig. 4; de Wit et al., 1987a; De Ronde and de Wit, 1994 - their Fig. 4). The Theespruit, Komati and Hooggenoeg Complexes on either side of the Dalmein Pluton are generally assumed to be the same, although there is no clear field evidence to support or refute this. For this reason the Komati and Hooggenoeg Complexes on Map 1 are depicted in different colors (blueish versus greenish) on either side of this pluton. Recent dating of rocks in the Theespruit Complex on both sides of the Dalmein Pluton (Van Kranendonk et al., 2009; Kröner et al., 2013, 2016) have yielded a similar range of ages (3530–3552 Ma) from volcaniclastic schists and are therefore shown in similar yellowish colors, despite the fact that there are conflicting interpretations of the geology, litho-tectonic stratigraphy and potential age range within this complex (de Wit et al., 1983, 1987a, b; de Wit et al., 2011; Cutts et al., 2014), which are further discussed below.

Ubiquitously, the mafic-ultramafic rocks of all complexes were metasomatised during early hydrothermal processes close to surface. In extreme cases pillow lavas and spinifex textured rocks are completely silicified over several km along strike and up to 20 m in thickness (Duchač and Hanor, 1987; de Wit et al., 1987a) These 'cherts' were generated during focussed silica-rich hydrothermal alteration (Hoffman et al., 1986; Hoffman et al., 1986, 2013; Paris et al., 1983; de Wit et al., 1987a, b; Duchač and Hanor, 1987; de Wit and Hart, 1994; De Ronde et al., 1994; Hofmann and Harris, 2008; Farber et al., 2016; de Wit and Furnes, 2016), in places clearly linked to white-smoker-like hydrothermal vents operating at ca. 200 °C, near and/or at the/a surface (de Wit and Furnes, 2016).

More regional metamorphic assemblages at amphibolite facies occur near the contacts of the greenstone belt with surrounding granitoids. The best studied examples are from the Theespruit Complex. Mafic assemblages in the lower Theespruit Complex, along the southern edge of the greenstone belt have peak local P/T conditions between 0.8 and 1.1 GPa (at temperatures of 650–700 °C), which are tectonically overlain by mafic sequences with metamorphic mineral assemblages that formed at 0.3–0.5 GPa and temperatures just below 500 °C (Dziggel et al., 2002; Diener et al., 2005; Van Kranendonk et al., 2009).

Regional assemblages reveal much lower metamorphic conditions across the overlying complexes within the greenstone belt. These range from sub-greenschist- to uppermost greenschist-facies conditions. Until recently the P–T conditions of these mafic-ultramafic rocks were only poorly quantified, based on traditional chlorite thermometry on mafic-ultramafic rocks of the Hooggenoeg and Kromberg Complexes. These yield temperature estimate of ca. 320 °C, interpreted to be due to burial metamorphism (Cloete, 1999).

The only modern P–T evaluations have been undertaken by Grosch et al. (2011, 2012). Their analyses of chlorite-actinolite-epidote-albite-quartz assemblages in massive and pillowed mafic units of the Kromberg Complex have yielded uppermost temperatures of around 450 °C at pressures close to 3 kbar. Based on surface and drill core samples along the Komati River, their analyses have also documented local inverted metamorphic profiles over vertical distance of about 1.5 km, from 390–450 °C at the top of the Kromberg and lower-most Mendon Complexes, to about 140–200 °C in the lower Kromberg Complex (see Map 2 for location of the drill sites, and Grosch et al., 2009 for details). This inverted metamorphic profile occurs across at least two shear zones and therefore likely reflects significant repetition across the Kromberg type-section by tectonic thrusting (Grosch et al., 2011).

Following the end of the 1st phase of deformation (D1), between ca. 3.45–3.43 Ga and possibly extended locally during back-thrusting at 3.3 Ga, 7–15 km of vertical exhumation of pillow lavas of the Komati and Hooggenoeg Complexes took place. Then, following the 2nd phase of deformation (D2) at about 3230 Ma, temperatures of all rock sequences around the edges of the greenstone belt and the old surrounding granitoids reached well below 300 °C by ca. 3140 Ma (Schoene et al., 2008, 2009).

Thereafter, the region was cut by a series of NW–SE dolerite-diorite dykes dated between 2.9 Ga and 2.8 Ga (U/Pb apatite; de Wit et al., 2011; Map 1), clearly defined also through magnetic surveys (Maré and Fourie, 2012). These are likely linked to the Usushwana complex in Swaziland (Inset Map 1).

4. General litho-tectonic stratigraphy and structure of the lower Onverwacht Suite

We have chosen to divide the original formations of the Onverwacht Suite of rocks into complexes. The reason is that each of these formations have complex stratigraphic and structural make ups, with at least 9 major shear zones, beyond that of simple formations (ss). We have provided details of this elsewhere (de Wit et al., 2011; Furnes et al., 2011). This is summarized in Figs. 3b and 4.

The oldest sequences, the Sandspruit and Theespruit Complexes are highly deformed and isoclinally folded, and at significantly

higher grades of metamorphism than the internal complexes (e.g., Stevens and Moyen, 2007, and references therein; Cutts et al., 2014). Estimated conditions during early deformation at 3.4 Ga are around 4 kbar at ca. 525 °C; and a later episode at 3.2 Ga, with local garnet-staurolite assemblages and rare kyanite megacrysts, at much higher pressures of 7–8 kbar but similar temperatures (560 °C). A monazite from the Theespruit Complex yielded an age of 3436 Ma, which has been interpreted as the early phase of metamorphism (Cutts et al., 2014).

The two complexes are parts of mafic-felsic schist belts that flank the SE margin of the Songimvelo Domain, herewith collectively referred to as the Theespruit Shear System (Fig. 2) that represents an oblique inclined section through an imbrication zone beneath the Komati/Theespruit shear systems (Map 2).

The type section near Tjakastad contains at least five imbricate tectonic slices each ca. 200 m or more in thickness, often with well-developed subvertical stretching lineation, which were rotated and flattened in bulk during a late schistosity forming event (de Wit et al., 1983, 1987b; Van Kranendonk et al., 2009), during which accretionary spheroids were significantly deformed into prolate ellipsoids (3:1:1). Adjacent TTG gneisses and linked sections of the Theespruit Complex have similar tectonic fabrics (e.g., Moyen et al., 2006, 2007; Schoene et al., 2008). Thus, the TTG cores (such as the Stolzburg and Theespruit) must at least in part have been in the solid state by 3.4 Ga (de Wit et al., 1983; Stevens and Moyen, 2007), as their zircon dates confirm (Schoene et al., 2008).

Previous interpretations suggested north directed thrusting of the Theespruit Complex (de Wit et al., 1987b), but this has been proved to be incorrect, except for local late back-thrusting (Map 2; Fig. 4).

Both Sandspruit and Theespruit Complexes comprise mafic-ultramafic amphibolites and felsic schists. In the case of the Sandspruit Complex the former dominate; whilst the felsic schists, together with tuffs, siliciclastic sandstones and mudstones, conglomerates, diamictites, cherts, accretionary lapilli and felsic volcanic breccias and agglomerates dominate the Theespruit Complex (de Wit et al., 1983; de Wit et al., 2011). The mafic rocks locally still display excellent pillow structures, which in places have been stretched into near vertical dipping ellipses of garnet amphibolites.

The Theespruit Complex has been dated between 3531 Ma and 3521 Ma, with detrital zircons dating back as far as 3552 Ma (Kröner et al., 2016). The tectonically lower Sandspruit Complex has been dated between 3521 Ma and 3531 Ma, and may be younger therefore than the Theespruit Complex (Dziggel et al., 2006). However, earlier analyses of detrital zircon from a felsic volcaniclastic horizon in the Theespruit sequence yielded ages as young as 3453 Ma and as old as 3531 Ma, and igneous zircons from a structurally lower deformed tonalite gneiss wedge dated at 3538 Ma (Fig. 3b; Armstrong et al., 1990). This would confirm the general stratigraphy of the lower Onverwacht Suite as originally suggested by Viljoen and Viljoen (1969a, b), and indicate that the Komati and Hooggenoeg Complexes were tectonically emplaced southwards across the Theespruit Complex. Van Kranendonk et al. (2009) did not accept the younger zircon dates in the Theespruit Complex to represent detrital material, and prefer to interpret the age of the Theespruit Complex to be much older. Robust lithostratigraphic chronology in the Theespruit and Sandspruit Complexes flanking the southern Songimvelo Domain is therefore missing and the contact between these two lowest complexes whilst not exposed, is likely tectonic. A lot more detailed mapping and drilling will be needed to resolve these issues beyond present rhetoric.

These major south facing imbricated thrust systems were subsequently later reworked as extensional shears, which are especially well-preserved flanking the northern margin of the Steynsdorp TTG gneiss dome (e.g., Kisters and Anhaeusser, 1995; Kisters et al., 2003; Schoene et al., 2008).

5. Faults and folds (Map 2)

Map 2 consolidates general structural data collected with a focus on fault and fold systems. Most of the NE–SW folds and faults are related to the D2 deformation dated between 3227 Ma and 3229 Ma, although the total range of this event has only been reliably dated across the Weltevreden and the northern sector of the Songimvelo Domains (De Ronde and de Wit, 1994). The age of the earlier D1 deformation remains controversial. The main evidence for this are from local pre D2 overturned sequences (Map 2). In addition large scale extensional deformation along regional listric normal faults across the Noisy Complex has been documented (Nijman and de Vries, 2009; de Vries et al., 2010). In the lower part of the complex these are linked and merge with a number of D0/D1 shear systems, including sub-horizontal extensional shears along the top of the Hooggenoeg Complex, and farther down often flanking the lower parts of the Hooggenoeg Complex chert layers (Map 2; de Vries et al., 2010). Similar normal faults occur in the Komati Complex (Dann, 2000), which likely are rooted in the major Komati-Theespruit Shear Zone (Figs. 2 and 3b). All these zones, including the thrusts and normal faults in the Theespruit Complex (and here called the Theespruit Shear System; Map 2; Fig. 2), bend to merge just to the west of the Dalmein pluton with NE striking D2 thrusts and shear zones. These E–W tectonic zones therefore predate D2 and are here marked as D1 structures.

Early D1 (or D0) structures are common throughout the Onverwacht Suite, best preserved where subvertical and steeply overturned cherts with linked fuchsite-gneiss zones were eroded and now unconformably overlain by sedimentary sequences of the Fig Tree and Moodies Groups that were sub-horizontal before D2. Some of the best preserved examples were mapped in great detail by Paris (1984, 1987) in the areas surrounding the Sigadeni, Waterfall and Xecacatu synclines/forms where the Onverwacht Suite represents undifferentiated Hooggenoeg, Kromberg and Mendon Complexes (Maps 1 and 2). Farther south, similar subvertical cherts and gneisses are folded and refolded both north and south of the Ekulindini and Steynsdorp Folds (Map 2; Fig. 3b).

The complex gneiss zones comprise intermingled and multi-generation extensional quartz-carbonate veins with whisks of schistose chlorite-fuchsite that have been interpreted as early brittle extensional phases and episodic ductile shear zones. These sequences are commonplace throughout the Onverwacht Suite, often flanking the lower margins of cherts, including the Middle Marker in the Hooggenoeg Complex (Fig. 29a, b). At least four such zones are tectonically repeated by D2 folding and/or thrusting, in the Kromberg and Mendon Complexes along northern sector of the Songimvelo Domain (Map 1, Fig. 3b; de Wit, 1983; de Wit et al., 1987a, b; Duchač and Hanor, 1987; De Ronde et al., 1994). Similar zones are also reported in the Weltevreden and Malalotsha Domains (Lamb, 1984a, b; Paris, 1984, 1987; De Ronde and Kamo, 2000).

Along the Komati River a similar well-exposed gneiss zone (named KSM by Grosch et al., 2011; and the Ekulindini thrust by de Wit et al., 2011) separates the Kromberg Complex from an overlying section of the Mendon Complex (as defined by Lowe and Byerly, 2007). This ca. 150 m thick gneiss zone records two metamorphic events at pressures of just less than 3 kbar, and temperatures of 390–450 °C and 240–350 °C, respectively (Grosch et al., 2011). These P–T conditions recorded in the highly altered mafic-ultramafic rocks of the Ekulindini zone do not support previous interpretations that the gneiss zones are low-temperature chemical

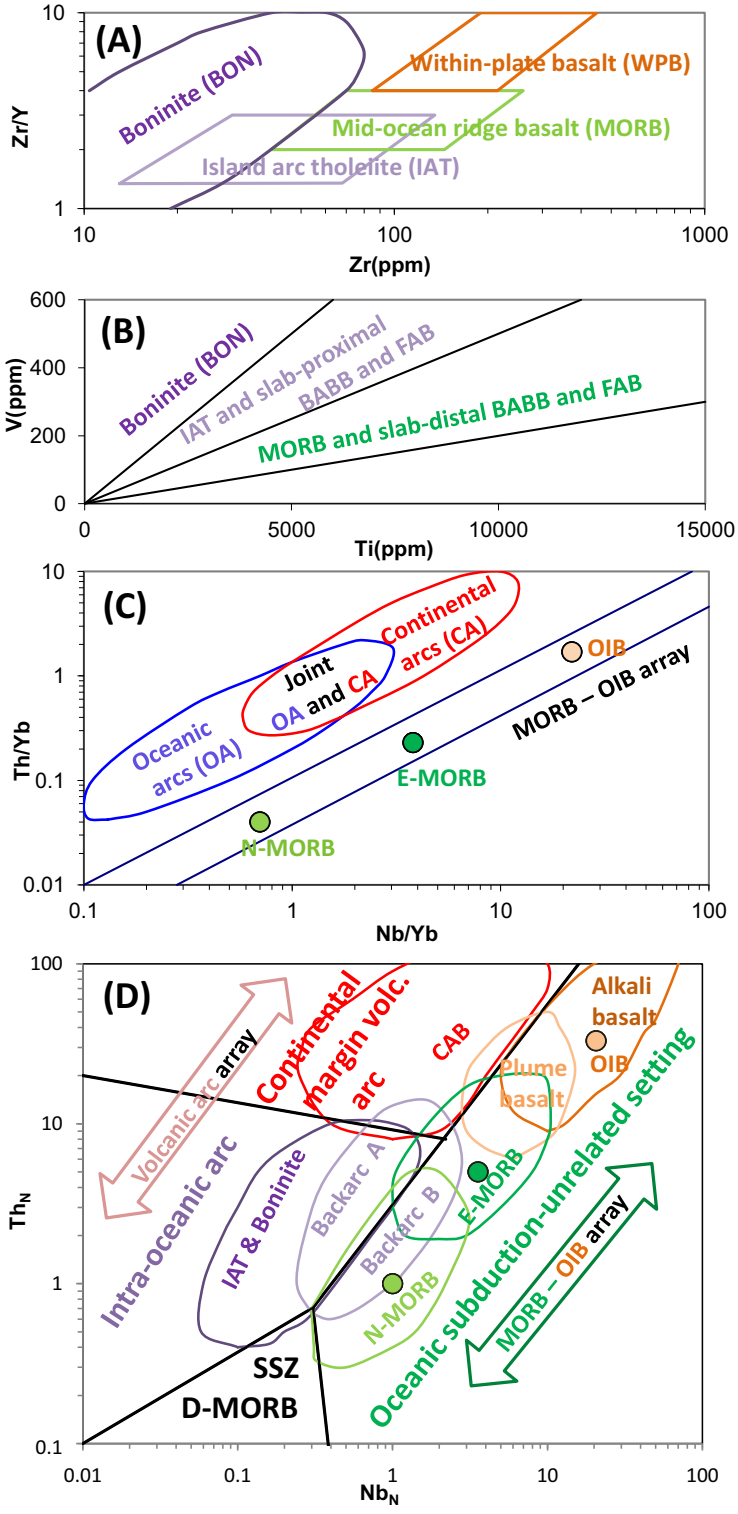

Figure 6. Templates for Zr/Y–Zr (A), V–Ti (B), Th/Yb–Nb/Yb (C), and Th_N–Nb_N (D) discrimination diagrams. The diagrams are after Pearce and Norry (1979) (diagram A); Shervais (1982) (diagram B), modified by Pearce (2008, 2014) (diagram C), modified by Pearce (2014), and Saccani, 2015 (diagram D). The boninite field in (A) has been inserted by Furnes et al. (2013). The Th and Nb values in diagram D are normalized against N-MORB (0.12 ppm and 2.33 ppm, respectively; after Pearce and Parkinson, 1993).

weathering products of komatiite or low-temperature alteration of volcanic tuffs (Viljoen and Viljoen, 1969a, b; Lowe and Byerly, 1986; and references therein), but rather linked to high temperature hydrothermal systems rooted down to 9–10 km deep below surface, and expressed at surface as white smokers at temperatures of 60–200 °C (de Wit and Furnes, 2016; and references therein), and within the complexes between 300 and 400 °C (Hoffman, 1985; Hoffman et al., 1986).

In addition, the deformation is expressed as schist-mylonite zones in underlying gabbros and pyroxenites of the Kromberg Complex (de Wit et al., 2011; Grosch et al., 2011). The Ekulindini zone is refolded and overturned by the Kromberg antiform (Map 2) and therefore

predates D2. It is likely to have been affected by early north-directed back-thrusting related to the early deformation sequences of the Songimvelo Domain. This fold and thrust deformation occurred during the deposition/emplacement of the felsic volcanics-intrusives and related conglomerates of the Noisy Complex around 3450–3433 Ma (Map 2) during tectonic uplift of the deep water mafic-ultramafic complexes (Map 1; Figs. 3b and 27; de Wit et al., 2011).

5.1. Onverwacht Bend

Traditionally the large scale change in the strike of the lower Onverwacht system along a north-west striking axis across the central part of the maps has been referred to as the Onverwacht anticline (Viljoen and Viljoen, 1969a, b). Structural mapping along its axis shows the fold to be plunging subvertical, albeit with local variations, including steep plunges both to the NW and SE, justifying renaming of this late tectonic structure as the Onverwacht Bend (de Wit, 1983; De Ronde and de Wit, 1994; de Wit et al., 2011), but which has not generally been inculcated in the subsequent literature. Structural mapping across this bend has revealed a complicated system of shear zones and variably trending fold-axis at different locations along the Onverwacht Bend axis (Map 2). Towards the southeastern margin, early fault systems of the Theespruit, Komati and Hooggenoeg Complexes merge and are affected by significant tectonic shortening, as quantified by a strong schistosity and highly deformed ocelli recording >80% shortening. Here, pillow lavas of the Komati Complex face west and are overturned. On Map 2 these convergent zones are shown as D2 structures (folds and fault systems; purple and blue, respectively) that are linked to northwest-southeast shortening across the western sectors of the region.

In the central part of the Onverwacht Bend, flanking the margin between Komati and Hooggenoeg sequences, a number of subvertical plunging fold axes within the Hooggenoeg Complex merge with faults that extend farther north across the Noisy Complex into a SW-younging system of Moodies sandstones and conglomerates that unconformably overly Kromberg/Mendon mafic-ultramafic rocks, cherts and Fig Tree like shales. Here the Moodies rocks are flanked by the SW plunging Sigadeni synform and related shear systems that represent the frontal thrust zone of the Malalotsha Domain situated to the east of the Manhaar-Msauli Shear System (Paris, 1984, 1987).

Clearly the Onverwacht 'Bend' has a long tectonic history that is still poorly understood. There is a great need to unravel the geology in this area further (rugged terrain between 700 and 1900 m.a.s.l and accessible only by foot) because it will enable a reliable connectivity to be unraveled between the rocks of the Noisy, Kromberg and Mendon Complexes in the north and east sectors of these complexes, which is presently not possible. It is for that very reason that the mafic-ultramafic (mostly serpentinite) rocks and cherts in the northeast section of the map as far as Emlembe (as mapped by Paris, 1984; Map 1) have been left as steeply dipping undifferentiated 'Onverwacht' rocks that were folded and in their near vertical position before being unconformably overlain by both marine FTG and alluvial MG (Map 1 and Fig. 4). 75% of the Onverwacht rocks in this area are affected by silicification. It is here that deep-water hydrothermal activity linked to hydrothermal vents was first documented to explain the origin of silicified deep water Onverwacht tuffs and pillows, which are underlain by early tectonic shear zones in the form of fuchsite gneisses (Map 1; Paris et al., 1983; Paris, 1984).

There is no geochemical data available from this area to provide potential distinctions and correlations to the East-West striking 'equivalents' that comprise the northern sector of the Kromberg and Mendon Complexes as mapped by C.E.J. De Ronde (De Ronde et al., 1994; De Ronde and Kamo, 2000; see Map 1 for locations); by Lowe and Byerly (1999, 2007, and references therein); and by Lowe et al. (2012). Nor is there any modern geochemical data to enable comparisons between mafic-ultramafic rocks here and to those of the Malalotsha Domain, west of the Manhaar-Msauli Shear

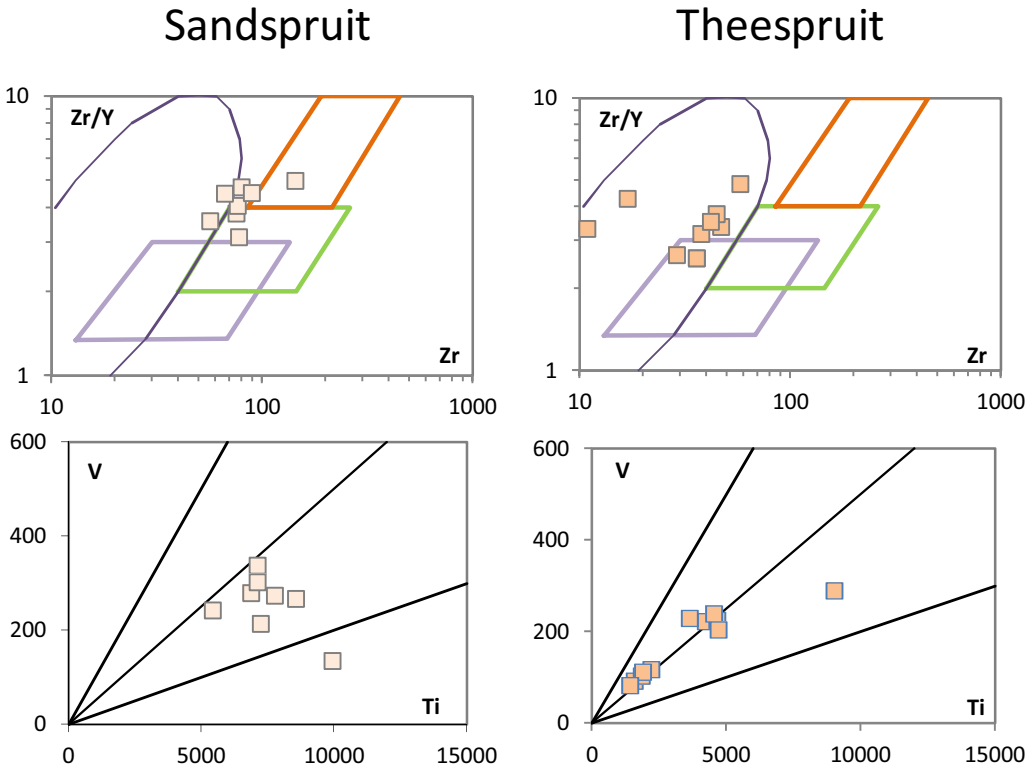

Figure 7. Zr/Y–Zr and V–Ti discrimination diagrams for the basaltic rocks of the Sandspruit and Theespruit Complexes. Date sources: see text.

System, along which large boudins of serpentinized ultramafic complexes similar to those flanking the Weltevreden Domain, are well preserved (Map 2).

In the central part of the Malalotsha Domain at least 9 tectonic units, separated by discrete planar zones of sheared and in parts silicified talcose-serpetinite schists that cut across upward younging sedimentary horizons, mark the repetition of similar subhorizontal sedimentary sequences. Movement of these slides is estimated to exceed 1 km as each unit covers an area of several kilometres of the unit below. The highest mafic-ultramafic unit covers lower units for 10 km in two orthogonal directions and movement on its lower bounding fault/shear exceeds 20 km (Lamb, 1984b). The entire tectonic package, including the early subhorizontal schistosity is refolded by the D2 Malalotsha synform and related thrusts with transport directions to the N and NW (Map 2; Lamb, 1984a, b).

6. Geochemistry of the rocks of the Onverwacht Suite and surrounding granitoids

In the this section we present general geochemical descriptions of the whole range of rocks from the oldest komatiite and basalt lavas of the Onverwacht Suite (OS) to the youngest granitic batholiths flanking the MMts, representing a time interval around 500 million years. The main focus is on the rocks of the OS. Each of the complexes has been comprehensively dealt with in the literature with respect to field geology, geochemistry and petrology as referred to below. We focus predominantly on the tectonic environments in which the various rock complexes formed.

6.1. The mafic-ultramafic volcanic/subvolcanic rocks of the Onverwacht Suite

Since the classical work of Viljoen and Viljoen (1969a, b) on the Barberton Greenstone Belt (BGB) the petrography and geochemistry of the intrusive and extrusive rocks of the Onverwacht Suite (OS) have been the focus of numerous publications, particularly the upper part comprising the Komati, Hooggenoeg, Kromberg, and Mendon Complexes (e.g., Jahn et al., 1982; Lahaye et al., 1995; Byerly, 1999; Chavagnac, 2004; Parman et al., 2004; Furnes et al., 2012, 2013). Different models related to the magmatic origin and tectonic setting of the lavas and intrusions of the OS, in particular the basic rocks, have been proposed as further discussed below.

Comprehensive petrographic descriptions and geochemical characterization of the basic lavas as well as some of the intrusive rocks of OS have been presented in Furnes et al. (2012, 2013). Here, only the general results are presented, starting from the oldest rocks (i.e., the Sandspruit Complex, Map 1; see de Wit et al., 2011).

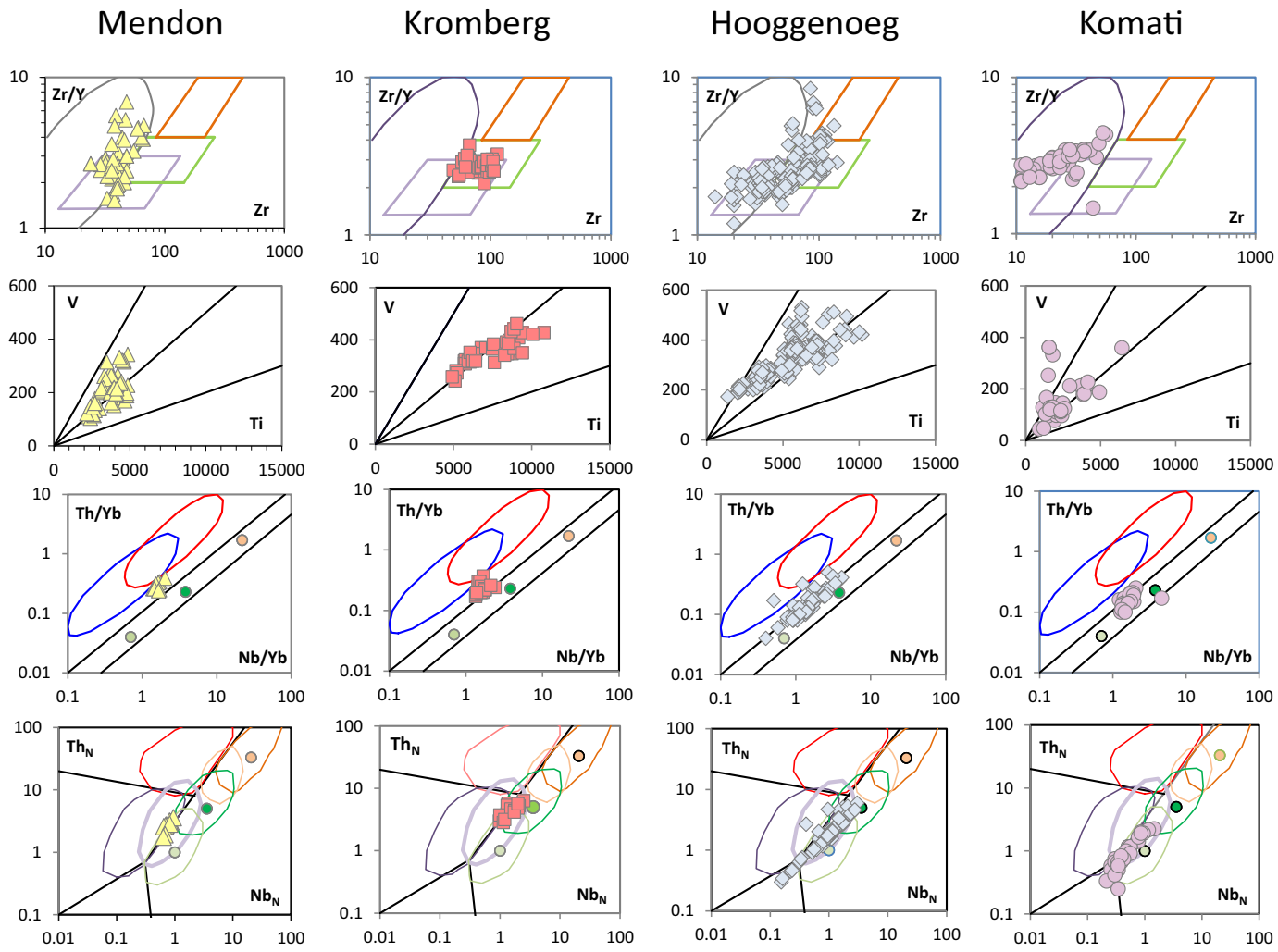

Figure 8. Zr/Y–Zr, V–Ti, Th/Yb–Nb/Yb, Th_N–Nb_N discrimination diagrams for the Mendon, Hooggenoeg, Kromberg and Komati Complexes. Date sources: see text.

For more detailed description and illustrations of the geochemistry of the basic rocks of OS, we direct the reader to the two papers by Furnes et al. (2012, 2013).

The basaltic samples of the Sandspruit and Theespruit Complexes are subalkaline and straddle the field between calc-alkaline and tholeiitic character (see SiO_2 vs Zr/Ti and Zr vs Y relationships, respectively in Fig. 6 of Furnes et al. (2013); Ross and Bedard (2009)). The komatiites to basaltic samples of the Komati Complex are predominantly subalkaline, and transitional between tholeiitic and calc-alkaline rocks. The lavas of the Hooggenoeg Complex are mainly subalkaline basalts and a minor part basaltic andesite; the majority is tholeiite, with a subordinate part of transitional character. The lavas of the Kromberg Complex, like those of the Hooggenoeg Complex, are mainly subalkaline basalts with minor basaltic andesites, and they all plot along the boundary between tholeiite and transition type rocks. The compositional range from komatiites to basalts of the Mendon Complex is more or less identical to those of the Komati Complex mentioned above.

The chondrite-normalized REE patterns of the samples of the Komati, Hooggenoeg, Kromberg and Mendon Complexes are mainly flat to slightly enriched in the LREE, and their MORB-normalized multi-element patterns show weak to significant negative Ta and Nb values, and are generally enriched in Ba and Cs (see Figs. 8 and 9 of Furnes et al. (2013), respectively). Robin-Popieul et al. (2012) also detected negative Nb anomalies (relative to La and Th) in Al-depleted komatiites from the Komati, Hooggenoeg, and Mendon Complexes, and attributed this feature to crustal contamination.

The Weltevreden Domain, to the NW of the Moodies Shear System, is dominated by komatiitic basalt sheet flows, minor komatiites, basalts, mafic pyroclastic rocks, and chert beds (Lahaye et al., 1995; Anhaeusser, 2001; Kareem, 2005; Thompson Stiegler et al., 2012). The komatiites are described as massive or layered, of which the former (and the komatiitic basalts) defines flat REE patterns, and the latter display depleted REE pattern (Thompson Stiegler et al., 2012). A large ultramafic igneous intrusive complex and an associated gabbro sill are described separately in the literature (de Wit et al., 1987a, b; MacLennan, 2012).

The magmas were generated by variable degrees of partial melting at different depths and temperatures of metasomatized mantle (Furnes et al., 2012). Tholeiitic basalts are produced over an interval of 5%–25% partial melting of mantle peridotites (e.g., McDonough et al., 1985), whereas komatiitic magmas are generated by 30%–50% of partial melting of mantle peridotites (e.g., Arndt, 2003; Maier et al., 2003). Further, Lu–Hf isotope studies of the OS komatiites and basalts also indicate formation by different degrees of partial melting, but from a common mantle source (Yamaguchi et al., 2015).

6.1.1. *Tectonic environment of the mafic-ultramafic rocks*

Since the mid-1970s a large number of geochemical discriminatory diagrams of basaltic rocks have been employed in order to give information about the tectonic environment in which they were generated. However, in altered and metamorphosed rocks not all employed elements represent the true concentration of the fresh parental rock; hence we have made a selection of diagrams constructed on elements that are immobile (or nearly so) during alteration and metamorphism.

The behaviour of major and trace elements during low-temperature alteration and low to medium grade metamorphism of oceanic rocks (mainly mafic rocks), is a highly complicated process that has been evaluated in many studies. In general the alteration process is affected and controlled by factors such as the composition and stability of the mineral phases in unaltered protoliths and in the alteration products. Further, the compositions, temperatures and volumes of fluid phases circulating through the lithospheric system also play a major role in element mobility. A general consensus is that Ti, Al, V, Y, Zr, Nb, REE (particularly HREE) and Th are relatively immobile (e.g., Staudigel and Hart, 1983; Seyfried et al., 1988; Hofmann and Wilson, 2007; Furnes et al., 2012). Seven of these elements (Ti, V, Zr, Y, Nb, Th and Yb) have been employed for four discrimination diagrams in order to assign the basic rocks to a specific tectonic environment. These diagrams are: Zr/Y vs. Zr, V vs. Ti, Th/Yb vs. Nb/Yb and Th_N vs. Nb_N, and their templates are shown in Fig. 6.

Before presenting the data, it is pertinent in this case to mention that some authors have questioned the use of discriminant diagrams for Archean rocks (e.g., Condie, 2015; Saccani, 2015). The reluctance of using discriminant diagrams (based on the geochemistry of modern basalts) for Archean basic rocks is based on the argument that the Archean mantle differed significantly

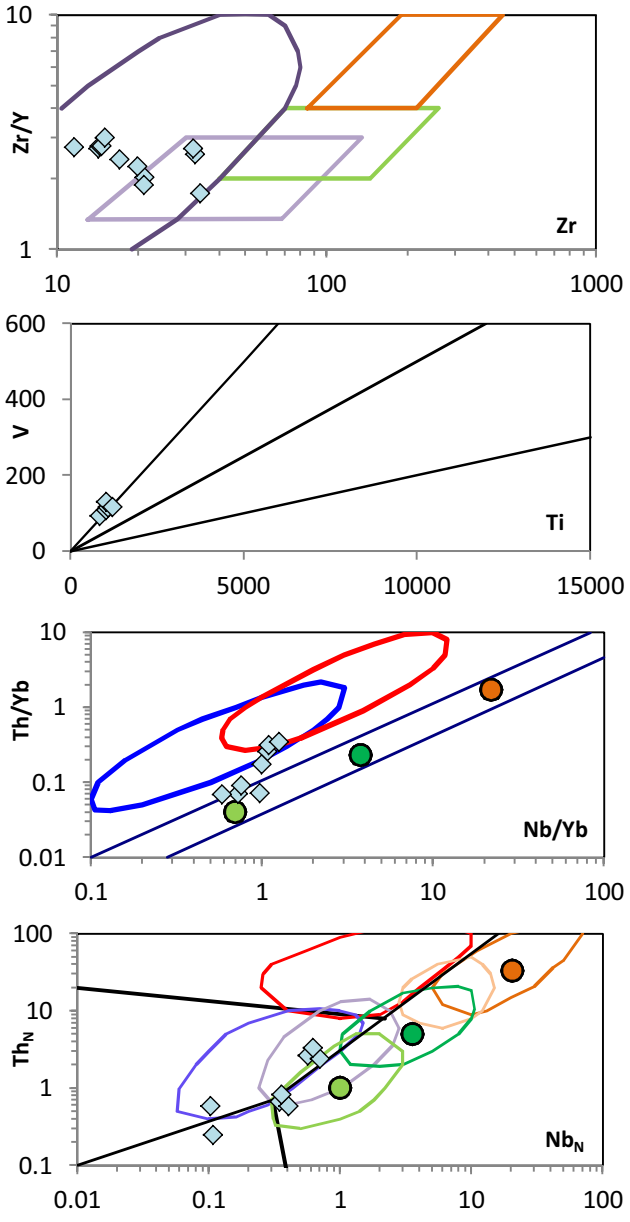

Figure 9. Zr/Y–Zr, V–Ti, Th/Yb–Nb/Yb, Th_N–Nb_N discrimination diagrams for the Weltevreden Complex. The geochemical data are from Lahaye et al. (1995), Kareem (2005), and Thompson Stiegler et al. (2012).

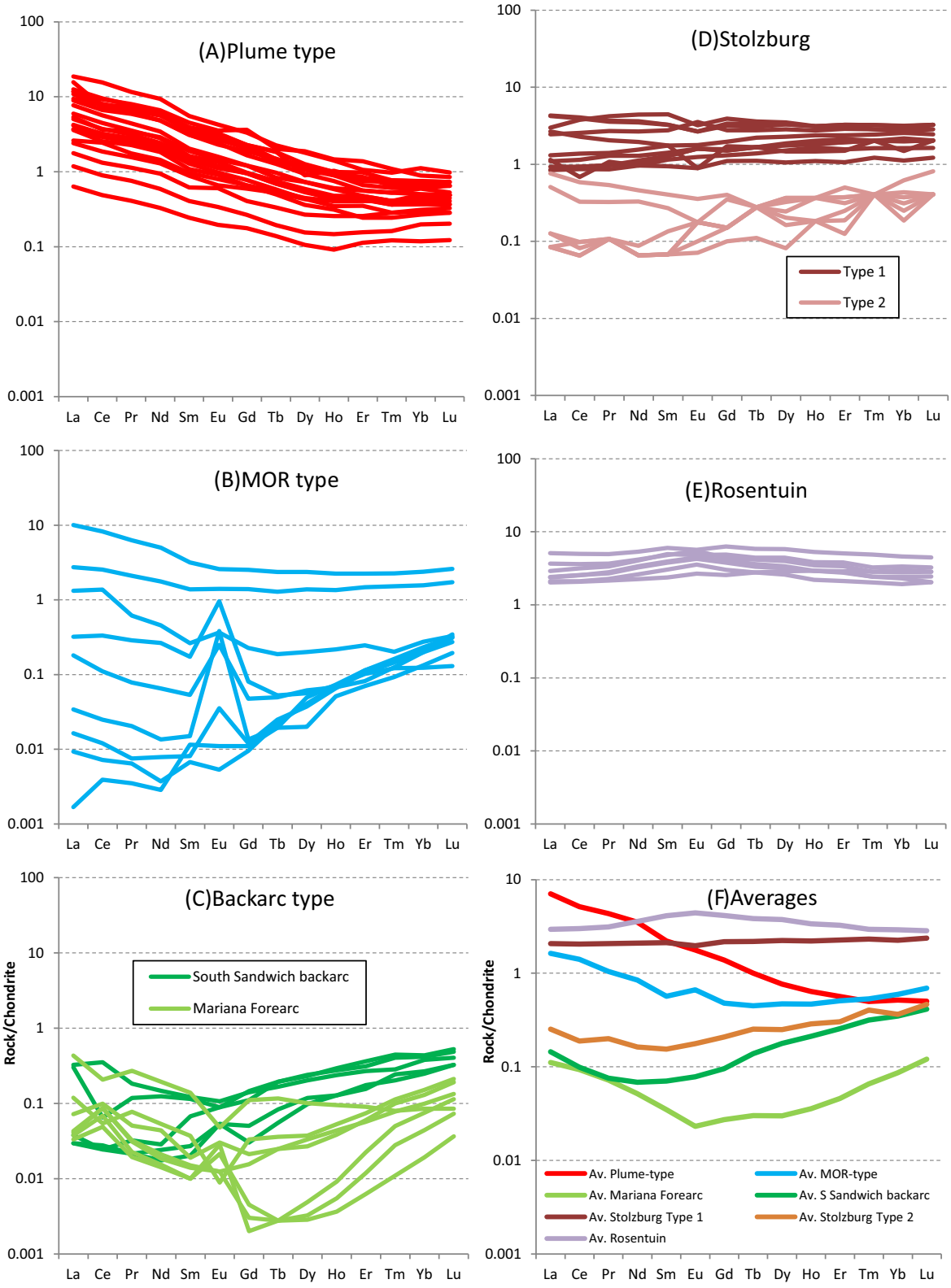

Figure 10. REE patterns of plume (A), MOR (B), and backarc (C) type ultramafic rocks from modern, magmatically active regions, compared with the REE patterns of ultramafic rocks of the Stolzburg Layered Ultramafic Body (D), Rosentuin ultramafic body (E), and averages of the various types (F). The Plume type represents harzburgites from Fuerteventure, Canary Islands (Neumann et al., 2015), the Mid-ocean ridge (MOR) type peridotites from the Atlantic Ocean (Paulick et al., 2006), and the backarc basin type harzburgites from South Sandwich Isl (Pearce et al., 2000), and the Mariana forearc (Savov et al., 2005). The geochemical data of the metaperidotites from the Stolzburg Layered Ultramafic body and the Rosentuin ultramafic body are from MacLennan (2012). Chondrite data are from Anders and Grevesse (1989). See text for further explanations and analyses.

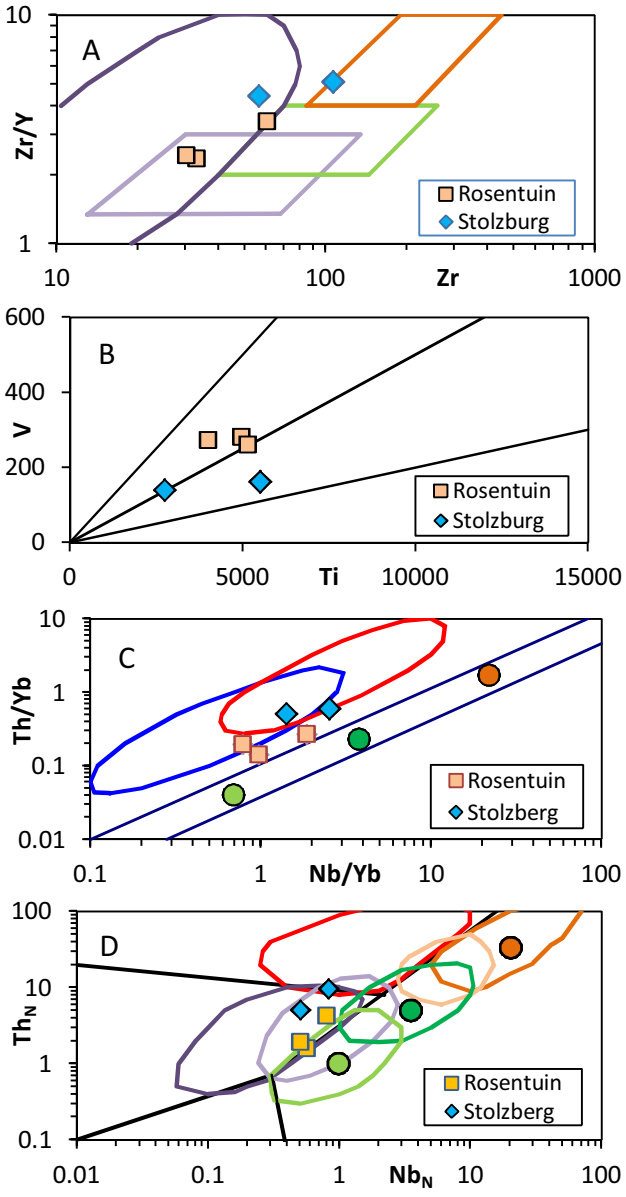

Figure 11. Zr/Y–Zr, V–Ti, Th/Yb–Nb/Yb, Th_N–Nb_N discrimination diagrams of metabasalts associated with the metaperidotites from the Stolzburg Layered Ultramafic body and the Rosentuin ultramafic body. The geochemical data are from MacLennan (2012).

from the post-Archean mantle (e.g., Griffin et al., 2003). However, if separation of the primordial mantle into crust (with high Th/Nb) and mantle (with lower Th/Nb) occurred in the Hadean, the Archean MORB-OIB array and the present-day MORB-OIB arrays would be similar (Pearce, 2008). There is evidence that significant geochemical differentiation of the primordial mantle occurred early in the Earth's history, even in the Hadean (Caro et al., 2006; Guitreau et al., 2013). It may therefore be justified to apply discrimination diagrams worked out on the basis of modern basaltic rocks from known tectonic regimes also for Archean rocks. Further, as pointed out in the literature (e.g., Vermeesch, 2006; Agrawal et al., 2008), individual tectonic discrimination diagrams may not be fully satisfactory to identify the tectonic regime, but become much more reliable when used in combination of several different types. On this basis we apply the discrimination diagrams shown on Fig. 6 to the basic rocks of the MMts.

For the Sandspruit and Theespruit Complexes the geochemical data base is very limited in terms of sample number and elements (Fig. 7), and only two of the four above-mentioned discrimination diagrams (Zr/Y–Zr and V–Ti) can be applied. The basalts of the Sandspruit Complex plot along the MORB/WPB/BON boundary (Zr/Y–Zr diagram) and in the MORB/slab distal field (V–Ti diagram). The basalts of the Theespruit Complex plot in the BON and IAT fields (Zr/Y–Zr diagram) and along the boundary between the IAT/slab proximal and MORB/slab distal fields (V–Ti diagram).

The komatiites and komatiitic basalts of the Komati Complex plot (Fig. 8) predominantly in the boninite field in the Zr/Y–Zr diagram, and the boninite and IAT fields in the V–Ti diagram. In the Th/Yb–Nb/Yb diagram the major part fall in the upper part of the MORB–OIB array and close to the OA field, and in the Th_N–Nb_N in the backarc B/N–MORB, indicating formation in a backarc basin. Recent research by Blichert-Toft et al. (2015) on Hf and Nd isotopes also indicate that deep-sea sediments (chert) provided part of the mantle source for some of the komatiites of the Komati Complex, thus providing independent evidence of Paleoarchean (or earlier) subduction.

The geochemical data of basaltic lavas (and a few associated dykes) of the Hooggenoeg Complex (Fig. 8) spread over the BON/IAT/MORB fields in the Zr/Y–Zr diagram, and plot in the IAT/slab-proximal field in the V–Ti diagram. In the Th/Yb–Nb/Yb diagram the majority fall in the upper part of the MORB–OIB array between N–MORB and E–MORB, and some samples plot within or close to the OA field. In the Th_N–Nb_N diagram the data define a spread from E–MORB to D–MORB, and the majority of the samples plot in backarc A+B/N–MORB. The combination of these diagrams would indicate formation in a backarc basin with subduction influence.

The basaltic lavas (and a few associated sills) of the Kromberg Complex plot in the MORB field of the Zr/Y–Zr diagram and in the V–Ti diagram along the boundary between the fields defined as IAT and MORB (Fig. 8). In the Th/Yb–Nb/Yb diagram the data plot between E–MORB and OA, and in the Th_N–Nb_N diagram in the joint area of the E–MORB and backarc A+B. The combination of these diagrams suggests formation in a backarc basin with subduction influence.

The komatiites and basaltic lavas and intrusions of the Mendon Complex plot predominantly in the BON and IAT fields for both the Zr/Y–Zr and V–Ti diagrams (Fig. 8). In the Th/Yb–Nb/Yb diagram all the samples plot above the MORB–OIB array, and close to the joint OA/CA field. In the Th_N–Nb_N diagram the data plot along the boundary between backarc A and B. The combinations of these diagrams indicate formation in a backarc basin with subduction influence.

The basaltic lavas from the Weltevreden Complex have been plotted in the discriminant diagrams, and show similar patterns as the other complexes of the OS (Fig. 9), i.e., they straddle the boundary between subduction-related and subduction-unrelated backarc environment.

Many models have been proposed for the tectonic environments in which the basic rocks of the MMts were formed. These vary from intracratonic volcanic activity with subsequent dome and keel formation (Van Kranendonk et al., 2009; Anhaeusser, 2010; Lana et al., 2010a, b; Van Kranendonk, 2011a, b), to formation as oceanic and/or continental plateaus (Kröner et al., 1996, 2016; Chavagnac, 2004; Van Kranendonk et al., 2015), to formation in backarc basins with associated subduction influence (de Wit et al., 1992; Parman et al., 1997, 2001, 2004; Grove and Parman, 2004; Parman and Grove, 2004a, b; Furnes et al., 2012, 2013). More recently, Grosch and Slama (2017) suggested that the magmatic rocks of the Kromberg Complex formed in a juvenile oceanic setting.

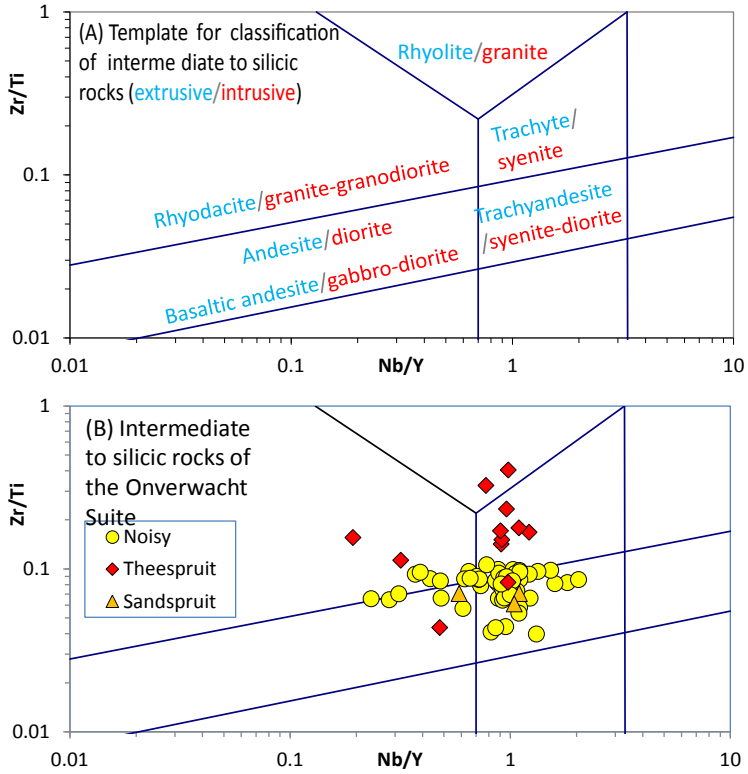

Figure 12. (A) Template for classification of intermediate to silicic rocks based in the Zr/Ti–Nb/Y relationships (after Floyd and Winchester, 1975; Winchester and Floyd, 1977). (B) Intermediate to silicic rocks of the Sandspruit, Theespruit and Noisy Complexes plotted in the Zr/Ti–Nb/Y diagram.

As a summary of the data presented in the four discrimination diagrams (Figs. 7–9), it should be stressed that much of the data plot at the boundary between the subduction-related and subduction-unrelated backarc setting, of which the latter category is also the field of juvenile ocean floor basalts. Thus we consider it most likely that all the complexes formed in backarc basins with zero to variable subduction influence.

6.1.2. Ultramafic intrusive rocks

The ultramafic rocks of the OS occur as a large number of variably sized bodies mainly within the Weltevreden Complex (de Ronde and de Wit, 1994), as well as within the Hooggenoeg Complex. Here we present geochemical data from two of these complexes, i.e., the Stolzburg Layered Ultramafic Complex (SLUC) within the Weltevreden Complex, and the Rosentuin Ultramafic body with the Hooggenoeg Complex (MacLennan, 2012), and compare these data with similar counterparts from plume, mid-ocean ridge, and backarc settings (Fig. 10A–C). As pointed out by MacLennan (2012), the SLUC comprises two types, a type 1 with flat REE patterns and a type 2 that defines REE patterns with progressive depletion from Lu through Gd, and from Gd to La slight to pronounced progressive enrichment (Fig. 10D). The Rosentuin ultramafics define the same pattern and REE concentrations as type 1 (of the SLUC; Fig. 10E). Fig. 10F shows the average patterns of Plume, MOR, and Backarc basin type of ultramafic rocks compared with those of the SLUC and Rosentuin. Type 2 is very similar to that of the South Sandwich backarc, whereas type 1 is more akin to the flat to slightly enriched MOR type. A few basalts are associated with the ultramafic rocks of the SLUC and Rosentuin, and in the discriminant diagrams these basalts plot within the subduction-related backarc environment (Fig. 11).

6.2. Intermediate to silicic rocks

Most of the geochemical data of the intermediate to silicic rocks are from the Noisy Complex (de Wit et al., 1987a, b; Louzada, 2003; Diergaardt, 2013). They consist of two varieties, i.e., (1) K_2O-rich and Na_2O-poor; and (2) K_2O-poor and Na_2O-rich, of which the former is the dominant type (Diergaardt, 2013).

6.2.1. Classification

We have plotted the intermediate to silicic rocks of the Sandspruit, Theespruit and Noisy Complexes in the Zr/Ti–Nb/Y classification diagram (Fig. 12). The samples of the Theespruit Complex show large variations and plot in the diorite, syenite-diorite, syenite, granite-granodiorite and granite fields, with the dominant part in the syenite field. Of the three analyzed samples of the Sandspruit Complex, two samples plot in the syenite-diorite field, and one sample in the diorite field. Most of the samples from the Noisy Complex plot in the syenite-diorite (trachyandesite) field, but some plot along the boundary between the diorite and granite-diorite (rhyodacite-andesite) fields.

6.2.2. Partial melting and fractional crystallization

Applying the experimental results of hydrous partial melting of cumulate gabbros (Koepke et al., 2004) and applying partition coefficients (D-values) from the literature, Brophy (2009) modeled the behavior of REEs and SiO_2 during melting and fractional crystallization of mid-ocean ridge basalt and gabbro. This modeling showed that hydrous melting (equilibrium and fractional) can yield melts with $SiO_2 > \sim 62$ wt.% with decreasing concentration of REE as SiO_2 values increase (particularly with high C_0), whereas during

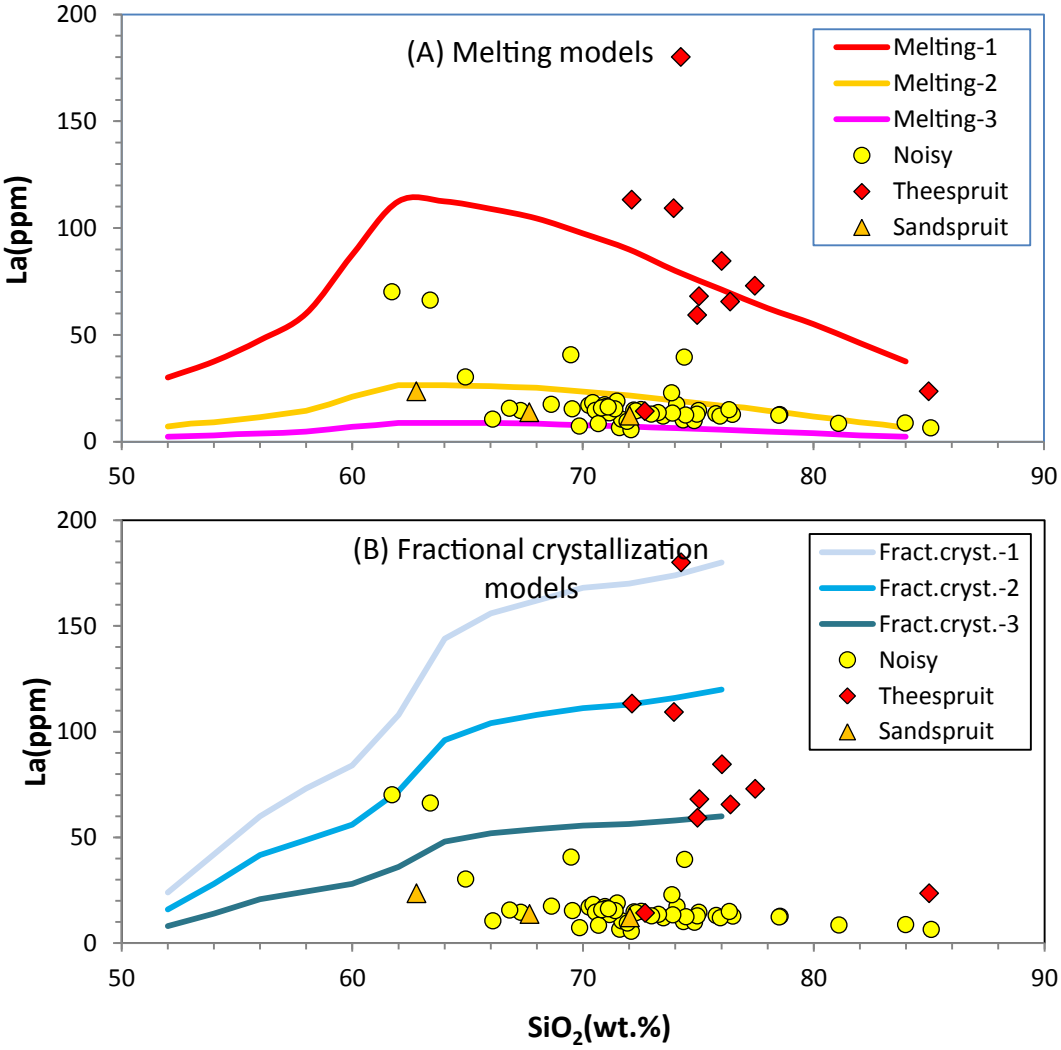

Figure 13. Modelled variations in the enrichment factor (C_l/C_0) for La with an increasing SiO_2 content during (A) batch melting, and (B) fractional crystallization (after Brophy, 2009), onto which the intermediate to silicic samples of the Sandspruit, Theespruit and Noisy Complexes have been plotted. For the melting models: Melting 1, 2 and 3: C_0 = 25, 6 and 2, respectively. For the fractional crystallization models: Fract.cryst. 1, 2 and 3: C_0 = 12, 8 and 4, respectively.

fractional crystallization of basaltic melt results in increasing concentrations of REE. We apply the results of the modeling of Brophy (2009) in an attempt to produce an *ad hoc* model of incompatible and compatible elements with progressive melting and fractional crystallization, using La and SiO_2 (Fig. 10). In modeling of trace-element enrichment with increasing SiO_2 we use C_l/C_0 (where C_0 = original concentration of La in a starting liquid, and C_l = concentration of La in the evolved liquid). The enrichment factor C_l/C_0 is dependent on relevant bulk distribution coefficients for partial melting and fractional crystallization. We have chosen the following initial values (C_0) for the melting and fractional crystallization models: 2, 6 and 25 for the melting models, and 4, 8 and 12 for the fractional crystallization models. For the melting model we use batch melting, and for the fractional crystallization model, we have chosen the experimental data produced under the QFM buffer conditions (see Fig. 6 of Brophy (2009)). The enrichment factors (C_l/C_0) as a function of increasing SiO_2 are shown in Fig. 13. The melting models are based on low pressure, hydrous melting (up to 6.5% H_2O) at temperatures of 900–1060 °C of mid-ocean ridge (MOR) cumulate gabbroic source.

The three samples of the Sandspruit Complex and most of the samples from the Noisy Complex are all very low in La, and get progressively lower as SiO_2 contents increase. This pattern is most compatible with partial melting of a parental source, similar to that of the model of Fig. 13A, with C_0 ranging between 2 and 6 ppm La. In general the trachyandesites/rhyodacites/andesites of the Noisy Complex are high in K_2O and Rb, and low in Na_2O, with averages of 4.8%, 94 ppm, and 1.9%, respectively (data from de Wit et al., 1987a, b; Louzada, 2003; Diergaardt, 2013). The study of Diergaardt (2013) concludes that the K_2O (and Rb) rich nature is a primary feature, and that biotite-bearing sediments may be the source. Alternatively, a highly depleted gabbroic/basaltic source, as shown by the melting models of Fig. 13A, together with K_2O-rich, biotite-bearing sediment (as proposed by Diergaardt (2013)), may account for the geochemical features of the majority of the Noisy rhyodacites/rhyolites. This way the high K_2O (Diergaardt, 2013), together with the low La-content shown in Fig. 13 can be explained.

The origin of the samples from the Theespruit Complex is more ambiguous. If produced by partial melting from a gabbroic/basaltic source, the initial La-concentration (C_0) would have to be on the

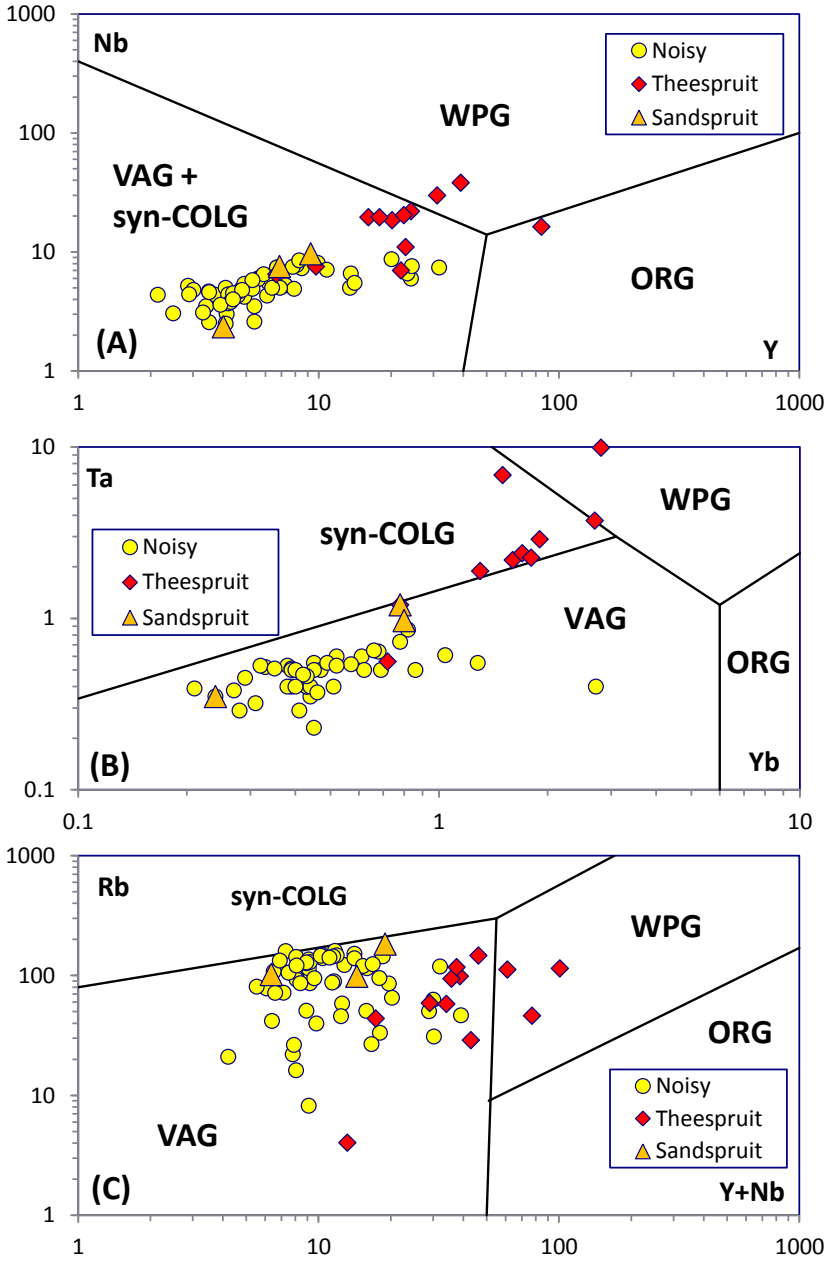

Figure 14. Geochemical data from the intermediate to silicic igneous rocks of the Sandspruit, Theespruit and Noisy Complexes plotted in the Nb–Y (A), Ta–Y (B) and Rb–(Y+Nb) (C) discrimination diagrams for granitoids (after Pearce, 1983; Pearce et al., 1984). ORG = ocean ridge granites, WPG = within-plate granites, VAG = volcanic arc granites, Syn-COLG = syn-collisional granites. Date sources: see text.

order of 25 ppm. Alternatively, most of the samples could also have been produced by fractional crystallization from a basaltic parent, with C_0 ranging between 4 and 8.

6.2.3. Tectonic environment

Fig. 14 shows the intermediate to silicic rocks of the Sandspruit, Theespruit and Noisy Complexes plotted in the Nb–Y, Ta–Yb and Rb–(Y+Nb) granitoid discrimination diagrams (Pearce et al., 1984). The rocks from all the three complexes plot in the joint field for volcanic arc granites (VAG) and syn-collisional granites (syn-COLG) (Fig. 14A). The majority of the rocks from the Theespruit Complex, however, differ from those of the two other above-mentioned complexes, and plot within or close to the field of within plate granites (WPG). The Ta–Yb diagram distinguished between VAG and syn-COLG, and in this diagram (Fig. 14B) the rocks of the Sandspruit and Noisy Complexes plot exclusively in the VAG field, whereas most of the rocks from the Theespruit Complex plot in the syn-COLG, close to the boundary of the VAG. Fig. 14C shows the rocks from the three above-mentioned complexes plotted in the Rb–(Y+Nb) diagram. We acknowledge that Rb is a highly mobile element; hence, in the Rb vs. Y+Nb diagram, some of the data may have been displaced from the VAG field into the Syn-COLG field by alteration. But, the distinction between the Theespruit and Noisy Complexes still remains.

The rock type adakite is geochemically characterized by high Sr and La, and low Y (thus high Sr/Y and La/Yb ratios), combined with

high SiO_2 (>56 wt.%), Al_2O_3(>15 wt.%) and Na_2O (>3 wt.%), and low high-field strength elements (for example Nb and Ta; see summary of the geochemistry of adakitic rocks in Table 1 of Castillo (2012)). This rock type may make up an important group of the intermediate to silicic rocks that are mainly restricted to subduction-related tectonic settings (e.g., Martin, 1999; Martin et al., 2005). Although adakites may form in different ways such as partial melting of the lower continental crust (e.g., Castillo, 2012; Ling et al., 2013), the melting of altered-hydrated metabasalts in a subducted slab, provides the best explanation for the generation of high-SiO_2 adakites (Moyen, 2009). Since the $(La/Yb)_N$ ratios in general are much higher in the lower continental crust than in the oceanic crust, Ling et al. (2013) also worked out a geochemical diagram to distinguish between adakites formed from the two different parental sources (Fig. 15).

Five of the samples of the Noisy Complex satisfy the geochemical criteria to be classified as adakite, and in Fig. 15 they are plotted in the Sr/Y–$(La/Yb)_N$ discrimination diagram. Two of the samples plot within the field of partial melt of subducted oceanic crust, whereas the other three samples plot at the boundary area between partial melts of subducted oceanic crust and lower crust.

The intermediate to silicic rocks of the Theespruit and Noisy Complexes have previously been attributed by Furnes et al. (2013) to a subduction-related island arc environment. New geochemical data from the Sandspruit Complex (Kröner et al., 2016) are similar to those of the Noisy Complex (Figs. 13 and 14), which would tentatively attribute the formation of this complex to an island arc setting. By contrast, based on Hf-in-zircon isotopic data, Kröner et al. (2016) suggested that the silicic rocks of the Sandspruit and Theespruit Complexes resulted from melting of a felsic continental basement, represented by the Ancient Gneiss Complex in Swaziland, and on this basis reject the possibility that these rocks were formed in a subduction-related environment. However, as an alternative interpretation, the isotopic signature as reported by Kröner et al. (2016) may represent contribution from older subducted clastic sediments, comparable to the present-day situation in which the Indonesian island arc magmas are influenced by the sediments from the old crustal rocks of the Australian margin (Vroon et al., 1995; Elburg and Foden, 1998). This is compatible with the abundance of siliciclastic and volcaniclastic rocks the Theespruit Complex (de Wit et al., 1983, 1987a, b; Armstrong et al., 1990; Van Kranendonk et al., 2009 and references therein), and with more recent detrital zircon analyses (Drabon et al., 2017).

From the renewed processing of the geochemical data from the Sandspruit and Noisy Complexes we suggest the following: (1) A certain proportion of the samples from the Noisy Complex are of adakitic character (Fig. 15), and to which we suggest formation by melting of a basaltic parent (that may be highly depleted in incompatible elements) in a subduction zone. (2) A dominant part of the Noisy Complex and the three analyses from the Sandspruit Complex are very low in La (+other incompatible elements) (Fig. 13), and can be modeled by partial melting of a source depleted in incompatible elements, as for example cumulate gabbros, and/or highly depleted basalts. This is by far the most common process responsible for the generation of intermediate to silicic rocks generation in backarc to forearc regions of any age (Furnes and Dilek, 2017). This process may occur along a subduction zone or at the base of backarc crust. When a melt lens solidifies (producing dikes + gabbro) and is hydrothermally altered, impingement of a younger melt lenses from below may result in the production of new intermediate to silicic melts, a process that may be repeated several times (Furnes and Dilek, 2017). Further, all discrimination diagrams (Fig. 11) indicate that the Sandspruit and Theespruit intermediate to silicic rocks are product of volcanic arc magmatism. The Theespruit samples show a large range in the content of incompatible elements (e.g., La), and some are pronouncedly different from those of the Sandspruit and Noisy Complexes (Fig. 13), which is also apparent from the discrimination diagrams (Fig. 14).

6.3. Granitoid rocks

6.3.1. The trondhjemite-tonalite-granodiorite (TTG) plutons

The TTG granitoids comprise two distinct age generations, i.e., approximately 3.5–3.4 Ga, and 3.3–3.2 Ga, and these are treated separately below. The petrography and geochemical data of these granitoids have been dealt with in a number of earlier works. The geochemical data used for the purpose of this compilation are from the following papers, i.e., the oldest group (Clemens et al., 2006), and the youngest group (Kleinhanns et al., 2003; Clemens et al., 2006; Moyen et al., 2007; Schoene and Bowring, 2010).

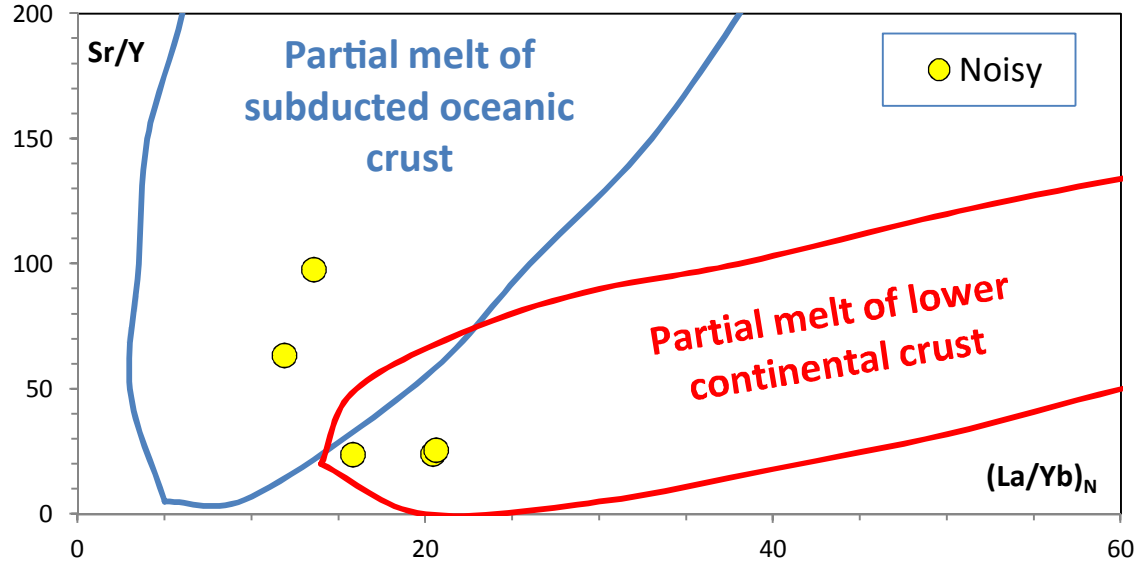

Figure 15. Sr/Y versus $(La/Yb)_N$ diagram for five samples from the Noisy Complex, discriminating adakites formed by partial melting of subducted oceanic crust and partial melting of lower continental crust. The $(La/Yb)_N$ ratios are chondrite-normalized values after Sun and McDonough (1989). The diagram is modified after Ling et al. (2013). Date sources: see text.

Fig. 16 shows the data from both age groups plotted in Sr/Y–Y diagrams that discriminate adakitic granitoids from the typical subduction-related calc-alkaline andesite-dacite-rhyolite (ADR) association. In subduction-related tectonic settings adakites make up an important group of the intermediate to silicic rocks, and are characterized by high Sr and low Y (hence high Sr/Y ratios), and high Al_2O_3, Na_2O, and low K_2O (e.g., Martin, 1999). We have applied a modified discrimination Sr/Y–Y diagram of Castillo (2006) and Naqvi et al. (2006), and taken the rocks with Sr/Y > 37 as adakites. For both age groups the majority of the rocks plot within the adakite field, but the youngest group displays a wider range than the oldest group in the Y-values (Fig. 16A and D), and exhibit a higher portion that plot in the ADR field. Further, all of the samples from both age groups that qualify as adakites on the basis of their Sr/Y ratios, plot in the high-SiO_2 adakite field (Fig. 16B and E). In the Ce/Sr–Y discriminant diagrams for different granitoids (TTGs and potassic granites), there is also a difference between the two age groups, shown by a wider range in the Ce/Sr values of the younger group (Fig. 16C and F). The geochemical data of the same rocks have also been plotted in the discriminant diagrams for granitoid rocks of Pearce et al. (1984), and for both age groups the vast majority plots in the volcanic arc granite (VAG) field (Fig. 17).

6.3.2. The granite batholiths/plutons

The geochemical data of the granites of the youngest magmatic generation (Kleinhanns et al., 2003; Yearron, 2003; Clemens et al., 2006, 2010) have been plotted in the Sr/Y–Y and Ce/Sr–Y discriminant diagrams (Fig. 18). For these granitoids the main part plots in the ADR field of the Sr/Y diagram. However, for some of the batholiths/plutons, i.e., the Heerenveen and Mpuluzi, the granites display large variations and plot in both the adakite and ADR fields (Fig. 18A). The large geochemical range is also shown by the Ce/Sr ratios (Fig. 18B). Fig. 19 shows the same rocks plotted in the Y–Nb and Rb–(Y+Nb) discriminant diagrams, and even though the majority plots in the VAG field, a high portion plot close to the VAG/WPG boundary.

6.3.3. Genetic considerations and tectonic environment

Based on Figs. 16–19, we discuss the genesis and tectonic environment in which the granitoid rocks were generated. Clemens et al. (2006) suggested that the most likely sources for TTG magmas are metabasaltic rocks, and that the different plutons represent separate magma batches. Moyen (2011) defined three TTG series using Sr/Y–Y, and Ce/Sr–Y relationships, and related the data distribution in these diagrams to the pressure under which the rocks were generated. Those with high Sr/Y and low Ce/Sr values were attributed to melting of garnet- and rutile-bearing sources (eclogite) under high pressure (20 kbar or higher), whereas those with low Sr/Y and high Ce/Sr ratios combined with high Y were ascribed to melting of amphibolite under pressure of 10–12 kbar, and with a medium-pressure series of 15 kbar with melting of garnet-amphibolite. The high- to medium-pressure granitoids plot in the adakite field, whereas the low-pressure examples plot in the ADR field (Fig. 16A and D).

Martin et al. (2005) divided adakites into high-SiO_2 and low-SiO_2 adakites (HSA and LSA, respectively), of which HSA represent slab-melts and LSA melts of peridotite previously metasomatized by slab-melt. Moyen (2009) further provided different pathways to explain the generation of HSA and LSA, in which slab melting yields the former, that can either be directly emplaced, or interact with the mantle peridotite toward its destination to form some member of the LSA. The majority of 3.5–3.3 Ga TTGs are thus HSA that can be attributed to generation under high- to medium-pressure conditions (Fig. 16), whereas the youngest granitoids (3.1–2.7 Ga) represent both adakites and ADR types (Fig. 17). The most remarkable example is provided by the granitoids of the Heerenveen Batholith (Fig. 17), for which Clemens et al. (2010) propose that the rocks with SiO_2 < 70 wt.% were generated from a source of intermediate to mafic igneous rocks having experienced different degree of K-metasomatism, whereas those with SiO_2 > 72 wt.% were generated from K-enriched intermediate to felsic sources.

Although there is a general consensus that the main source for TTGs is a mafic igneous rock, there is controversy regarding the tectonic environment is which the melting took place, i.e. subduction-related versus unrelated to plate boundaries. Strong advocates in favor of subduction-related environments include: Martin 1986, 1994; Rapp et al., 2003; Martin et al., 2005; Moyen, 2009, 2011; Moyen and Martin, 2012. Those in favor of a generation unrelated to plate tectonics are: Smithies, 2000; Bédard, 2006; Van Kranendonk et al., 2007; Willbold et al., 2009.

For the production of granitoid magmas from a basaltic parent, no matter what the tectonic environment, water is an essential component, and in most volcanic and plutonic examples the water content is between 2 wt.% and 4 wt.% (e.g., Whitney, 1988). In the case of the subduction-related model, the main sources of water come from the dehydration of hydrous silicates as well as volatile components transported into the crust from subducted oceanic crust. For the other, subduction-unrelated model, “the drip model”, the main responsible mechanism for granitoid magmas is partial melting in the lower portions of thick basalt accumulation, such as a plume-generated oceanic plateau (e.g., Bédard, 2006). In such cases the necessary water supply to produce granitoid melts is a problem, as circulation of water in such thick basalt accumulations is restricted to the uppermost parts of the pile (e.g., Arndt, 2013).

In the case of the granitoid rocks within and surrounding the MMts, all geological field and geochemical evidence point to the fact that they are generated in relation to a subduction-related environment. This is evidenced by their geochemical character as shown in Figs. 16–19, as also supported by Nd-isotope data of the Usutu granitoid rocks in Swaziland (Schoene and Bowring, 2010). Further, returning to the mafic lavas of the Onverwacht Suite, there is no evidence that any of these lavas can be regarded as plume-generated and thus could have been the source for the granitoid magmas by partial melting at the bottom of the basalt pile (or from detached drips), but instead represents subduction-related back-arc-generated magmas.

Thus, the entire magmatic complex of the MMts we relate to a plate-tectonic, backarc and arc tectonic environment.

6.4. Selected isotope signatures of granitoids

Sm–Nd and Lu–Hf isotopic data from granitoids and orthogneisses in the eastern Kaapvaal craton have been used to confirm the locations of lithospheric boundaries and to constrain the balance of crustal recycling versus mantle input to crustal growth, ca. 3.66–2.70 Ga. Whole rock Sm–Nd data (Fig. 20) show offsets in ε_{Nd} values for 3.2–3.3 Ga granitoids across the MMts that are consistent with accretion of ca. 3.3–3.23 Ga lithosphere north of the BGB onto pre-existing ca. 3.66 Ga lithosphere south of the BGB in Swaziland (Schoene et al., 2009). Larger datasets of U–Pb dates and Hf isotopic signatures from individual zircons separated from similar samples support this finding (Zeh et al., 2009, 2011). These data confirm a model where subduction-accretion and associated magmatism created new Archean lithosphere from depleted mantle-derived melts north of the BGB, whereas a mixture of re-melting of enriched crust and addition of new mantle derived melts contributed to crustal growth south of the BGB. After ca. 3.2 Ga, however, the Nd and Hf signatures of ca. 3.1

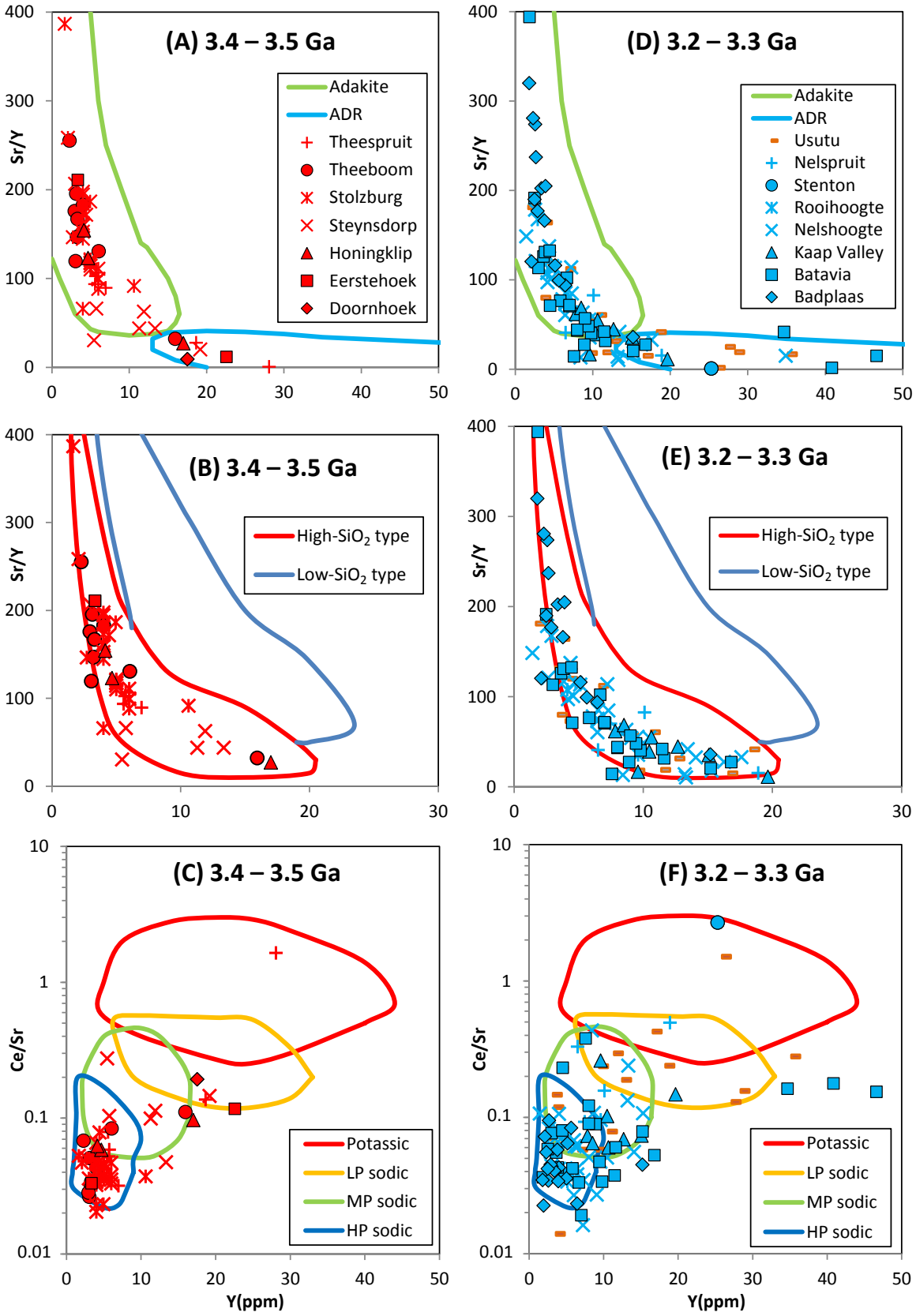

Figure 16. Granitoids of the 3.5–3.2 Ga TTGs plotted in Sr/Y–Y diagrams showing adakite and ADR (andesite, dacite, rhyolite) fields (A and D) (modified from Castillo, 2006; Naqvi et al., 2006). Diagrams B and E separating high-SiO_2 and low-SiO_2 are from Martin et al. (2005). Diagrams C and F (Ce/Sr–Y) show the fields defined by TTGs generated under high, medium and low pressures (HP sodic, MP sodic and LP sodic, respectively), and potassic granites (after Moyen, 2009, 2011). The Usutu rocks (marked by orange colour) are from Swaziland (data from Schoene and Bowring, 2010). Data sources from the MMt rocks: see text.

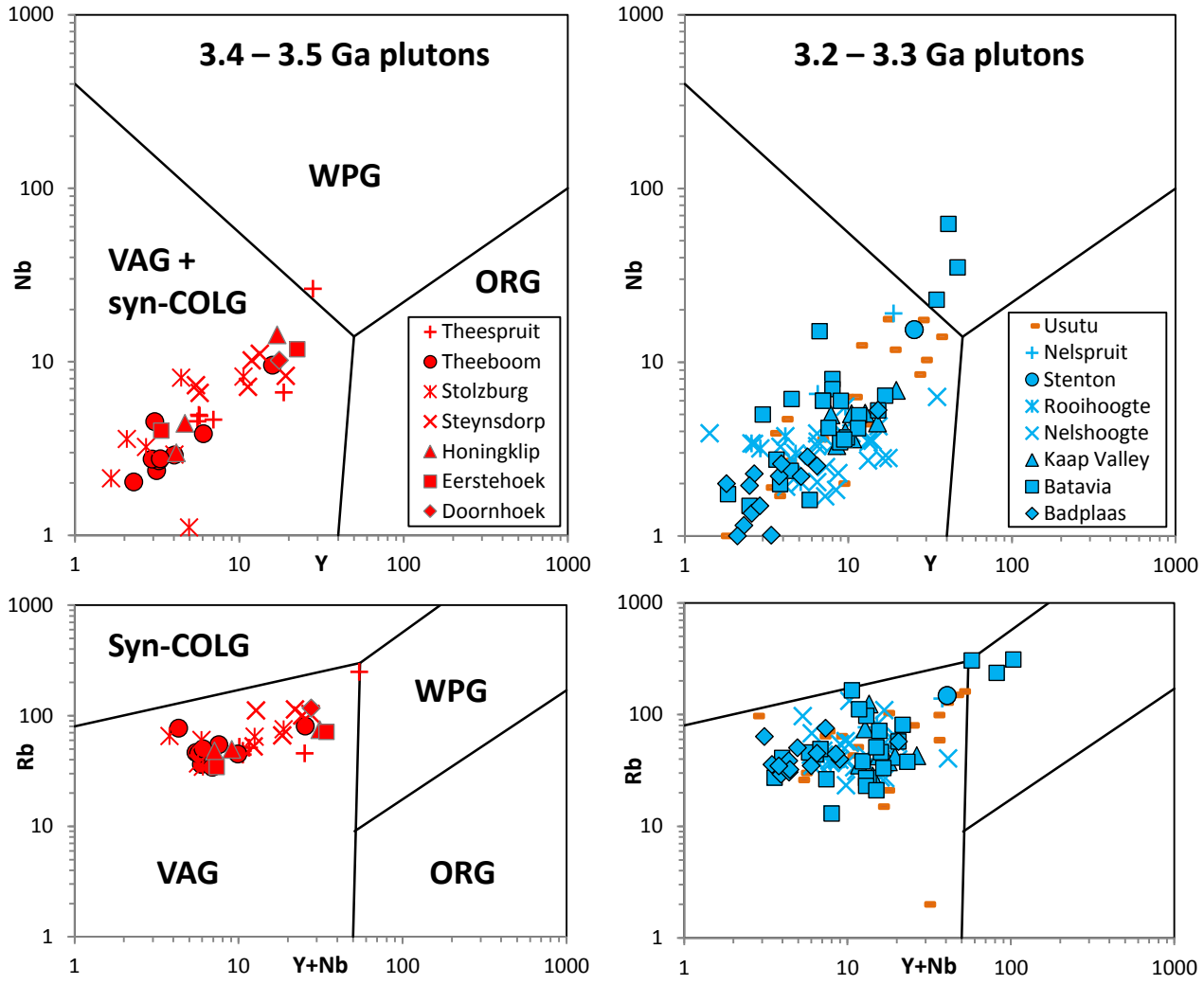

Figure 17. Granitoids of the 3.5–3.2 Ga TTGs plotted in Nb–Y, and Rb–(Y+Nb) discriminant diagrams (after Pearce et al., 1984). Data sources: see text.

and 2.7 Ga plutonic rocks are dominated by intracrustal recycling rather than by new additions from the mantle, perhaps signaling a transition to cratonic stability (Schoene et al., 2009; Zeh et al., 2009, 2011).

7. Magnetic tests for paleo-subduction zones

7.1. High resolution aeromagnetic-based shallow sections (>10 km)

A high strain zone that forms a boundary between the Badplaas and Stolzburg plutons is known as the Inyoni Shear Zone (ISZ: Moyen et al., 2006; Nédélec et al., 2012; Van Kranendonk et al., 2014). The ISZ is directly linked south to the external Schapenburg Schist Belt (Fig. 2). It has played a prominent role in modeling the tectonic history of the region in that it has been interpreted as (1) a Paleoarchean suture zone on the basis of its metamorphic mineral assemblages that record high-pressure and moderate-temperature conditions and apparent low geotherms indicative of a subduction environment (Moyen et al., 2006); or subsequently as (2) a negative thermo-tectonic diapir or 'drip' through partial convective overturn caused by density contrasts between the upper and middle crust, and increased *in situ* heat production (Van Kranendonk, 2011a, b, 2014).

It has also been suggested that the Stolzburg Schist Belt (SSB) may continue to the south, and specifically linking the Inyoka-Saddleback Shear System (ISSS) with the ISZ, either directly (Diener et al., 2005; Moyen et al., 2006; Kisters et al., 2010), or offset by a late (ca. 3.1 Ga) mylonite zone (Van Kranendonk et al., 2014). However, asserting this connection (e.g., Fig. 2) is thwarted by very poor outcrop, and in the field this connectivity cannot be confirmed. The purported connectivity cannot be tested with available geophysical data because the regional aeromagnetic data from the national archives (Council for Geosciences) is of low resolution. Thus potential connection between the ISSS and ISZ remains uncertain. To test the continuation of the SSB into the adjacent TTG core complexes and their internal shear zones, as possible subduction-related sutures, we conducted a high resolution aeromagnetic survey linked to *in situ* magnetic susceptibility measurements to trace these zones at surface and at depth.

The aeromagnetic survey was conducted using the GyroLAG Kriek IIB gyrocopter. Line spacing was at 100 m as 6000 line km were flown across much of the southwestern Stolzburg Schist Belt and surrounding granitoid complexes at an average speed and height above ground of 100 km/h and 40 m, respectively (Fig. 21a, b). Vector fluxgate magnetometers were positioned 2.6 m from the centre on both sides of the aircraft and the signal sampling rate was

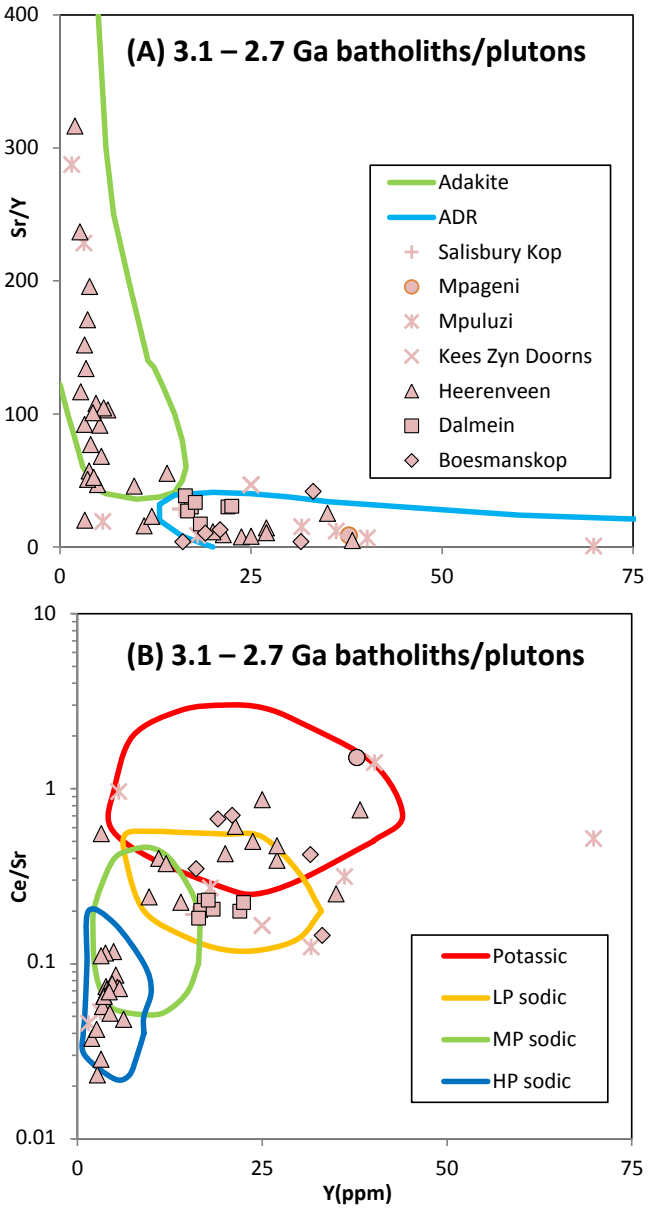

Figure 18. Granites of the youngest batholiths/plutons plotted in the Sr/Y–Y (A) and Ce/Sr–Y (B) diagrams. See Fig. 14 for reference to the diagrams. Data sources: see text.

30 Hz. This resulted in an accuracy of approximately 1 nT (see MacLennan (2012) for further details).

A number of distinct magnetic anomalies are visible on the total Magnetic Intensity (TMI) Map that in general correlates with the greenstone belt lithologies (Fig. 22a). 1000 m upward continuation of the TMI shows that the major magnetic anomalies are deep seated. Reduction to the pole and the first vertical derivative of the total magnetic intensity assist in the identification and interpretation of these major anomalies. Analytic signal transformation of the reduced-to-the-pole TMI whereby magnetic peaks associated with the centre of their causative bodies shows that only the deeper sourced anomalies remain clearly visible (Fig. 21c).

Compared to the mafic-ultramafic rocks of the MMts, all surrounding granitoid complexes have relatively poor magnetic susceptibility and low remnant magnetization (Figs. 21b and 22). The two very strong anomalies D and G show a spatial correlation with syenites (e.g., the Kees Zyn Doorns (G) and Boesmanshoek syenite and syenogranite (D) dated at between 3.1 Ga and 3.15 Ga (Kamo and Davis, 1994). The syenites contain interstitial magnetite (Anhaeusser, 1980; MacLennan, 2012) and are associated with high magnetic susceptibility (35–39 SI units). It is possible therefore that the syenite intrusions are responsible for these magnetic anomalies.

The largest anomaly (F) is spatially closely associated with the Stolzburg Layered Ultramafic Complex (SLUC; Fig. 5, Map 1). The SLUC has abundant magnetite due to intense serpentinization. *In situ* magnetic susceptibility measurements related to detail mapping at 10 m scale confirm that both the positive and negative parts of this anomaly are caused by serpentinized ultramafic rocks of the SLUC (MacLennan, 2012). The anomaly at location E forms part of a broader area of elevated magnetisation that correlates well with the mafic and ultramafic lithologies of the Weltevreden Complex. The anomaly at location E visually continues towards the southwest in the direction of the Sterkspruit Asbestos Mine (Fig. 5).

There is a distinct margin between the magnetisation of the Weltevreden Complex and the very low magnetisation of the SLUC. Due to the precise correspondence of the magnetic margin with the contact between the Weltevreden Complex and the SLUC mapped at surface, it is unlikely that the juxtaposition of magnetic high and low is purely a dipolar effect. Rather this likely represents a tectonic break, with the very low magnetic values being recorded as a result of the steep gradient in the magnetic field across the contact. This interpreted tectonic break has been named the Mawelawela Fault (Map 2).

A number of other magnetic anomalies correlate with the Moodies, Inyoka, Komati and Theespruit Faults. These faults, along with the Mawelawela Fault, all converge towards the west into one schist zone, containing a subvertical stretching lineation (de Wit, 1983; Fig. 5), where they amalgamate with the magnetic anomaly that trends between location G and E. Associated with these faults is a major magnetic anomaly that correlates well with the SLUC and Weltevreden Complex (Figs. 22 and 23). This magnetic anomaly continues to the west and northwest in a broad arc that trends towards the mafic-ultramafic rocks in the Kalkkloof Schist Belt (Fig. 23; Map 2; Menell et al., 1981). There is thus no geophysical evidence for these shear zones to continue to the south linking with the Inyoni Shear Zone.

By contrast, the magnetic gradients across lithological boundaries with the TTG gneisses can be interpreted as Weltevreden mafic-ultramafic material linked to a north-dipping unit beneath the TTG gneisses of the Nelshoogte complex. This unit is likely responsible for the gradient towards the north since the TTG gneisses of the Badplaas and Nelshoogte are geochemically (and magnetically) very similar.

To test this further, forward modelling of the aeromagnetic data was conducted along 3 profiles (Figs. 23 and 24). A western profile (Profile 1) that crosses the anomaly reveals a relatively steep north dipping slab between 50° and 60°, and which becomes slightly thicker with depth down to 6.5 km, fits the observed data well. A second profile across the anomaly in the central part of the survey area is weaker than those to the west or east. Different models show that either a thin, highly magnetic body or thicker, less magnetic rectangular body best approximates the observed data. In both cases, the bodies dip to the north down to 0.8–1.2 km below surface, with dips 20°–40°, respectively. Profile 3 runs across the major magnetic anomaly at location E. This anomaly can be approximated with a simple north dipping rectangle of mafic-ultramafic material at an intermediate slope down to about 3 km. In all three cases the greenstone materials dip beneath the Nelshoogte TTG.

As with all forward models, the solutions may be non-unique and the derived physical parameters could remain poorly

constrained without additional datasets such as gravity measurements. Therefore, the forward models used here were purposely kept simple and geologically consistent across the survey area in order to minimise over-interpretation of the magnetic data.

The aeromagnetic and geologic maps reveal a number of faults that coalesce within the western extent of the Stolzburg Schist Belt. The Komati and Hooggenoeg Complexes at the southern margin of the supracrustal sequence are also well-delineated by the aeromagnetic data, and a sharp gradient is present at the contact with the higher grade Sandspruit and Theespruit Complexes. These magnetic anomalies continue toward the western extent of the SSZ, where they are isoclinally folded and coalesce into the same trend as the extension of Anomaly F. Isolated positive magnetic anomalies within the Sandspruit Complex correlate well with mapped enclaves of partially serpentinized rocks (Diener et al., 2005). However, neither the isolated amphibolite-ultramafic slivers within the ca. 3.45 Ga Stolzburg TTG core complex (e.g., those situated around location D) and along its contact with the Badplaas TTG gneiss complex (ca. 3.25 Ga), induce such magnetic signatures.

In terms of delineating the continuation of the SISS, there is no aeromagnetic evidence that it continues to the south. Rather the highly magnetized material associated with the Nelshoogte schist belt seems to coalesce with the aeromagnetic anomaly associated with the Kees Zyn Doorns syenite. The most favorable interpretation for the continuation of the material with high magnetic susceptibility associated with the Nelshoogte schist belt and the SLUC, and by association the continuation of the SISS, seems to be that it continues in a thinned zone to the NW. The subsequent subvertical intrusion of the Kees Zyn Doorns syenite is here interpreted to obscure the original magnetization. In this respect, the SSB is more likely to be linked to the greenstone remnant known as the Kalkkloof Schist Belt some 15 km to the west of the BGB and 10 km north of Badplaas (Hall, 1930; Visser et al., 1956; Menell et al., 1981; and Map 2), where it is in part unconformably covered by the sub-horizontal rocks of the Transvaal Supergroup. The predominant rock type of the Kalkkloof Schist Belt is the Kalkkloof ultramafic layered complex (KULC), a serpentinite body surrounded by hornblende-actinolite-talc-tremolite and felsic schists. The compositions of the mafic-ultramafic schists are similar to those of the lower Onverwacht Suite, but detailed chemistry is lacking. The KUMC has been previously compared to the SLUC. Detailed analyses of these two complexes have been linked to the abundant chrysotile

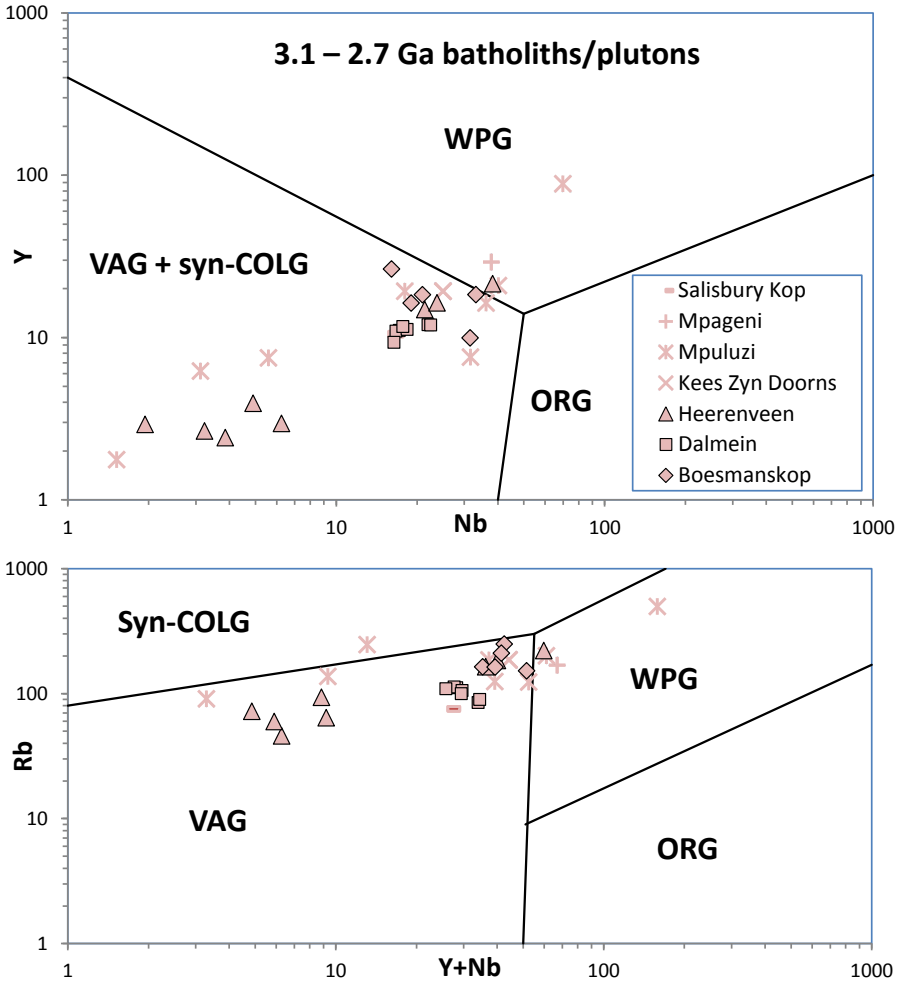

Figure 19. Granites of the youngest batholiths/plutons plotted in Nb–Y, and Rb–(Y+Nb) discriminant diagrams (after Pearce et al., 1984). Data sources: see text.

asbestos mines (now abandoned) in both complexes (Sterkspruit and Stolzburg in the SLUC; e.g. Anhaeusser, 1972). Both complexes consist of well-defined serpentinized dunites (olivine) and orthopyroxenites (enstatite-bronzite), with lesser harzburgites and wehrlites, and are heavily tectonized as evident from a wide variety of sheared talc-tremolite schists and carbonated ultramafic varieties, including local development of the rare serpentine mineral stichtite (an hydrated carbonate-hydroxide of Mg and Cr, Ashwal and Cairncross, 1997); and all enriched in magnetite and altered chromite. Adjacent to parts of KUMC are felsic schists and cherts similar to those in the Stolzburg Schist Belt that can be linked farther west to both the Theespruit and Noisy Complexes (Map 1; Fig. 5).

The HR magnetic data and modelling confirms a continuation of the ISSS to the west and that part of the Weltevreden Complex can best be interpreted to dip moderately to steeply north to northwest beneath the Nelspruit TTG core down to depths of close to 7 km (Figs. 24 and 25). We suggest this represents the upper remnants of a ca. 3.2 Ga subduction zone.

7.2. Magneto-Telluric (MT) based deep electrical conductivity sections (>10 km)

Magnetotelluric (MT) surveys across the study region, in 2009 and 2010, resulted in 2D and 3D conductivity models of the region (Kuetter et al., 2016). Electrical conductivity is generally sensitive to small conductive mineral constituents and pore fluids in large rock sequences. Imaging the electrical conductivity may thus help test for paleo-processes that focused metamorphic fluids and/or mineralization along shear planes.

From the results of the 3D inversion studies we show a selected section of a refined 3D conductivity model, cutting across the Moodies, Inyoka-Saddleback, Maanhaar-Msauli and Forbes Reefs Shear Systems down to depths of ca. 15 km (Fig. 2). The majority of the resistive features can be directly linked to rocks of the Onverwacht Suite and Fig Tree/Moodies Groups at surface and which were found to extend to a maximum depth of approximately 8 km, whilst nearly electrically homogeneous bodies adjacent to the belt extend down to a depth of at least 20 km, suggesting they are part of the granitic upper crust inferred to be preserved below the MMts (Kisters et al., 2003; Schoene et al., 2008, and references therein). These findings across the sequences of the MMts agree well with other electric and gravity data (de Beer et al., 1988).

The 3D inversion models in the NE part of the MMts, correlate with zones of high conductivity across major shear systems and in the south-central part resistive structures extend deeper to mid-crustal levels (Fig. 26; profile 40–60 km, down to 8 km) and the two major shear systems of the Moodies/Inyoka-Saddleback and Maanhaar-Msauli, are underlain by inclined zones of enhanced

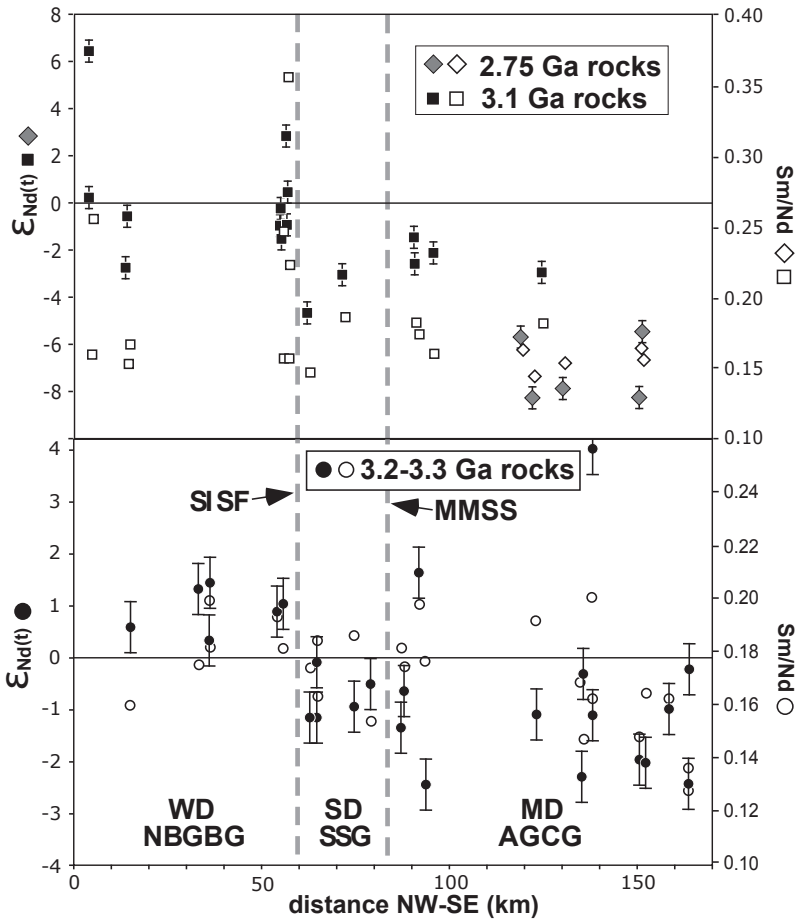

Figure 20. Nd isotopic data and Sm/Nd for magmatic granitoids dated at 3.2–3.3, 3.1 and 2.73 Ga, plotted across the study area along the transect shown on Fig. 2, and onto which the granitoid samples were perpendicularly projected. NBGBG: Granites NE of the greenstone belt, as part of the Weltevreden Domain (WD); SSG: Stolzburg and Steynsdorp Granitoids, as part of the Songimvelo Domain (SD); AGCG: Ancient Gneiss Complex Granitoids linked to the Malalotsha Domain (MD). Error bars on ε_{Nd} are fixed at ±0.5 at the 2σ level, and errors in Sm/Nd are smaller than symbol (modified from Schoene et al., 2009).

conductivity possibly down to 10–12 km (Fig. 26). These compare well with the doubly-verging 3.2–3.3 Ga paleo-subduction zones inferred from the Sm–Nd isotope systematics and in ε_{Nd} values for granitoids across the greenstone belt (BGB), and consistent with existing models for ca. 3.23 Ga accretion of newly formed lithosphere north of the MMts onto pre-existing ca. 3.66 Ga lithosphere south of the MMts (Schoene et al., 2008), and their subsequent exhumation history (e.g., Kisters et al., 2003; Schoene et al., 2008). These zones may indicate pathways for metamorphic fluids from lower crustal levels that may also have induced focused mineral deposits asbestos, iron and gold deposits (Barton, 1982; and see below).

8. Ocean depth estimates

At a certain depth (and pressure) volatiles (predominantly water) are dissolved in basaltic magma, and erupted pillow lavas will be non-vesicular (Moore, 1965). With decreasing depth (and pressure) volatiles become a separate phase in the basalt magma and will result in gas-filled pores upon eruption, particularly in the upper part of pillows. The relationship between water depth and vesicularity, however, is a function of the water content in the magma (Jones, 1969; Moore, 1970); thus, water-rich alkali basalts will be more vesicular then water-poor tholeiitic basalts when erupted at the same depth.

The vesicularity of pillows at various stratigraphic levels of the Hooggenoeg and Kromberg Complexes has been calculated, and employing the vesicularity-depth relationship as defined by the modern oceanic, tholeiitic basalt, compositionally comparable with those of the MMt metabasalts, the depth of eruption has been estimated (Furnes et al., 2011). Using this technique, and applying the depth-vesicularity relationships of Moore (1965), the lavas of the Hooggenoeg Complex formed at depths of 2.4–4 km, whereas those in the lower part of the Kromberg Complex formed at shallower depths of around 1.7 km. Higher in the Kromberg Complex the vesicularity decreases and suggests eruption at water depths of >2 km.

The depths of modern active back-arc basins vary considerably; for example in the Mariana back-arc basin, the depths ranges from 3200 to 5300 m (Stüben et al., 1998), and the depth of the zero-age Philippine Sea back-arc basin is 3200 m (Chung-Hwa et al., 1990). The estimates of the eruption depths of the pillow lavas in the Hooggenoeg and Kromberg Complexes are thus comparable with the depths of spreading ridges in modern ocean back-arc basins.

9. Ocean and arc-like hydrothermal processes

There is ample evidence that hydrothermal processes operated at deep sea and shallow to subaerial levels throughout the depositional stages of the Onverwacht Suite (e.g., de Wit et al., 1983, 1987a, b; Paris et el., 1983; De Ronde et al., 1994; de Vries and Touret, 2007; de Wit and Furnes, 2016).

9.1. Silica-fuchsite chimneys – deep water

A large number of volcanic tuff horizons across the Onverwacht Suite are well-preserved because of their silicification to cherts and associated micas, especially chrome-rich fuchsite (Map 1; Fig. 3b). The cherts have been extensively described elsewhere (Viljoen and Viljoen, 1969a, b; Paris et al., 1985; Duchač and Hanor, 1987; de Wit et al., 1987a; Hanor and Duchač, 1987; Lowe and Byerly, 2007; de Wit and Furnes, 2016). The cherts have been used as marker horizons in almost all lithostratigraphic studies; indeed the Middle Marker (Fig. 3b) has become an iconic Paleoarchean marker horizon. The origin of the silicification processes was long regarded to be related to sedimentary processes and direct chemical precipitation from seawater (Knauth and Lowe, 2003 and references therein). Today they are generally accepted as secondary deposits related to deep water and near surface hydrothermal alterations, during large-volume fluid circulation. Recent stable isotope analyses in the Hooggenoeg Complex of vertical silica-fuchsite pipes rooted in breccias of a chert horizon, and extending 14 m into the overlying pillow lavas that formed at a depth of 2–4 km below sea-level, has verified their formation temperatures of 150–200 °C, analogous to that of 'white smokers' (de Wit and Furnes, 2016).

9.2. Iron chimneys - shallow water

Both in the Songimvelo and Malalotsha Domains, ironstone pods and chimneys of goethite and hematite rooted in silicified ultramafic rocks and linked across and along strike with ferruginous shales and laminated iron-oxide facies banded iron-formation (BIF) inferred to represent episodic discharge of iron-oxide and silica-rich flocculates from the iron-chimneys (Barton, 1982; De Ronde et al., 1994). Just below the Pylon Nappe (Map 2), such iron chimneys yielded fluid temperatures between 90 and 150 °C (low salinity (5–16 wt.% NaCl; and 33–109 °C), and high salinity (24–30 wt.% $CaCl_2$) (De Ronde et al., 1994). These deposits resemble low-temperature hydrothermal iron-oxide deposits on the seafloor. Fluid inclusion analyses provided constraints on the seawater of about 3.1 wt.% NaCl and $\delta^{18}O$ values (−1.2 to 1.4‰) close to modern values. These deposits formed in shallow seawater (60–100 m), and in places linked to mud deposits that reached above sea-level where fossil gas-escape structures are preserved in dehydrated mudpools (de Wit et al., 1982; De Ronde et al., 1994). Similar structures have been described in the Malalotsha Domain both in Swaziland (Barton, 1982; Lamb, 1984a) and across the border in the to Josefsdal area (Paris, 1986; Map 2). Paris (1984) was the first also to discover possible air-fall rain and/or mudpool-fluid drops in these silicified muds (Fig. 29d). These still require modern analyses to determine Paleoarchean atmospheric conditions (c.f., Som et al., 2012 for the Neoarchean).

9.3. Felsic breccia pipes – shallow water to subaerial

Detailed field mapping, together with abundant fluid inclusion work on veins and breccia pipes across the felsic volcano-sedimentary sequences of the Noisy Complex indicates a shallow water to subaerial environment of deposition for the sediments, with contemporaneous hydrothermal activity at temperatures below 200 and 300 °C (de Vries and Touret, 2007). Such temperatures are consistent with paleomagnetic studies on these same rocks (Tarduno et al., 2010; Biggin et al., 2011). Hydrothermal quartz contains coeval two-phase aqueous inclusions (with variable salinities) and mixed H_2O–CO_2 inclusions, and the phase relations in the CO_2–H_2O system show that unmixing of immiscible fluids occurred at relatively low pressure (ca. 100 bars). Clasts and matrix have undergone extensive hydrothermal alteration by the CO_2–H_2O fluids, which have altered much of the primary mineralogy to sericite, fuchsite, carbonates and magnetite (de Vries and Touret, 2007). The origin of the hydrothermal fluids is interpreted to be partly related to felsic magmatism linked to deep rooted TTG plutons (de Wit et al., 1987b, 2011). The similarities of the aqueous fluids compared to those of present day hydrothermal systems, and the absence of reduced gases in inclusions strengthen the conclusion from field observations that the Noisy hydrothermal system operated in a near-surface environment related to felsic magmatism in arc related systems such as recorded, for example, in the Taupo zone of New Zealand and in Japan.

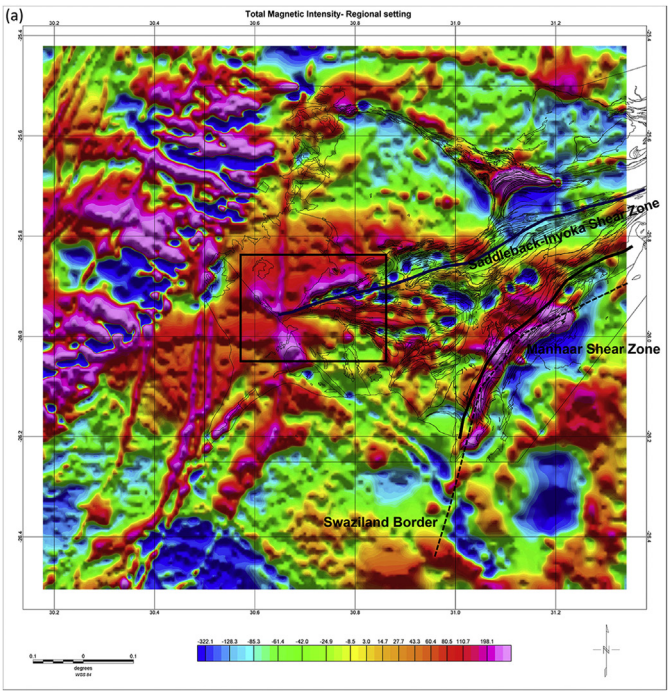
(a)
Total Magnetic Intensity- Regional setting
Saddleback-Inyoka Shear Zone
Manhaar Shear Zone
Swaziland Border

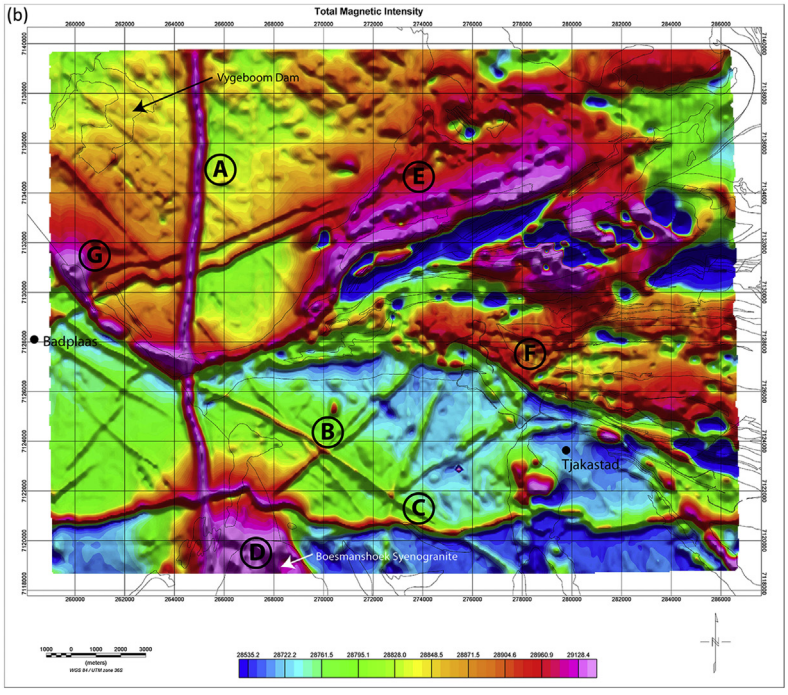
(b)
Total Magnetic Intensity
Vygeboom Dam
A
E
G
Badplaas
F
B
Tjakastad
C
D
Boesmanshoek Syenogranite

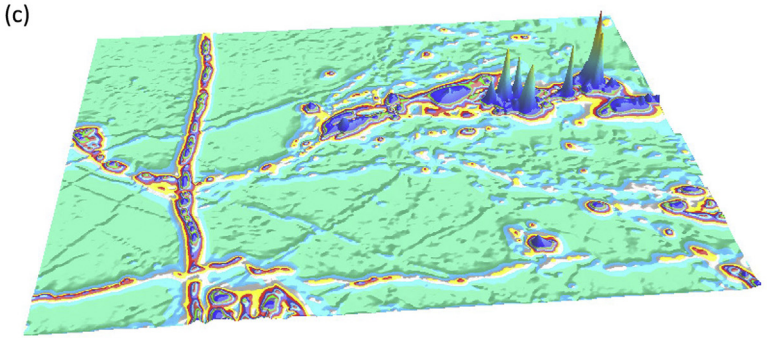
(c)

10. Selected hydrothermal ore deposits

10.1. Barite

Barite deposits in the Malalotsha Domain, with an estimated reserve of near 300 thousand tons, represent the largest stratiform sulphate body in the MMts. At Londosi, close to the Manhaar-Msauli Shear System, barite occurs continuously for 1250 m, and discontinuously for more than 10 km along strike into adjacent parts of South Africa. The composite thickness of the deposits averages 1.2 m (Reimer, 1980; Barton, 1982). The footwall of the deposits comprises silicified mafic-ultramafic schists and talcose serpentinites, consistent with basaltic komatiite composition of Onverwacht Suite rocks, whilst the hanging walls also contain felsic volcanics and tuffs (Barton, 1982). Viljoen and Viljoen (1969a) first proposed a hydrothermal origin for the Londosi barite deposits, and Barton (1982) interpreted these deposits to be related to hydrothermal activity during the alteration of the mafic-ultramafic sequences, similar to those found along fault zones in the Pacific marginal Lau Basin. Associated siliceous breccias and conglomerates are consistent with local sedimentary reworking of the hydrothermal deposits. This is similar to barite horizons and barite clasts found in the coarse sedimentary sequences tectonically below the Pylon Nappe in the northern sector of the Songimvelo Domain (de Wit, 1982; De Ronde et al., 1994; Lowe and Byerly, 1999), and farther north (Reimer, 1980; where recent ICDP drilling has re-investigated these deposits; e.g., Ledevin et al., 2015) as well as within the eastern and western extremities of the Stolzburg Schist Belt (de Wit, 1983).

10.2. Gold

The MMts first became famous for its potential gold mineralization in the early 1890s (Hall, 1918). There is a vast formal and informal literature on these deposits and mines, and it is beyond the scope of this contribution to review this. Recent work confirms that the major deposits occur on thrust/extension faults closely flanking the ISSZ, and, to a lesser degree, the MMSZ (Fig. 27), and especially within relatively short distance of 3.2 Ga TTG plutons, where dominated by normal movements (Dirks et al., 2013).

Individual mineralized shear zones are typically normal or transtensional brittle–ductile structures, $<$ 300 m in length and $<$1 m in width, active at sub-greenschist to lower amphibolites facies conditions (De Ronde et al., 1992; Ward, 1999; Dirks et al., 2009, 2013). Major mine camps display a cluster spacing of ~12 km, which suggests a regular distribution of controlling shears, and detailed stress analyses suggests that their gold mineralization occurred during a single tectonic stage around 3015 Ma (Munyai et al., 2011; Dirks et al., 2013).

Dziggel et al. (2010) have provided the only direct age estimates at 3027 ± 7.5 Ma for hydrothermal titanite intergrown with auriferous minerals. A date of ca. 3084 Ma was suggested for major mineralization based on hydrothermal rutile (De Ronde et al., 1992), but this mineral cannot unequivocally be linked to gold mineralization (Dirks et al., 2009. 2013). Zircon ages between 3017 Ma and 3009 Ma have been determined at mineralized dykes (Dirks et al., 2013).

Whether these major deposits occur in late-tectonic structures along which pre-existing mineralization was remobilized, remains unresolved. Dziggel et al. (2010) showed that mineralization likely occurred in two phases, one during the peak compressional deformation and metamorphism close to 3230 Ma, and a main phase around 3030 Ma linked to extension and exhumation of the MMt sequences and the rise of adjacent TTG cores. Thus the major deposits may occur only in areas where the network of brittle–ductile shears interacts and upgrades zones that were already gold enriched. This suggests that gold is locally derived and stripped from deep MMt sequences by mineralizing fluids, concentrated and deposited at suitable structural sites (e.g., Foster, 1985; Anhaeusser, 1986).

It is likely then that some stratigraphic or early tectonic horizons of the MMts were relatively enriched in gold soon after formation. Indeed many small deposits and occurrences are distributed in the central Songimvelo Domain flanking the early (ca. 3.45 Ga) deformation zones (including quartz-carbonate-fuchsite shear zones) underlying chert horizons well away from the 3.2 Ga thrust zones (Fig. 27). For example, flanking the Komati River and the Mbjega Shear, north of Tjakastad, and just beneath the Middle Marker north of Steynsdorp; and along the early tectonic zones separating the Kromberg and Mendon Complexes near Ekulindeni (Viljoen et al., 1969; Map 1). Similarly in the major gold area of the Malalotsha Domains, there are over 30 named gold occurrences in the Forbes Reef area, most of which occur in the talcose schists and fuchsite-bearing cherts flanking the tectonic boundary of the Malalotsha Nappe (Barton, 1982, and references therein; compare Fig. 27 with Map 2). It thus appears that early, relatively low-grade gold mineralization was associated with the deep-water hydrothermal shear systems; and which were later dispersed or concentrated into more economically viable deposits during deep fluid migration. This is consistent with the findings of the conductivity survey.

Thus a model has emerged in which the underlying complexes locally enriched in gold during early pre-D1 hydrothermal systems were truncated by late D2 extensional shear zones at depths sufficient to allow ingress of fluids perhaps as late as 3015 Ma, to form large, high-grade gold deposits (see Fig. 3b). By ca. 3075 Ma regional erosion down to the Mpuluzi granitoid sheets had led to deposition of Neoarchean sequences such as the Witwatersrand and Pongola (Dirks et al., 2013; see inset Map 1). This reveals a long term recycling of gold over 475 Ma, and rapid local enrichment within less than 12–70 million years.

11. Rates of Paleoarchean processes

Below we highlight some of the findings from our field mapping, integrated with geochemistry and linked to time lines derived from published geochronology. We collate these into Table 1, which summarizes a first order set of rates of Paleoarchean processes to test reliability of our plate tectonic model summarized as Fig. 28.

11.1. Subduction-exhumation processes

Exhumation up to 18 km of unroofing took place between 3140 and 3230 Ma, exposing high pressure mineral assemblages formed,

Figure 21. (a) Regional Magnetic map for the southern Makhonjwa Mountains (Council for Geoscience of South Africa) overlain with general geology (Ward, 2000). (b) Total Magnetic Intensity map of High Resolution survey, with locations A–G referred to in the text. Note NE=Nelshoogte TTG gneiss core, which shows slightly greater magnetic susceptibility than the Badplaas, Stolzburg or Theespruit TTG gneiss domes, and in turn slightly greater than that across the late Mpulusi granite sheet. A number of prominent linear magnetic anomalies (e.g., A, C and likely B) show very close spatial association with either the Neoarchean dyke swarms (NE–SW and NW–SE orientated, and dated at 2.981–2.989 Ga; de Wit et al., 2011), and N–S Jurassic Karoo dykes (dated at ca. 183 Ma; Maré and Fourie, 2012). (c) Perspective image of the analytic signal of the reduced-to-the-pole TMI from the HR Magnetic data. The image shows energy peaks in the magnetic data associated with the location of causative sources. Note the high anomalies related to serpentinites beneath the Moodies Group of the Stolzburg syncline, and exposed along local antiforms (Fig. 5 and Map 2). Note the continuation of the rocks of the Stolzburg Schist Belt towards the NW. There is no sign of a connection of these rocks to the south (see text).

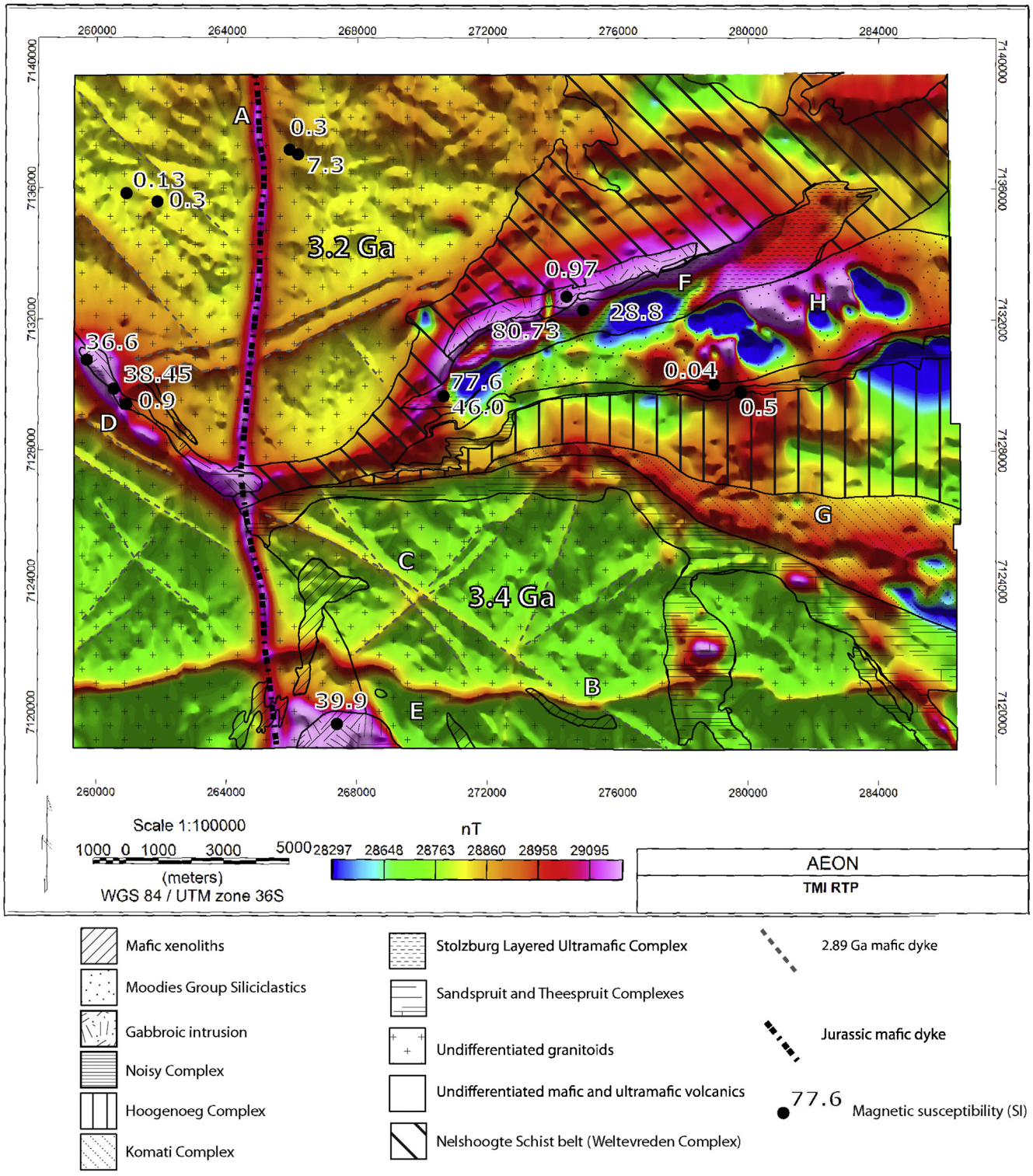

Figure 22. TMI Magnetic map showing ground control measurements. Strong positive and negative magnetic anomalies (H) fall within the mapped extent of the Stolzburg syncline. It seems unlikely that the causative body for these anomalies is within this folded siliciclastic unit given the low magnetic susceptibility recorded from field measurement within this unit, including the banded iron formation and ferruginous shales. However, structural field data shows that the syncline is directly underlain by mafic-ultramafic lithologies of the Weltevreden Complex and which outcrop in tight antiforms within the syncline (see Map 1; Fig. 5). The anomaly at Location D correlates in part with the surface outcrop of the Kees Zyn Doorns syenite. This could indicate that the observed magnetic anomaly is due at least in part to this late stage felsic intrusion (3107 Ma). However, there are also mafic-ultramafic tectonic boudins at surface along the anomaly at Location G (Kisters et al., 2010; Fig. 5). Moreover, the Kees Zyn Doorns syenite is part of a set of NW trending vertical intrusions, yet the magnetic gradient shows the magnetic anomaly dips to the north, and is thus more likely to be due to north dipping mafic-ultramafic rocks possibly linked to the back-thrusts flanking the Weltevreden Complex (De Ronde and de Wit, 1994; Map 2).

during relatively low geothermal gradients along the southern margin of the MMts (Dziggel et al., 2002, 2006; Diener et al., 2005, 2006; Moyen et al., 2006; Stevens and Moyen, 2007; Fig. 28). This episode followed external subduction-like processes associated with folding, thrusting and molasse-type sedimentation within the MMts; all comparable to modern ocean subduction to continental collision processes. During this period, younger complexes were assembled, and the older complexes re-cycled and eroded, at rates and with geotherms comparable to those in modern orogenic belts (e.g., Hodges, 2017; Yamato and Brun, 2017).

11.2. Uplift and obduction rates

The Hooggenoeg Complex is separated by an unconformity from the overlying fluvial to shallow water clastic sequences of the Noisy Complex. The conglomerates contain clasts of the metasomatized lithologies and early shear zones from the underlying Hooggenoeg Complex (de Wit et al., 2011). Uplift and exposure of the deep water Hooggenoeg Complex above sea level is suggested by the reworking of its uppermost chert horizon and clasts of silicified spinifex-textured komatiite and basalt in the conglomerates of the Noisy Complex. This suggests the Hooggenoeg Complex was uplifted by 3.5–5.5 km (2–4 km uplift from oceanic depth, plus a minimum of 1–1.5 km down-cutting of the Noisy conglomerates into the Hooggenoeg Complex) between about 3445 Ma and 3433 Ma giving an uplift rate of some 0.5 mm/yr. This rate of uplift must be a minimum, because the youngest volcanic rocks of the Hooggenoeg Complex were erupted at the greatest depth (ca. 4 km), because an unknown thickness of the Hooggenoeg Complex must have been exhumed across the unconformity. However, within an order of magnitude, the rate is comparable to those reported from modern tectonic plate boundaries and during emplacement of Mesozoic

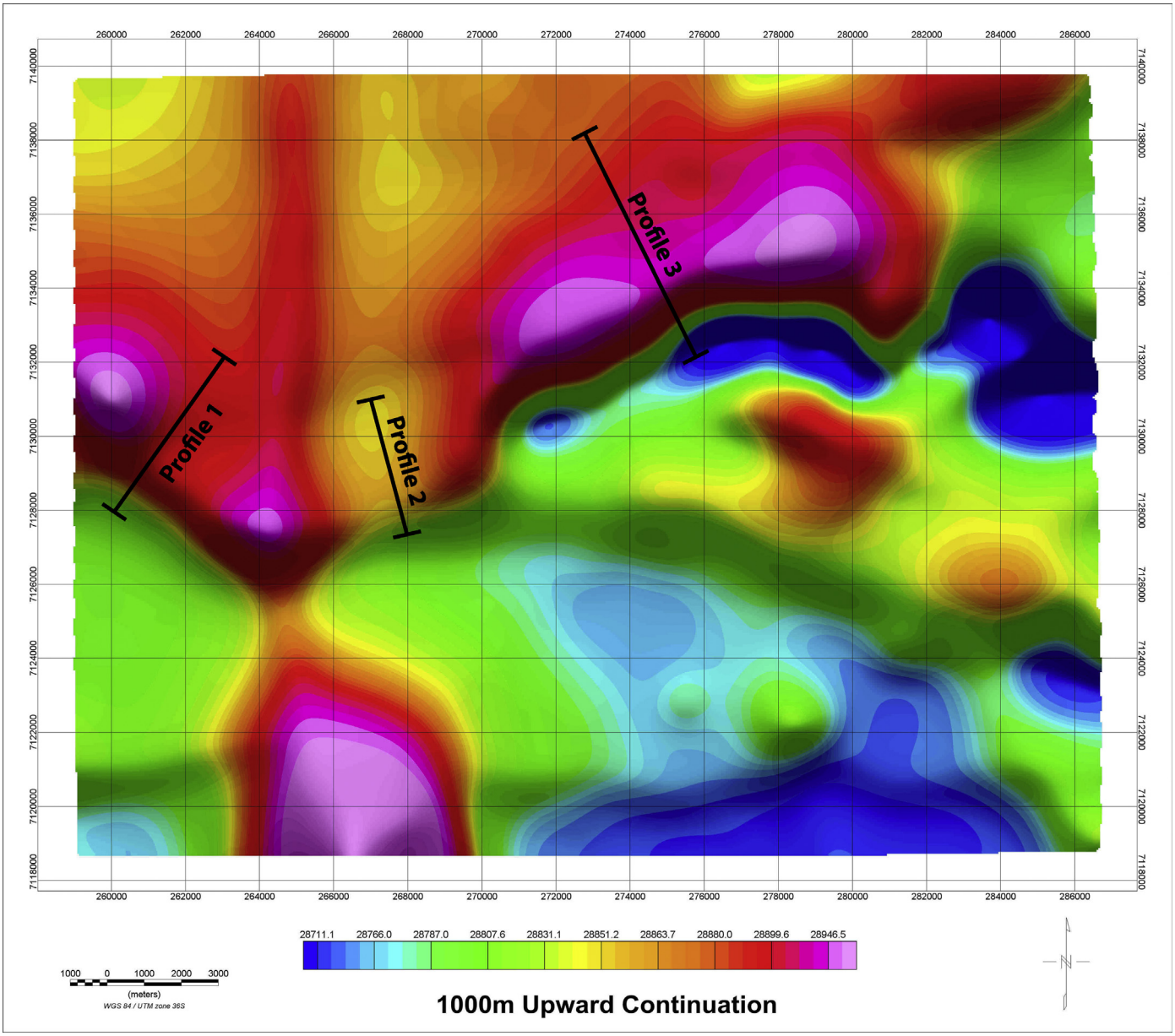

Figure 23. 1000 m upward continuation of high resolution aeromagnetic data. The locations of the three profiles used for forward modelling are shown. Observed and calculated values and model geometry for each profile are presented in Fig. 24.

oceanic crust preserved as ophiolite complexes such as the 8 mm/yr rate of obduction of the Oman Ophiolite (e.g., Searle et al., 2004; Searle, 2007).

11.3. Exhumation rates

Variable uplift of the MMts sequences and their marginal granitoids are documented by U–Pb thermochronology (Schoene and Bowring, 2007; Schoene et al., 2008). On the basis of this, given a geotherm of 15–35°C/Myr, about 7–15 km of vertical exhumation of the southern MMts, and surrounding granitoids originally emplaced at amphibolite to granulite depths, took place at a rate of 10–100 m/Myr, comparable to erosion rates between that of the Alps/Himalayas and the Appalachians (Scharf et al., 2012). By ca. 2.8 Ga, 2.89 Ga mafic dikes and 3.01 Ga granites eroded down to depths of ca. 6–10 km, were exposed at surface and unconformably covered by late Archean shallow marine sequences as still exposed along the present day escarpment (Fig. 1A and B2; Map 1).

11.4. Formation rates of lava sequences

The lava sequence of minimum 2700 m thick that makes up the Hooggenoeg Complex formed during a time span of less than ca. 10 Ma (ca. 3472–3460 Ma; de Wit et al., 2011). It is interesting to note that the Early to Middle Eocene ca. 6 km thick basaltic lava sequence of the Izu-Bonin-Mariana (IBM), ranging from early island arc tholeiite/MORB to boninite and finally to calc-alkaline lavas, formed in a time span of ca. 7 Ma (Ishizuka et al., 2014). Thus, the formation thicknesses and chemical compositions of the IBM and Hooggenoeg Complex are very comparable, suggesting their rates of magmatism were similar too.

11.5. Rates of change in dip-angle of subduction zone

Furnes et al. (2012) calculated Th-enrichment (relative to an estimated Th-concentration without subduction-influence) throughout the lava sections of the Hooggenoeg, Kromberg and Mendon Complexes. In the lava pile of the Hooggenoeg Complex, whose duration is about 10 million years, the variation in Th-enrichment varies from zero to nearly 100% (see Fig. 12 of Furnes et al. (2012)). Enrichment of Th can be attributed to melting of sediments in the deeper parts of a Benioff zone (Pearce et al., 2005). Thus, the pronounced temporal variation in Th-enrichment of the Hooggenoeg Complex, supposedly related to various amounts of sediment-derived partial melts added to the mantle source, Furnes et al. (2012) attributed these variations to the depth and angle of subducting crust. At low and high angles of the subduction zone, the Th-enrichment will be relatively low and high, respectively.

In the active subduction systems around the Pacific Ocean, the dip-angle of subduction show large variation from <30° to near-vertical (e.g., Gvirtzman and Stern, 2004; Lallemand et al., 2005), and the slab geometry may vary laterally as well as time-wise at a fixed position (Guillaume et al., 2013). It is particularly in basins with backarc spreading that the steepest dips occur (>51°), whereas in the case of backarc shortening the dips < 31° (Lallemand et al., 2005). Further, as demonstrated by Lallemand et al. (2005) the slab-dip is controlled by the upper plate strain, the absolute motion of the overriding plate, and the absolute motion of the arc/trench. Given the long time period of about 10 million years for the production of the Hooggenoeg Complex it is highly probable that some, if not all of the above-mentioned slab-dip controlling parameters, would change their character, and thus, as earlier suggested (Furnes et al., 2012), that significant changes in the slab-dip occurred at rates comparable to modern processes. According to Lallemand et al. (2005), in individual subduction-related systems with active backarc spreading, the slab-dip varies with about 10° (mostly 50°–60°, 60°–70°). As we propose active backarc spreading for the crustal formation of the upper Onverwacht Suite, comparable slab-dip variations (between 50° and 70°) may be accounted for, although this remains speculative, given the possible changes in mantle temperatures since the Archean.

11.6. Paleomagnetism and potential rates and of horizontal displacements

Paleomagnetic measurements have yielded a positive conglomerate tests with a minimum age of 3455.2 ± 7.5 Ma from

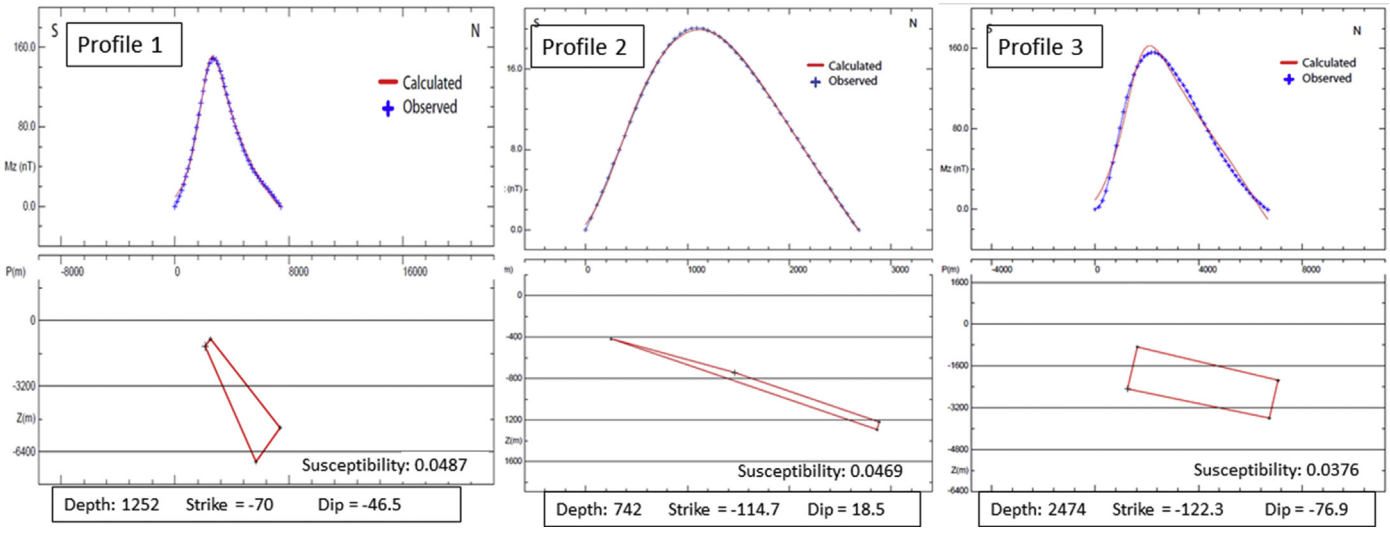

Figure 24. Forward modelling of magnetic profiles showing best-fit models achieved with dipping slab configurations of source bodies. Modelling parameters are shown under each profile including depth (to the top of the body) below surface, the magnetic susceptibility in SI units, and strike and dip in degrees from geographic north. Profile 1 crosses the anomaly in the West central part of the survey area and the observed data are here best fitted by a North dipping relatively steep slab. Iterative modelling confirms that the anomaly becomes slightly thicker with depth. Profile 2 runs across the anomaly within the central part of the survey area and the anomaly appears weaker than to the West or East. The source body here dips to the North at an angle substantially less than that of Profile 1. Profile 3 is the easternmost profile and runs across the major magnetic anomaly at location E on Fig. 21.

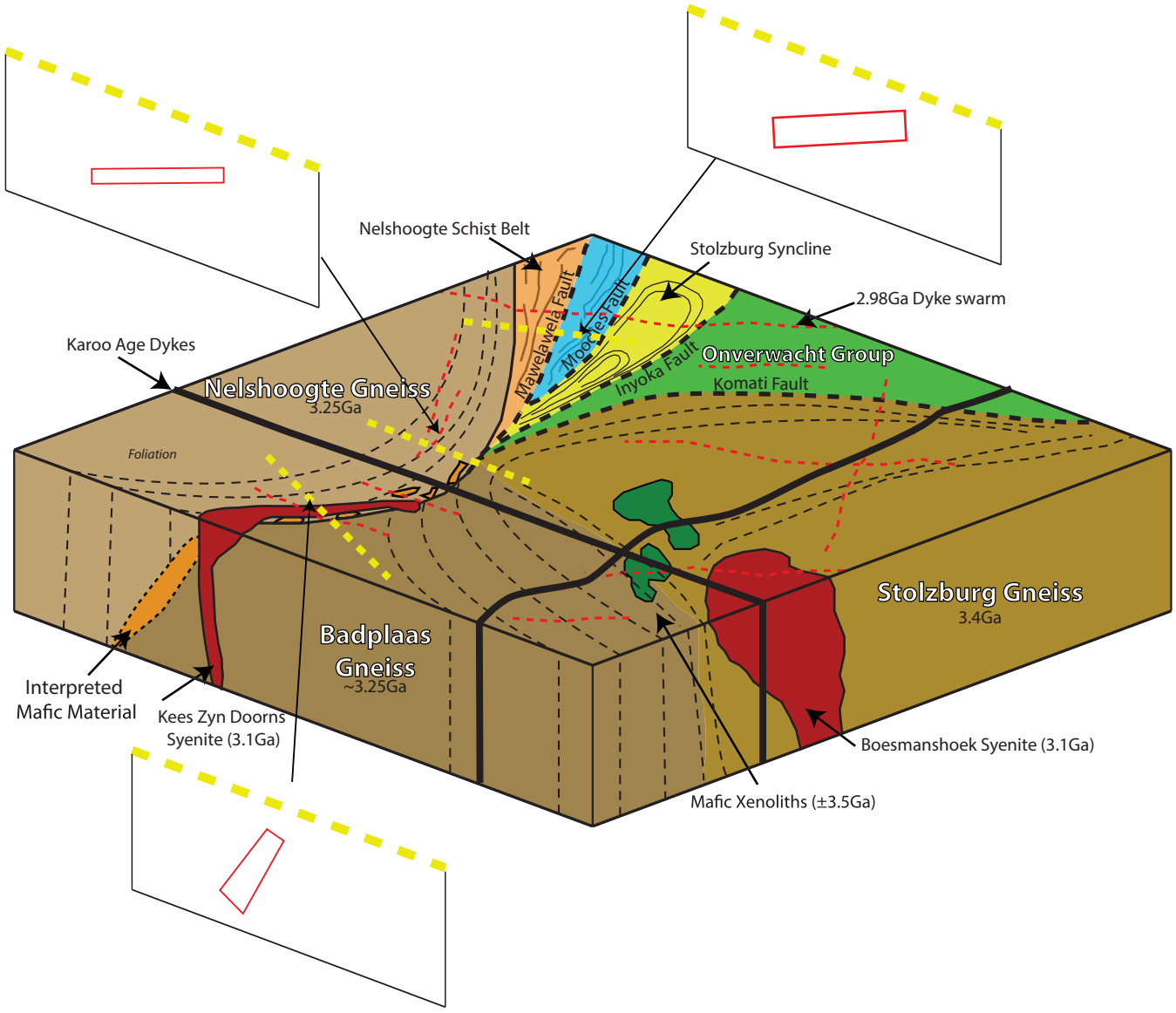

Figure 25. Summary Block Diagram for visual interpretations and forward model of aeromagnetic data from the southwestern part of the Makhonjwa Mountains. The three profiles modelled are shown, as well as simplifications of the bodies that satisfy the observed data. The magnetic body dips towards the northwest and becomes gradually steeper to the west.

the Noisy Complex, which was deposited within 30° of the equator (Biggin et al., 2011). Consistency in stratigraphic coordinates and the absence of any clear indications of remagnetisation from comparison with younger poles has strengthened the claim that these are the most trustworthy palaeomagnetic results yet produced from any rocks of Paleoarchaean age. When taken in conjunction with other published data (Usui et al., 2009), these MMt results present the most compelling evidence to date that the Earth had a stable geomagnetic field at ca. 3.5 Ga, in addition to presenting tentative evidence that it was undergoing polarity reversals (Biggin et al., 2011). The uncertainties associated with the most reliable poles overlap with those produced from the ca. 3.46 Ga rocks from the Pilbara Craton (W. Australia) when reconstructions of the Vaalbara Supercraton previously-proposed for the Neoarchean are used (Suganuma et al., 2006). These results provide intriguing evidence that continental drift rates were not excessively fast relative to today, and leaves open the possibility that parts of the Kaapvaal and Pilbara Cratons may have been conjoined in the Palaeoarchean. Given the average 9 Myr difference in age estimates between the two units, this ca. 1100 km motion translates to latitudinal velocity of ca. 12 cm/yr (Biggin et al., 2011). This is faster compared to today's standards but well within the range of plate velocities observed in the Phanerozoic and consistent with the lowest limits of drift rates suggested previously for the Paleoarchaean (Suganuma et al., 2006). However, the uncertainties in the numbers are large, and greater resolution is needed before these rates can be used with confidence.

11.7. Ophiolites and their emplacement

Sections of the Onverwacht Suite have been compared to Phanerozoic ophiolites (e.g., de Wit, 2004; Parman and Grove, 2004a, b) although there is no universal agreement on this (e.g., Dann and Grove, 2007). This may be because of the simplistic

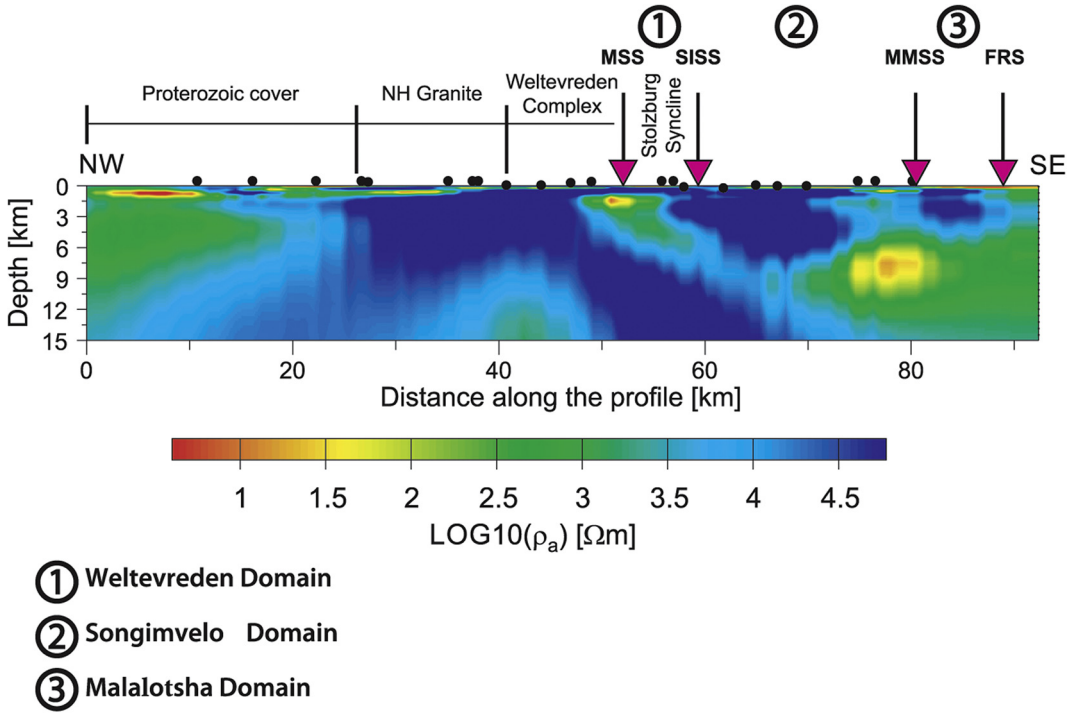

Figure 26. Conductivity section along the MT profile (Fig. 2) derived from a 3D inversion model (ModEM; Meqbel, 2009; Egbert and Kelbert, 2012; Kelbert et al., 2014) with horizontal grid sizes of 850 m; and error floors set to 5% for off-diagonal and 10% for diagonal MT impedances; the inversion stopped with an rms of 4.2. Red and yellow reflect zones of enhanced electrical conductivity; blue colours for high resistivities. MT stations are marked by black circles; red diamonds indicate location of major shear systems at surface. The TTG cores and greenstone lithologies of the Onverwacht Suite, and Fig Tree-Moodies Groups generally consist of highly resistive rocks. Conductive rocks in the northwester link to the sub-horizontal post-Archean sequences cover the escarpment. Note that the major Shear Systems within the greenstone belt are underlain by inclined zones of enhanced conductivity. M(SS) = Moodies; SI(SS) = Saddleback-Inyoka; MM(SS) = Manhaar-Msauli; FR(SS) = Forbes Reef (Shear Systems).

descriptions in the literature of what constitutes typical ophiolites (Furnes et al., 2015). Phanerozoic ophiolites have been classified now into two major types, (1) subduction-unrelated, and (2) subduction-related, and these can further be subdivided into several subtypes (Dilek and Furnes, 2011, 2014). In the subduction-unrelated types, the Continental-Margin type ophiolite represents the embryonic stage of ophiolite formation, and at more advanced stage of development and onset of seafloor spreading with oceanic crust formation, the Mid-Ocean type ophiolite is formed. A third ophiolite type, the Plume type, may be part of oceanic plateaus or plume-proximal oceanic ridges, such as Iceland. The subduction-related ophiolites can, on the basis of crustal construction and geochemical characteristics, be classified as the four following types: (1) Backarc, (2) Forearc, (3) Backarc–Forearc, and (4) Volcanic Arc. While the Backarc and MOR types structurally and lithologically may look alike, the Forearc type comprises intermediate to silicic magmatic components, and characteristically contains boninites. The Volcanic Arc type represents a longer term development (20–30 Ma), and is dominated by intrusions of diorite, tonalite and granodiorite (Dilek and Furnes, 2011, 2014; Furnes and Dilek, 2017). By applying the geochemical discrimination diagrams of Pearce (2014), the various complexes of the upper Onverwacht Suite have been classified in terms of the ophiolite types as outlined above (Furnes et al., 2015). In this geochemical classification, combined with field geological features, the Komati, Hooggenoeg and Kromberg Complexes were classified as Backarc to Forearc type, the Mendon Complex as Forearc type, and the Noisy Complex as Volcanic Arc type. Of crucial importance with respect to oceanic crust generation and its subsequent on-land tectonic emplacement as an ophiolite, is the process-related comparison between Phanerozoic ophiolites and the Paleoarchean examples of the Onverwacht Suite. From several ophiolites whose magmatic crystallization and emplacement ages are well-constrained, it appears that the time period from formation to on-land emplacement is rather short, i.e., in the range of 1–3 million years (e.g., Harper et al., 1994; Hacker et al., 1996; Smith, 2006), and the emplacement rates are on the order of 0.1–2 cm/yr (Harper et al., 1994; Hacker et al., 1996). This range of emplacement rate is within the same order of magnitude as estimated for the tectonic obduction of the Hooggenoeg Complex (ca. 0.5 cm/yr).

12. Discussion and conclusions

Recent work reveals that at least 11 major shear zones and a regional unconformity separate the rocks of the southern MMts into seven igneous complexes that make up the Onverwacht Suite. These complexes, each with different tectonic histories, resemble parts of different types of ophiolite complexes (c.f., Furnes and Dilek, 2017), and related sedimentary basins. The most characteristic features of the MORB-normalized, multi-element diagrams for the lavas of the Hooggenoeg, Kromberg and Mendon Complexes, as well as the Komati Complex, are concentrations of about 1–0.2× MORB and relative enrichment in the large ion lithophile elements. When compared to global patterns of subduction-related volcanic rocks and in particular those from the Izu-Bonin-Mariana there are strong similarities between these and the volcanic rocks of the MMts (Reagan et al., 2010). Our interpretation of the different element enrichments may reveal that the angle of the subduction zone varied during the build-up of the different complexes of the Onverwacht Suite. At stages of only Cs, Pb and Ba enrichments the subduction zone had a shallow dip, whereas during additional enrichments of

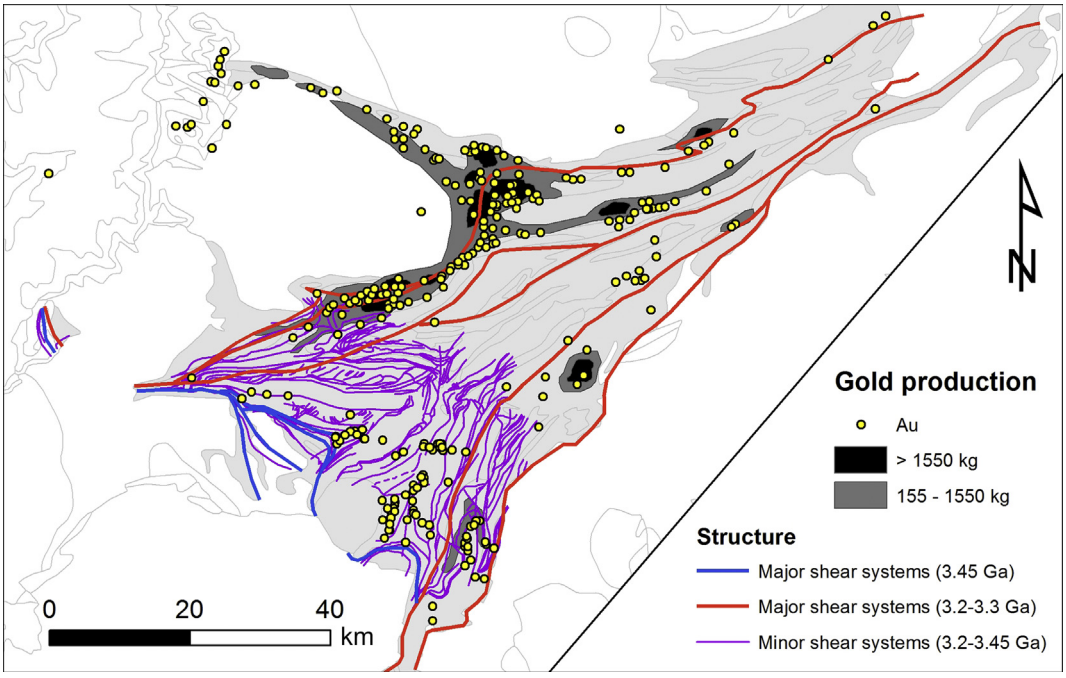

Figure 27. Distribution and production of gold deposits across the MMts. The distribution reveals that major deposits formed along a common network of late brittle–ductile shear zones that developed during late extension-exhumation between 3015 Ma and 3027 Ma (Dirks et al., 2013), and following accretion processes around 3284 Ma (De Ronde et al., 1991), linking main gold mineralization to greenstone belt regional accretion and exhumation (see Fig. 3b). Smaller gold occurrences are found away from the main Shear Systems and are related to earlier geothermal fluid-induced concentrations linked to early oceanic hydrothermal activity during formation of the mafic-ultramafic complexes. See text for further information. Gold deposit locations and data are from Ward (2000).

Th, U and LREE, the dip of the subduction zone was steeper. Based on these observations, it appears that significant changes in subduction angles must have occurred within a period of 10 million years.

Others propose that the basaltic rocks were derived from an earlier generation of high-magnesium basaltic rocks, suggesting that the arc-like signature in Archaean TTGs was inherited from an ancestral source lineage. This protracted, multistage process for the production and stabilization of the first continents—coupled with the high geothermal gradients—favours the formation of TTGs near the base of thick, plateau-like basaltic crust. Thus in those models subduction is not required to produce TTGs in the early Archaean. Such a model has been proposed for the origin of the mafic and ultramafic rocks of the Onverwacht Suite, as a thick continental-flood basalt sequence derived from mantle plumes, which was subsequently recycled *in situ* to produce the tectonics of the MMt, including its 'drips' into the mid-lower crust (Van Kranendonk et al., 2014, 2016; Kröner et al., 2016). In the MMt sequences, such proposed 'flood basalts' must have formed as ocean plateaus to account for the ubiquitous pillow lavas formed at depths close to 2–4 km below sea-level. But the time gap between these two epeirogenic processes, e.g., uplift during igneous plateau formation, followed by convective lithosphere dynamics, is about 200–300 Myrs, between their

Table 1
Rates and related data of Early Archean processes derived from the Makhonjwa Mountains

Processes	Rates	Within order magnitude of modern rates	References and comments
Volcanic stratigraphy and magmatism	Lava successions	✓	Dann and Grove, 2007; Furnes et al., 2011.
	Hooggenoeg Complex: 300 m/Myr	✓	
	Komati Complex: 250 m/Myr		
Plate motions	12 cm/yr over 9 Myrs across 1000 km	✓	Suganuma et al., 2006; Biggin et al., 2011
	12–673 cm/yr over 20 Myrs	×	
Uplift and unroofing	1.5–5 mm/yr	✓	Kisters et al., 2003; Diener et al., 2005, 2006;
	2–5 mm/yr	✓	Stevens and Moyen 2007; de Wit et al., 2011
Regional Exhumation	10 –100 mm/Myr	✓	Schoene et al., 2008
Slab-angle changes in back arc basins	30°–90° over 10 Myrs active spreading	✓	Furnes et al., 2011
Accretion and arc magmatism	ca. 2.3 Ga: 9–17 Myrs	✓	De Ronde and Kamo 2000; Schoene and Bowring, 2010
Tectonic obduction	Hooggenoeg Complex: 0.5 mm/yr	✓	de Wit et al., 2011
Gold mineralization	Major deposits <12 Myrs	✓	Dirks et al., 2013
Hydrothermal activity	Deep water White smokers: 60–200 °C	✓	Hoffman et al., 1986
	Deep water general: 300–400 °C	✓	De Ronde et al., 1991
	Shallow water Fe pipes: 30–270 °C	✓	De Vries and Touret, 2007
	Subaerial: < 200–300 °C	✓	de Wit and Furnes, 2016
P/T during subduction	1.2–1.5 GPa @ 600–650 °C, 12–15 °C/km	✓	Moyen et al., 2006; Stevens and Moyen 2007
Ocean depth back arc basin	2–4 km	✓	Furnes et al., 2011

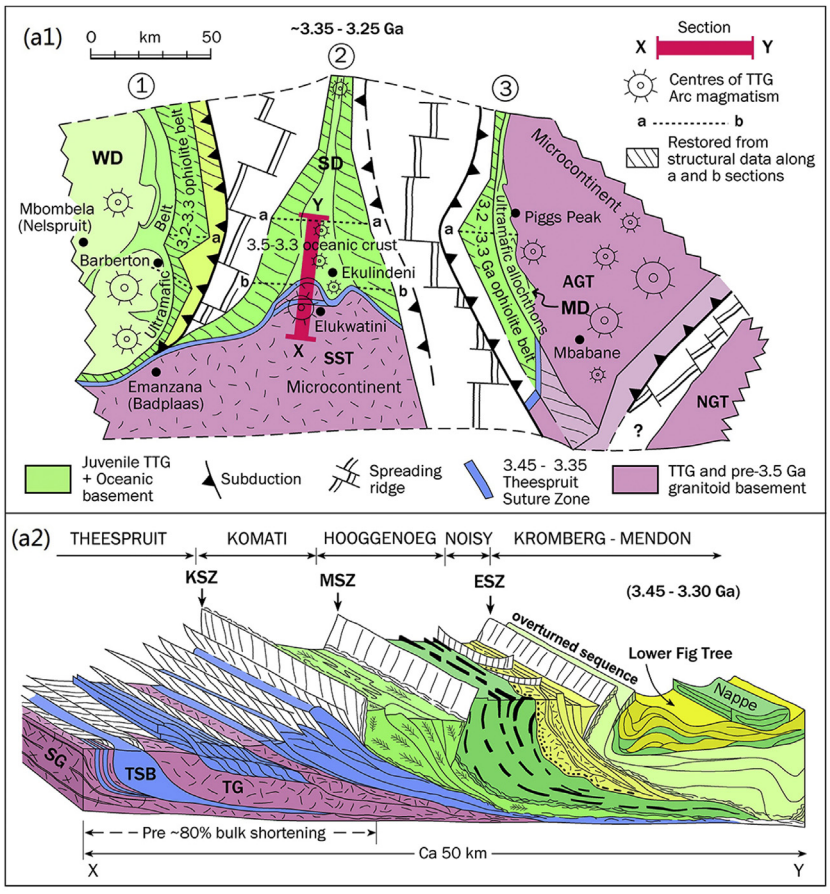
(a1)
0 km 50
~3.35 - 3.25 Ga
Section
X Y
Centres of TTG Arc magmatism
a ---------- b
Restored from structural data along a and b sections
WD
SD
Microcontinent
Mbombela (Nelspruit)
Barberton
Ultramafic Belt
3.2-3.3 ophiolite belt
3.5-3.3 oceanic crust
Ekulindeni
Elukwatini
SST
Emanzana (Badplaas)
Microcontinent
Piggs Peak
AGT
MD
Mbabane
3.2-3.3 Ga ophiolite belt
Ultramafic allochthons
NGT
?
Juvenile TTG + Oceanic basement
Subduction
Spreading ridge
3.45 - 3.35 Theespruit Suture Zone
TTG and pre-3.5 Ga granitoid basement
(a2)
THEESPRUIT
KOMATI
HOOGGENOEG
NOISY
KROMBERG - MENDON
KSZ
MSZ
ESZ
(3.45 - 3.30 Ga)
overturned sequence
Lower Fig Tree
Nappe
SG
TSB
TG
Pre ~80% bulk shortening
Ca 50 km
X
Y
(b1)
WELTEVREDEN
SONGIMVELO
3.35 - 3.25 Ga
MALALOTSHA
NST
K+MC
NC
HC
KC
TC
SST
AGT
NGT
D
(b2)
3.25 - 3.22 Ga
(b3)
3.22 - 3.20 Ga
Barberton
Elukwatini
Mbabane
Badplaas
Spreading ridge
Subduction zone
Reverse shear zone
Normal shear zone
Composite shear zones
Exhumation zones

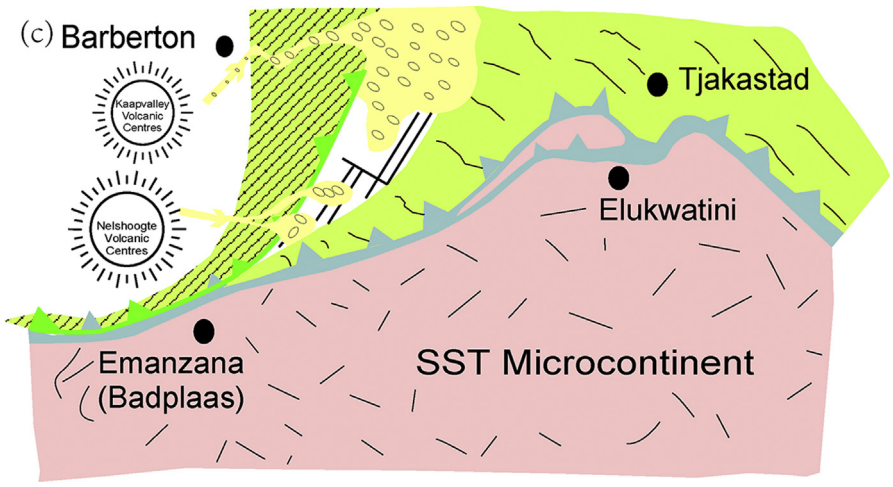

Figure 28. (*continued*).

formation about 3.5–3.4 Ga and their burial ca. 3.2 Ga. Such a long term history does not fit a simple drip tectonics model to explain the geometry and history of the MMts, nor even closely resembles timing of drip geometry in numerical models by an order of magnitude (e.g., Fischer and Gerya, 2016). From regional geology, geophysics and isotope geochemistry, which all suggest outward-dipping paleo-subduction zones along both NE–SW margins of the belt (c.f., Schoene and Bowring, 2010), it is clear that the MMts do not have a 'simple dome and keel' pattern, or a regional 'drip' geometry.

The age range and tectonostratigraphic thickness of the Onverwacht Suite is about 120 million years and, by our estimations, about 18 km, respectively (Fig. 3b). Whilst we have selected to divide the original formations of the Onverwacht Suite of rocks into complexes, this new stratigraphic terminology remains generally unsupported, and will require further field work to be tested before it is or not officially accepted by the South African Committee of Stratigraphy. The precise age range of the rocks present in each complex is poorly constrained, whilst the original spatial relationships between the complexes can in most cases only be inferred. The complexes were tectonically stacked during the final stages of their development during two subsequent orogenic events. At least one complex (the Hooggenoeg Complex) was uplifted and deeply eroded at about 3.45 Ga with a minimum uplift rate (ca. 0.5 mm/yr) within an order of magnitude of that during emplacement of Phanerozoic ophiolites.

The emergence of the deep water pillow lavas of the Hooggenoeg Complex above sea level, the start of its deep erosion through fluvial and glacial activity over a period of 25 million years (between about 3458 Ma and 3433 Ma), represents the onset of oceanic crust emplacement to the south across older and younger complexes, some of which are now preserved in the Theespruit Shear System and in old TTG cores farther south. Younger oceanic slabs (the Kromberg and the Mendon Complexes) were subsequently emplaced across the Noisy Complex, and locally affected by north-directed back-thrusting (Fig. 29).

The Songimvelo Domain subsequently accreted with the Malalotsha and Weltevreden Domains, within about 5 million years (between 3228–3223 Ma and 3227–3222 Ma, respectively), indicating doubly-verging subduction zones beneath granitoid terrains flanking the greenstone belt along both NE–SW trending margins (Schoene and Bowring, 2010). The subduction zones, directed outward below the main shear systems (MMSS and SISS) created high volumes of granitic magmatism and likely felsic volcanism over a period of at least 17 million years (3219–3236 Ma) across the AGC in Swaziland (and thus a continental arc setting; see also van Schijndel et al., 2017), and 9 million years (ca. 3227–3236 Ma) across deformed TTG cores flanking the NE margin as an oceanic arc system; and since the Dalmein Pluton is dated at 3216 Ma, the timing of cessation of magmatism within the MMts (or at least the Songimvelo Domain) is perhaps similar to that as within the Swaziland Domains Such rates are similar to those observed both in present and Phanerozoic continental as well as oceanic arcs (Schoene and Bowring, 2010, and references therein). The full time range of the magmatism along both margins was much longer, lasting possibly as long as 80 million years starting around 3366–3280 Ma (for summary, see Fig. 15 of Schoene and Bowring, 2010). This provides a maximum time span from onset of subduction to final accretion that is similar to that found along the present western Pacific.

The Saddleback-Inyoka Shear System continues in a W and then NW orientation where it links to the Kalkkloof ultramafic complex. The magnetic rocks within the contact between the Nelshoogte and Badplaas plutons dip to the north and have deep origins. The last phase of deformation experienced by the Stolzburg Layered Ultramafic Complex has a right lateral strike slip with a vertical

Figure 28. (a) Paleo-reconstruction of the Makhonjwa Mountains region. (a1) Schematic reconstruction of the three tectonic domains: WD = Weltevreden (left); SD = Songimvelo (centre); MD = Malalotsha (right). (a2) Schematic N-S section across SD prior to east-west D2 collision-related deformation. South directed (D1) thrusting is likely related to north dipping subduction below SD, initiated about 3.45 Ga. Note the back-thrusting as inferred from the overturned sequences of the Kromberg and Mendon Complexes. K(SZ) = Komati; M(SZ) = Mbjega; E(SZ) = Etimambeni (Shear Zones). (b) Conceptional plate-tectonic model for the tectonic evolution (b1-b3) inculcating subduction related final terrane amalgamation of three Paleoarchean crustal blocks of MMTs region between 3.45 Ga and 3.25 Ga. Note (in b3) how the geochemical-geophysical and structural data along the margin of the Stolzburg Schist belt are consistent with southerly directed extensional exhumation of the Stolzburg TTG core and exposure of the high-pressure metamorphic assemblages in the supracrustal rocks of the Inyoni zone, as part of a lower plate (e.g., Moyen et al., 2006, 2007) with progressive decreasing P/T conditions from the highest P conditions closest to the MMts and thus derived from the deepest section of subduction zone beneath the Nelspruit complex, as also suggested by the magnetic models (e.g., Fig. 25). This is consistent with sudden pressure drops in subduction-accretion zones followed by rapid exhumation in modern subduction zones (e.g., Yamato and Brun, 2017). The SE directed subduction beneath the Ancient Gneiss Complex is consistent with field and isotope data (Schoene and Bowring, 2010; Van Schijndel et al., 2017). NS(T) = Nelspruit; SS(T) = Stolzburg-Steynsdorp; AG(T) = Ancient Gneiss; NG(T) = Natal Granitoid Terranes. (c) Conceptional model of the late sedimentation of the Moodies Group' coarse siliciclastics (yellow) are deposited during the final stages of accretion/collision processes across the subduction system across remnant back-arc oceanic crust (black lines).

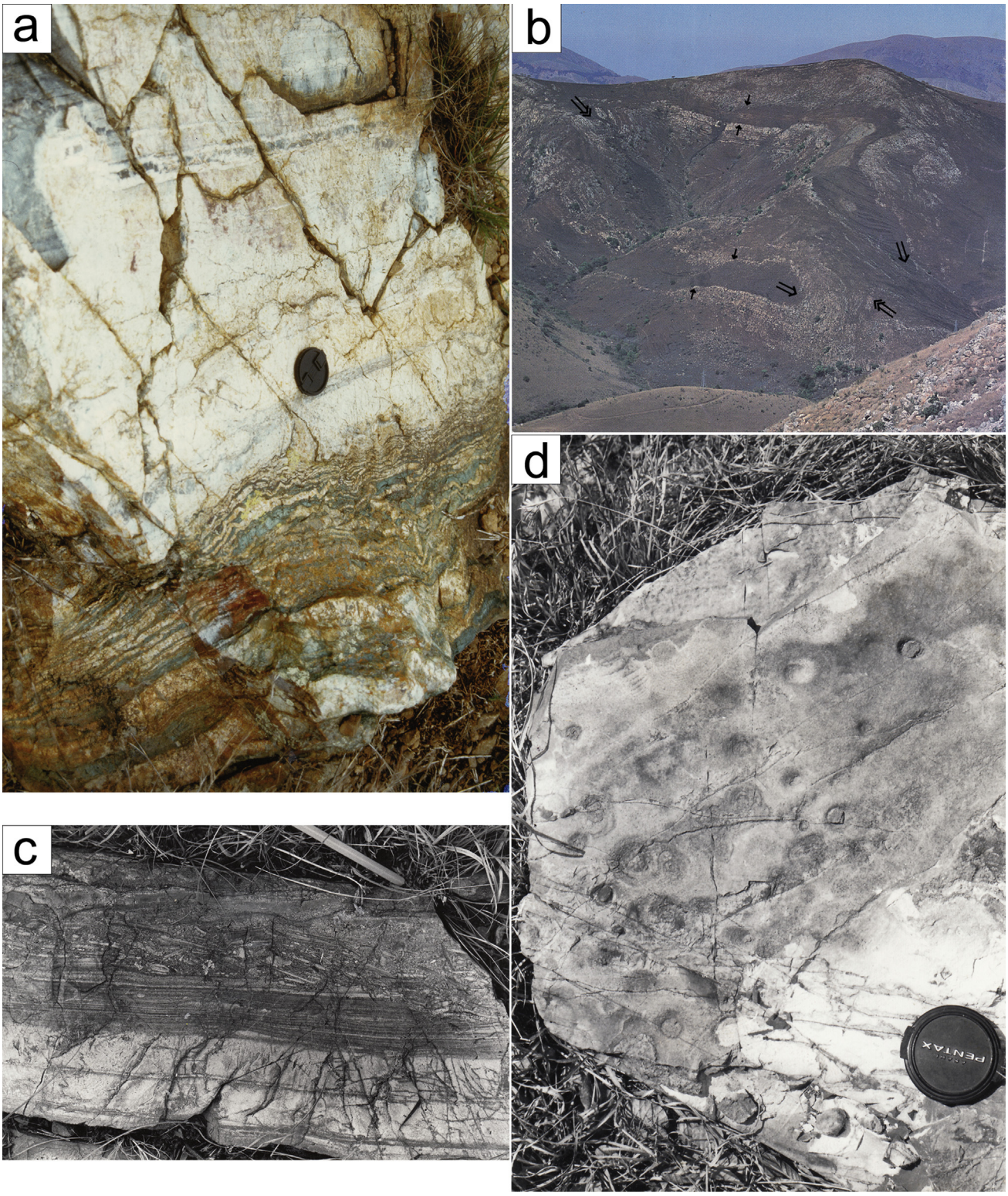

Figure 29. Selected example of many controversial field interpretations, and which illustrate the need for continued detailed mapping to further resolve complex Paleoarchean geotectonic models. (a) Typical Onverwacht chert layer (white, top) underlain by complex green 'gneiss' zones comprising intermingled deformed quartz-veins (white) and schistose fuchsite-carbonate micoliths (green). The gneisses have been interpreted as paleo-weathering surfaces or shear zones related to complex extensional and simple shear zones (see text); boulders of similar gneisses occur in conglomerates of the lowest section of the Noisy Complex. (b) Large scale nappe-structure of cherts (white-grey) and ultramafic sequences (dark), showing early sub-horizontal fold closures (single arrow heads) refolded by upright folds (double arrow heads). The cherts are irregularly underlain by green gneiss zones (see a). For scale note the large electric pylons in the foreground (hence 'Pylon Nappe'; see text, Map 2, and Fig. 3B). Detailed maps of this large-scale structure are available in de Wit (1982) and De Ronde et al. (1991). The age and emplacement mechanisms of the Pylon Nappe remain controversial (e.g., Grosch, 2011). Emplacement, related either to late D1 or early D2, is linked to syntectonic deposition and destruction of a partially consolidated shale sequence ((c) see Fig. 3b, red rectangle for location). Closely underlying the Nappe, are hydrothermal pipes (de Ronde et al., 1991) linked to the shales. The shales themselves preserve gas escape structures formed in hydrothermal-driven mud-pools (de Wit et al., 1983, and see text). It has also been suggested that fluids exploding from the mud-pools created drops (d) on the surrounding shales (Paris, 1984). The genetic, if any, time-link between the gneisses underlying the Nappe cherts, the 'bulldozing' of sediments ahead of the Nappe, and the gas escape features from underlying hydrothermal systems remains unknown, but these tectono-stratigraphic features resemble the emplacement of the classic Appalachian Taconic slices by gravity sliding of klippen (allochthonous sheets, slides, mélanges, wildflysch) as described by Bird (1969) and Bird and Dewey (1970). These few selected examples reflect many complex field relationships across the Makhonjwa Mountains that will continue to require more detailed mapping if we are to resolve Paleoarchean geodynamic models against empirical data.

component. The ultramafic complex moved up relative to the Moodies Group sediments in the Stolzburg Syncline, based on vertical lineation in the fault gouge of the Moodies and Belvue faults. It is along these zones that the major gold deposits are hosted (Fig. 28).

Finally, the relative stability of more than 200 million years following the onset of deposition of the mafic-ultramafic complexes of the central Songimvelo Domain and its early deformation at ca. 3.45 Ga before the onset of inferred crustal convective overturn and 'drip' tectonics at ca. 3.2 Ga (c.f., Van Kranendonk et al., 2007, 2014, 2015; Van Kranendonk, 2011a, b; Kröner et al., 2016) is at odds with substantial density contrast and the high crustal heat production that is used to support rapid pre-plate tectonic 'drip' tectonics (Arndt, 2013, for references related to this; Stern, 2013). Moreover, for such drip tectonics to occur, the lithosphere must have had a relatively lower viscosity, for which at present there is no evidence. To the contrary, the preservation of diamonds derived from the lithosphere at the same time as the inferred convective overturn (e.g., ca. 3.2 Ga) and thereafter deposited in early Neoarchean Basins filled with sediments and detrital gold derived from regional sources like the MMts (Smart et al., 2016) would appear to contradict regional convective overturn. In addition existing geophysical data, albeit scarce, do reveal shallow horizontal rectangular images for the rocks of the MMts rather than deep drips or large synclinoria (Kuetter et al., 2016, and references therein). Instead, our data reveals significant horizontal tectonics linked to subduction and collision processes that resemble modern plate boundary conditions.

There is still considerable local controversy about the interpretation of field observations and rock assemblages. For example, sections of the Onverwacht Suite have been compared to Phanerozoic ophiolites (e.g., de Wit, 2004; Parman and Grove, 2004a, b; de Wit et al., 2011; Furnes et al., 2011). Whilst this comparison remains unacceptable to some (e.g., Lowe and Byerly, 2007; Robin-Popieul et al., 2012), to others this remains an open debate (e.g., Dann and Grove, 2007).

There is also a distinct lack of understanding of the extensional shear systems and their subsequent structural evolution of the almost ubiquitous fuchsite-carbonate veining below and occasionally cutting across the cherts of the Onverwacht Suite and in places the Fig Tree sequences, where they are also associated with nappe emplacement apparently during sedimentation nearby hydrothermal venting at surface (Fig. 29a–d). These extensional shear systems were interpreted as early layer parallel extension zones (D0) formed during hydrothermal processes (de Wit et al., 1982; Duchač and Hanor, 1987; Hanor and Duchač, 1987; Grosch et al., 2012; de Wit and Furnes, 2016). Initial failure along these zones was brittle and tensile. In many places these zones are commonly reworked under ductile compressional conditions and shear failure brought about by the changes in the palaeostress systems. These early structures resemble ocean-floor detachment zones (e.g., Karson et al., 2005; MacLeod et al., 2009), which thereafter were preferentially remobilized as thrust zones in response to compressional deformation episodes, during both the early and late tectonic events (D_1 and D_2), forming a variety of flaser banded fuchsite carbonate schists and gneisses during tectonic stacking (e.g., de Wit, 1982; Paris, 1984; De Ronde and de Wit, 1994; De Ronde and Kamo, 2000; de Wit et al., 2011; Grosch et al., 2012). By contrast, many of these zones are interpreted as (deformed) volcanic ash, tuffs and breccias, and weathering profiles by other field geologists (e.g., Lowe and Byerly, 2007 and references therein). Thus the tectonic and metamorphic history of the MMt complexes is far from resolved. There is a need to address these issues using modern high resolution electron microscope imaging linked to geochemical techniques.

Similarly there are disagreements about the interpretation of the origin and deposition of the regionally extensive stacked and graded accretionary lapilli tuff that occur in almost all cherts throughout the Onverwacht Suite. Whilst there appear to be lapilli linked to large meteorite impacts (e.g., Lowe and Byerly, 2007; Lowe et al., 2012; Drabon et al., 2017), the depositional environment of these uniquely preserved layers remains controversial. The layers have been described as deep water turbidites, or as tidal deposits in shallow water systems (see Lowe and Byerly, 2007, page 507, for references). More recent work has shown many of these deposits to have been deposited at water depths between 2 and 4 km (de Wit and Furnes, 2016), but whether they represent turbidites, ash falls or both, remains to be resolved.

We hope that the rates of processes presented above will serve at least as first approximation to be incorporated into future numerical models of the Paleoarchean. But we stress also, these rates must be tested and improved further, based on high-precision geochronology linked to detailed field mapping as well as geochemical and structural analyses, before geodynamic processes of the Paleoarchean Earth can be quantified with greater precision and confidence; and the term 'greenstone belt' can be finally laid to rest.

Acknowledgements

Field work for this MMt project was rooted in the SA Geodynamics Project, coordinated by Louis O. Nicolaysen, and funded from 1978 by the SACUGS (South African Committee for the International Union of Geological Sciences) on behalf of the CSIR (Council for scientific and Industrial Research). After 1981, funding continued through the South African FRD (Foundation for Research and Development) and its successor, the NRF (National Research Foundation). By 2004, NRF funding was largely met through the joint SA-German Inkaba yeAfrica program, which by 2014 had evolved into Iphakade funded through the Global Change Program of DST (Department of Science and Technology). In the 1980s and early 1990s, geochemistry and isotope analyses for this project were driven through Hugh Alsop, Bill Compston, Derek York, Don Davies and Ed Spooner, undertaken by Richard Armstrong, Rodger and Roger Hart, Marian Tredoux, Alan Wilson, Sandra Kamo and Cornel de Ronde. From 2004, geochemistry was undertaken in Bergen, Norway, funded through the Norwegian Research Council and the Meltzer Fund (University of Bergen). Drilling through the Noisy and Kromberg/Mendon Complexes in 2007 was enabled by funding from the Centre for Geobiology, University of Bergen. Paleomagnetic work was funded through Cor Langereis and Andrew Biggin (University Utrecht) by the Dutch ALWNWO (Aarden Levenswetenschappen division of the Nederlandse Organisatie voor Wetenschappelijk Onderzoek); MT work through DFG and the GFZ-Potsdam. The foundation of this work is based on field mapping, much of which was undertaken by dedicated students and postdoctoral researchers as mentioned in the text. We are grateful to Hugh Berg, Roger Hart, Hubert Staudigel, Karlis Muehlenbachs, Neil Banerjee and Tanja Zegers for help in the field. We would like to thank the local communities, farmers and mine owners for their help and generous access to, and camping on, their communal land, properties and mines, respectively; Johan Eksteen and Louis Loock of the Mpumalanga Parks Board, and Reserve Managers Property Mokoena, Jerry Myeni and S. Shoba, for access to the Songimvelo nature reserve; and Fred Daniel for his generosity in hosting many field teams in his cottage and across his 'Cradle of Life' game reserve. The maps were initially digitized and collated into GIS by Laura Middlemann, refined and completed by Uma Martinez (Map 1) and Bastien Linol (Map 2). We would like to thank anonymous reviewers for critical comments, which improved this contribution, and we express our gratitude to the editors of this volume to

provide the space and opportunity to include our maps. MdW would like to dedicate this work to Roger Hart, Seal Rock, Oregon, USA, who passed away in 2011. He was an exceptionally generous person, an astute, creative scientist and ecosystem champion. Roger first explored the concepts of Archean hydrothermal processes during collaborative fieldwork in 1981 across the Makhonjwa Mountains, just after the first active black and white smokers were discovered in the Pacific Ocean; and for the next 15 years helped to apply these concepts to the rocks of the MMts. This is AEON contribution number 175 and Iphakade number 186.

References

Adam, J., Rushmer, T., O'Neil, J., Francis, D., 2012. Hadean greenstones from the Nuvvuagittuq fold belt and the origin of the Earth's early continental crust. Geology 40, 363–366. https://doi.org/10.1130/G32623.1.

Agrawal, S., Guevara, M., Verma, S.P., 2008. Tectonic discrimination of basic and ultrabasic volcanic rocks through log-transformed ratios of immobile trace elements. International Geology Review 50, 1057–1079. https://doi.org/10.2747/0020-6814.50.12.1057.

Anders, E., Grevesse, N., 1989. Abundances of the elements: meteoritic and solar. Geochimica et Cosmochimica Acta 53, 197–214.

Anhaeusser, C.R., 1972. The nature of chrysotile asbestos occurrences in southern Africa: a review. Economic Geology 71, 96–116.

Anhaeusser, C.R., 1976. A Bibliography of the Geology Relating to the Barberton Mountian Land and Surrounding Terrane, vol. 102. Economic Geology Research Unit, Information Circular, 51pp.

Anhaeusser, C.R., 1980. A geological investigation of the Archean granite-greenstone terrane south of the Boesmanskop syenite pluton, Barberton Mountain Land. Transactions of the Geological Society of South Africa 83, 93–106.

Anhaeusser, C.R., 1986. Archaean gold mineralization in the Barberton Mountain land. In: Anhaeusser, C.R., Maske, S. (Eds.), Mineral Deposits of Southern Africa, vol. 1. Geological Society of South Africa, Johannesburg, pp. 359–375.

Anhaeusser, C.R., 1987. A Bibliography of the Geology Relating to the Barberton Mountian Land and Surrounding Terrane, 1976–1986, vol. 184. Economic Geology Research Unit, Information Circular, 48 pp.

Anhaeusser, C.R., 1997. A Bibliography of the Geology Relating to the Barberton Mountian Land and Surrounding Terrane, vol. 306. Economic Geology Research Unit, Information Circular, 44 pp.

Anhaeusser, C.R., 2001. The anatomy of an extrusive-intrusive archaean mafic-ultramafic sequence: the Nelshoogte Schist belt and Stolzburg layered ultramafic complex, Barberton Greenstone Belt, South Africa. South African Journal of Geology 104, 167–204.

Anhaeusser, C.R., 2006. A re-evaluation of Archean intracratonic terrane boundaries on the Kaapvaal Craton, South Africa: Collisional suture zones? In: Reimold, W.U., Gibson, R.L. (Eds.), Processes on the early Earth, Geological Society of America, Special Paper, 405, pp. 193–210.

Anhaeusser, C.R., 2010. Magmatic and structural characteristics of the ca. 3440 Ma Theespruit pluton, barberton mountain land, South Africa. American Journal of Science 310, 1136–1167.

Armstrong, R.A., Compston, W., de Wit, M.J., Williams, I.S., 1990. The stratigraphy of the 3.5–3.2 Ga Barberton Greenstone Belt revisited: a single zircon ion microprobe study. Earth and Planetary Science Letters 101 (1), 90–106.

Arndt, N., 2003. Komatiites, kimberlites, and boninites. Journal of Geophysical Research 108 (B6), 2293. https://doi.org/10.1029/2002JB002157.

Arndt, N., 2013. Formation and evolution of continental crust. Geochemical Perspectives 2 (3), 404–533.

Ashwal, L.D., Cairncross, B., 1997. Mineralogy and origin of stichtite in chromite-bearing serpentinites. Contributions to Mineralogy and Petrology 127, 75–86.

Banerjee, N.R., Furnes, H., Muehlenbachs, K., Staudigel, H., de Wit, M., 2006. Preservation of similar to 3.4–3.5 Ga microbial biomarkers in pillow lavas and hyaloclastites from the Barberton Greenstone Belt, South Africa. Earth Planetary Science Letters 241, 707–722.

Barton, C.M., 1982. Geology and mineral resources of northwest Swaziland (Barberton Greenstone Belt). Swaziland Geological Survey and Mines Department Bulletin 10, 97 pp.

Bédard, J.H., 2006. A catalytic delamination-driven model for coupled genesis of Archean crust and sub-continental lithospheric mantle. Geochimica et Cosmochimica Acta 70, 1188–1214.

Biggin, A., de Wit, M.J., Langerijs, C., Zegers, T.E., Voûte, S., Dekkers, M.J., Drost, K., 2011. Palaeomagnetism of archaean rocks of the Onverwacht group, Barberton Greenstone Belt (southern Africa): evidence for a stable and potentially reversing geomagnetic field at ca. 3.5 Ga. Earth and Planetary Science Letters 302, 314–328. https://doi.org/10.1016/j.epsl.2010.12.024.

Bird, J.M., 1969. Middle Ordovician gravity sliding—Taconic region. In: Kay, M. (Ed.), North Atlantic—Geology and Continental Drift, vol. 12. American Association of Petroleum Geologists. Memoir, pp. 670–686.

Bird, J.M., Dewey, J.F., 1970. Lithosphere plate: continental margin tectonics and the evolution of the Appalachian orogen. Geological Society of America Bulletin 81, 1031–1060.

Blichert-Toft, J., Arndt, N.T., Wilson, A., Coetzee, G., 2015. Hf and Nd isotopic systematics of early Archean komatiites from surface sampling and ICDP drilling in the Barberton Greenstone Belt, South Africa. American Mineralogist 100, 2396–2411.

Brophy, J.G., 2009. La-SiO_2 and Yb-SiO_2 systematics in mid-ocean ridge magmas: implications for the origin of oceanic plagiogranite. Contributions to Mineralogy and Petrology 158, 99–111.

Büttner, W., 1984. The Serpentinites and Related Rocks of the Msauli Asbestos Deposits in the Archean Barberton Greenstone Belt, South Africa, vol. 168. Economic Geology Research Unit, University of the Witwatersrand, p. 32. Circular.

Byerly, G.R., 1999. Komatiites of the Mendon formation: late-stage ultramafic volcanism in the Barberton Greenstone Belt. In: Lowe, D.R., Byerly, G.R. (Eds.), Geologic Evolution of the Barberton Greenstone Belt, South Africa, vol. 329, pp. 189–211. Boulder, Colorado, Geological Society of America Special Paper.

Caro, G., Bourdon, B., Birck, J.-L., Moorbath, S., 2006. High-precision $^{142}Nd/^{144}Nd$ measurements in terrestrial rocks: constraints on the early differentiation of the Earth's mantle. Geochimica et Cosmochimica Acta 70, 164–191.

Castillo, P.R., 2006. An overview of adakite petrogenesis. Chinese Science Bulletin 51 (3), 257–268.

Castillo, P.R., 2012. Adakite petrogenesis. Lithos 134–135, 304–316.

Cawood, P.A., Kröner, A., Pisarevsky, S.A., 2006. Precambrian plate tectonics: criteria and evidence. GSA Today 16, 4–11. https://doi.org/10.1130/GSAT01607.1.

Chavagnac, V., 2004. A geochemical and Nd isotopic study of Barberton komatiites (South Africa): implication for the Archean mantle. Lithos 75, 253–281.

Chowdhury, P., Gerya, T., Chakraborty, S., 2017. Emergence of silicic continents as the lower crust peels off on a hot-plate tectonic Earth. Nature Geoscience 10, 698–702.

Chung-Hwa, P., Tamaki, K., Kobayashi, K., 1990. Age-depth correlation of the Philippine Sea back-arc basins and other marginal basins in the world. Tectonophysics 181, 351–371.

Clemens, J.D., Yearron, L.M., Stevens, G., 2006. Barberton (South Africa) TTG magmas; Geochemical and experimental constraints on source-rock petrology, pressure of formation and tectonic setting. Precambrian Research 151, 53–78.

Clemens, J.D., Belcher, R.W., Kisters, A.F.M., 2010. The Heerenveen Batholith, Barberton Mountain Land, South Africa: mesoarchaean, potassic, felsic magmas formed by melting of an ancient subduction complex. Journal of Petrology 51 (5), 1099–1120.

Cloete, M., 1999. Aspects of volcanism and metamorphism of the Onverwacht group lava in the southwestern portion of the Barberton Greenstone Belt. Memoirs of the Geological Survey of South Africa 84, 232 p.

Compston, W., Kröner, A., 1988. Multiple zircon growth within early Archean tonalite gneiss from the Ancient Gneiss Complex, Swaziland. Earth and Planetary Science Letters 87, 13–28. https://doi.org/10.1016/0012-821X(88)90061-1.

Condie, K., 2015. Changing tectonic settings through time: indiscriminate use of geochemical discriminant diagrams. Precambrian Research 266, 587–591.

Cutts, K.A., Stevens, G., Hoffmann, J.E., Buick, I.S., Frei, D., Münker, C., 2014. Paleo- to Mesoarchean polymetamorphism in the Barberton Granite–Greenstone Belt, South Africa: constraints from U–Pb monazite and Lu–Hf garnet geochronology on the tectonic processes that shaped the belt. Geological Society America Bulletin 126, 251–270.

Dann, J.C., 2000. The Komati Formation, Barberton Greenstone Belt, South Africa. P [art I: new map and magmatic architecture. South African Journal of Geology 103, 43–68.

Dann, J.C., 2001. Vesicular komatiites, 3.5-Ga Komati Formation, Barberton Greenstone Belt, South Africa: inflation of submarine lavas and origin of spinifex zones. Bulletin of Volcanology 63, 462–481.

Dann, J.C., Grove, T.L., 2007. Volcanology of the Barberton Greenstone Belt, South Africa: inflation and evolution of flow fields. In: van Kranendonk, M.J., Smithies, R.H., Bennett, V.C. (Eds.), Earth's Oldest Rocks. Developments in Precambrian Geology, vol. 15. Elsevier, Amsterdam, pp. 527–570.

Davies, G.F., 2007. Dynamics of the Hadean and Archean mantle. In: Kranendonk, M.J., Smithies, R.H., Bennett, V.C. (Eds.), Earth's Oldest Rocks, Developments in Precambrian Geology, vol. 15. Elsevier, Amsterdam, pp. 61–73.

De Beer, J., Stettler, E., du Plessis, J., 1988. The deep structure of the Barberton Greenstone Belt: a geophysical study. South African Journal of Geology 91, 194–197.

De Kock, M.O., Evans, D.A.D., Beukes, N.J., 2009. Validating the existence of Vaalbara in the neoarchean. Precambrian Research 174, 145–154.

De Ronde, C.E.J., de Wit, M.J., 1994. Tectonic history of the Barberton Greenstone Belt, South Africa: 490 million years of archean crustal evolution. Tectonics 13, 983–1005.

De Ronde, C.E.J., Kamo, S., 2000. An Archean arc-arc collisional event: a shortlived (ca. 3Myr) episode, Weltevreden area, Barberton Greenstone Belt, South Africa. Journal of African Earth Sciences 30, 219–248.

De Ronde, C.E.J., Kamo, S., Davis, D.W., de Wit, M.J., Spooner, E.T.C., 1991. Field, geochemical and U-Pb isotopic constraints from hypabyssal felsic intrusions within the Barberton Greenstone Belt, South Africa: implications for tectonics and the timing of gold mineralization. Precambrian Research 49, 261–280.

De Ronde, C.E.J., Spooner, E.T.C., de Wit, M.J., Bray, C.J., 1992. Shear zone related, Au quartz vein deposits in the Barberton Greenstone Belt, South Africa: field and

petrographic characteristics, fluid properties, and light stable isotope geochemistry. Economic Geology 87, 366–402.
De Ronde, C.E.J., de Wit, M.J., Spooner, E.T.C., 1994. Early Archean (>3.2 Ga) Fe-Oxide-rich, hydrothermal discharge vents in the Barberton Greenstone Belt, South Africa. Geological Society of America Bulletin 106, 86–104.
de Vries, S.T., 2004. Early archean sedimentary basins: depositional environment and hydrothermal systems. Examples from the barberton and coppin gap greenstone belts. Geologie Ultraiectina 244, 160 pp.
de Vries, S.T., Touret, J.L.R., 2007. Early archaean hydrothermal fluids; a study of inclusions from the ~3.4 Ga Buck Ridge chert, Barberton Greenstone Belt, South Africa. Chemical Geology 237, 289–302.
de Vries, S.T., Nijman, W., Armstrong, Richard, A., 2006. Growth-fault structure and stratigraphic architecture of the Buck Ridge volcano-sedimentary complex, upper Hooggenoeg formation, Barberton Greenstone Belt, South Africa. Precambrian Research 149, 77–98.
de Vries, S.T., Nijman, W., de Boer, P.L., 2010. Sedimentary geology of the palaeoarchaean Buck Ridge (South Africa) and Kittys gap (Western Australia) volcano-sedimentary complexes. Precambrian Research 183, 749–769.
de Wit, M.J., 1982. Gliding and overthrust nappe tectonics in the Barberton Greenstone Belt. Journal of Structural Geology 4, 117–136.
de Wit, M.J., 1983. Notes on a preliminary 1:25 000 geological map of the southern part of the Barberton Greenstone Belt. Special Publication of the Geological Society of South Africa 9, 185–187.
de Wit, M.J., 1998. On Archean granites, greenstones, cratons and tectonics: does the evidence demand a verdict? Precambrian Research 91, 181–226.
de Wit, M.J., 2004. Archean greenstone belts do contain fragments of ophiolites. In: Kusky, T.M. (Ed.), Precambrian Ophiolites and Related Rocks. Developments in Precambrian Geology, vol. 13. Elsevier, Amsterdam, pp. 599–614.
de Wit, M.J., 2007. The Kalahari Epeirogeny and climate change: differentiating cause and effect from Core to Space. Inkaba yeAfrica special volume. South African Journal of Geology 110, 367–392.
de Wit, M.J., 2010. The deep-time treasure chest of the Makhonjwa mountains. South African Journal of Science 106 (5/6). https://doi.org/10.4102/sajs.v106i5/6.277.
de Wit, M.J., Ashwal, L.D., 1995. Greenstone belts: what are they? South African Journal of Geology 98, 505–520.
de Wit, M.J., Hart, R.A., 1994. Earth's earliest continental lithosphere, hydrothermal flux, and crustal recycling. Lithos 30, 309–335. https://doi.org/10.1016/0024-4937(93)90043-C.
de Wit, M.J., Hynes, A., 1996. The onset of interaction between the hydrosphere and oceanic crust, and the origin of the first continental lithosphere. In: Coward (Ed.), Early Precambrian Processes. In: Ries (Ed.), Geol Soc London Spec Publication 95, pp. 1–9.
de Wit, M.J., Furnes, H., 2016. 3.5 Ga Hydrothermal fields and diamictites in the Barberton Greenstone Belt – Paleo-Archean crust in cool environments. Science Advances 2, e1500368.
de Wit, M.J., Hart, R., Martin, A., Abbot, P., 1982. Archean abiogenic and probable biogenic structures associated with mineralised hydrothermal systems and regional metasomatism, with implications for greenstone belt studies. Economic Geology 77, 1783–1801.
de Wit, M.J., Fripp, R.E.P., Stanistreet, I.G., 1983. Tectonic and stratigraphic implications of new field observations along the southern part of the Barberton Greenstone Belt. Special Publication of the Geological Society of South Africa 9, 21–30.
de Wit, M.J., Hart, R.A., Hart, R.J., 1987a. The Jamestown ophiolite complex, Barberton mountain belt; a section through 3.5 Ga oceanic crust. Journal of African Earth Sciences 6, 681–730.
de Wit, M.J., Armstrong, R., Hart, R.J., Wilson, A.H., 1987b. Felsic igneous rocks within the 3.3- to 3.5-Ga Barberton Greenstone Belt: high crustal level equivalents of the surrounding Tonalite- Trondhjemite Terrain, emplaced during thrusting. Tectonics 6, 529–549.
de Wit, M.J., Roering, C., Hart, R.J., Armstrong, R.A., de Ronde, C.E.J., Green, R.W.E., Tredoux, M., Peberdy, E., Hart, R.A., 1992. formation of an archean continent. Nature 357, 553–562.
de Wit, M.J., Furnes, H., Robins, B., 2011. Geology and tectonostratigraphy of the Onverwacht suite, Barberton Greenstone Belt, South Africa. Precambrian Research 186, 1–27.
Dhuime, B., Wuestefeld, A., Hawkesworth, C.J., 2015. Emergence of modern continental crust about 3 billion years ago. Nature Geoscience 8, 552–555.
Diener, J.F.A., Stevens, G., Kisters, A.F.M., Poujol, M., 2005. Metamorphism and exhumation of the basal parts of the Barberton greenstone belt, South Africa: constraining the rates of Mesoarchaean tectonism. Precambrian Research 143, 87–112.
Diener, J.F.A., Stevens, G., Kisters, A.F.M., 2006. High-pressure- intermediate-temperature metamorphism in the southern Barberton granitoid-greenstone terrain, South Africa: a consequence of subduction-driven overthickening and collapse of Mid-Archean continental crust. In: Benn, K., Mareschal, J.-C., Condie, K. (Eds.), Archean Geodynamics and Environments. American Geophysical Union Geophysical Monograph Series, vol. 164, pp. 239–254.
Diergaardt, B.N., 2013. Rhyolitic Volcanism in the Onverwacht Group, Barberton Greenstone Belt. Master of Science thesis. University of Stellenbosch, p. 104.
Dilek, Y., Furnes, H., 2011. Ophiolite genesis and global tectonics: geochemical and tectonic fingerprinting of ancient oceanic lithosphere. Geological Society of America Bulletin 123, 387–411.
Dilek, Y., Furnes, H., 2014. Ophiolites and their origins. Elements 10, 93–100.
Dirks, P.H.G.M., Charlesworth, E.G., Munyai, M.R., 2009. Cratonic extension and archaean gold mineralization in the sheba-Fairview mine, Barberton Greenstone Belt, South Africa. South African Journal of Geology 112, 291–316.
Dirks, P.H.G.M., Charlesworth, E.G., Munyai, M.R., Wormald, R., 2013. Stress analysis, post-orogenic extension and 3.01 Ga gold mineralization in the Barberton Greenstone Belt, South Africa. Precambrian Research 226, 157–184.
Drabon, N., Lowe, D.R., Byerly, G.R., Harrington, J.A., 2017. Detrital zircon geochronology of sandstones of the 3.6–3.2 Ga Barberton greenstone belt: No evidence for older continental crust. Geology 45, 803–806.
Duchač, K.C., Hanor, J.S., 1987. Origin and timing of the metasomatic silicification of an early Archean komatiite sequence, Barberton Mountain Land, South Africa. Precambrian Research 37, 125–146.
Dziggel, A., Stevens, G., Poujol, M., Anhaeusser, C.R., Armstrong, R.A., 2002. Metamorphism of the granite-greenstone terrane south of the Barberton Greenstone Belt, South Africa: insights into the tectono-thermal evolution of the 'lower' portions of the Onverwacht Group. Precambrian Research 114, 221–247.
Dziggel, A., Knipfer, S., Kisters, A.F.M., Meyer, F.M., 2006. P-T and structural evolution during exhumation of high-T, medium-P basement rocks in the Barberton Mountain Land, South Africa. Journal of Metamorphic Geology 24, 535–551.
Dziggel, A., Otto, A., Kisters, A.F.M., Meyer, F.M., 2007. Tectono-metamorphic controls on archean gold mineralization in the Barberton Greenstone Belt, South Africa: an example from the new consort gold mine. In: Van Kranendonk, M.J., Smithies, R.H., Vickie, C.B. (Eds.), Earth's Oldest Rocks. Development in Precambrian Geology, vol. 15. Elsevier, Amsterdam, pp. 699–727.
Dziggel, A., Poujol, M., Otto, A., Kisters, A.F.M., Trieloff, M., Schwarz, W.H., Meyer, F.M., 2010. New U-Pb and Ar-40/Ar-39 ages from the northern margin of the Barberton Greenstone Belt, South Africa: implications for the formation of Mesoarchaean gold deposits. Precambrian Research 179, 206–220.
Egbert, G., Kelbert, A., 2012. Computational recipes for electromagnetic inverse problems. Geophysical Journal International 189, 251–267.
Elburg, M., Foden, J., 1998. Temporal changes in arc magma geochemistry, northern Sulawesi, Indonesia. Earth and Planetary Science Letters 163, 381–398.
Ernst, W.G., Sleep, N.H., Tsujimori, T., 2016. Plate-tectonic evolution of the Earth: bottom-up and top-down mantle circulation. Canadian Journal of Earth Sciences 53, 1103–1120. https://doi.org/10.1139/cjes-2015-0126.
Farber, K., Dziggel, A., Meyer, F.M., 2016. Petrology, geochemistry and fluid inclusion analyses of altered komatiites of the Mendon Formation in the BARB4 drill core, Barberton Greenstone Belt, South Africa. South African Journal of Geology 119.4, 639–654.
Fischer, R., Gerya, T., 2016. Regimes of subduction and lithospheric dynamics in the Precambrian: 3D thermomechanical modelling. Gondwana Research 37, 53–70.
Floyd, P.A., Winchester, J.A., 1975. Magma type and tectonic setting discrimination using immobile elements. Earth and Planetary Science Letters 27, 211–218.
Foster, R.P., 1985. Major controls of Archaean gold mineralization in Zimbabwe. Tansactions of the Geological Society of South Africa 88, 109–133.
François, C., Philippot, P., Rey, P., Rubatto, D., 2014. Burial and exhumation during Archean sagduction in the east Pilbara granite-greenstone Terrane. Earth and Planetary Science Letters 396, 235–251.
Furnes, H., Dilek, Y., 2017. Geochemical characterization and petrogenesis of intermediate to silicic rocks in ophiolites: a global synthesis. Earth-Science Reviews 166, 1–37.
Furnes, H., Banerjee, N.R., Muehlenbachs, K., Staudigel, H., de Wit, M., 2004. Early life recorded in Archean pillow lavas. Science 304, 578–581.
Furnes, H., de Wit, M.J., Staudigel, H., Rosing, M., Muehlenbachs, K., 2007. A vestige of Earth's oldest ophiolite. Science 315, 1704–1707.
Furnes, H., Rosing, M., Dilek, Y., de Wit, M.J., 2009. Isua supracrustal belt (Greenland) - a vestige of a 3.8 Ga suprasubduction zone ophiolite, and the implications for Archean geology. Lithos 113, 115–132.
Furnes, H., de Wit, M., Robins, B., Sandstå, N.R., 2011. Volcanic evolution of the upper Onverwacht suite, Barberton Greenstone Belt, South Africa. Precambrian Research 186, 28–50.
Furnes, H., Robins, B., de Wit, M.J., 2012. Geochemistry and petrology of lavas in the upper Onverwacht suite, barberton mountain land, South Africa. South African Journal of Geology 115 (2), 171–210.
Furnes, H., de Wit, M.J., Robins, B., 2013. A review of new interpretations of the tectonostratigraphy, geochemistry and evolution of the Onverwacht Suite, Barberton Greenstone Belt, South Africa. Gondwana Research 23, 403–428.
Furnes, H., de Wit, M.J., Dilek, Y., 2014. Four billion years of ophiolites reveal secular trends in oceanic crust formation. Geoscience Frontiers 5, 571–603.
Furnes, H., Dilek, Y., de Wit, M.J., 2015. Precambrian greenstone sequences represent different ophiolite types. Gondwana Research 27 (2), 649–685.
Greber, N.D., Dauphas, N., Bekker, A., Ptáček, M.P., Bindeman, I.N., Hofmann, A., 2017. Titanium isotopic evidence for felsic crust and plate tectonics 3.5 billion years ago. Science 357, 1271–1274.
Griffin, W.L., O'Reilly, S.Y., Abe, N., Aulbach, S., Davis, R.M., Pearson, N.J., Doyle, B.J., Kivi, K., 2003. The origin and evolution of Archean lithosphere mantle. Precambrian Research 127, 19–41. https://doi.org/10.1016/S0301-9268(03).
Grosch, E.G., 2011. Determining the Physico-chemical Conditions on the Early Earth: Barberton Scientific Drilling Project, South Africa. Unpublished PhD thesis, 166 pp.
Grosch, E.G., McLoughlin, N., 2015. Questioning the biogenicity of titanite mineral trace fossils in Archean pillow lavas. Proceedings of the National Academy of Science, USA. https://doi.org/10.1073/pnas.1506995112.

Grosch, E.G., Slama, J., 2017. Evidence for a 3.3-billion-year-old oceanic crust in the Barberton Greenstone Belt. Geology 45 (8), 695–698.
Grosch, E.G., McLoughlin, N., de Wit, M.J., Furnes, H., 2009. Drilling for the archean roots of life and tectonic earth in the barberton mountains. Scientific Drilling 8, 24–28. https://doi.org/10.2204/iodp.sd.8.03.2009.
Grosch, E.G., Kosler, J., McLoughlin, N., Drost, K., Slama, J., Pedersen, B., 2011. Paleoarchean detrital zircon ages from the earliest tectonic basin in the Barberton Greenstone Belt, South Africa. Precambrian Research 191, 85–99.
Grosch, E.G., Vidal, O., Abu-Alam, T., McLoughlin, N., 2012. P-T constraints on the metamorphic evolution of the paleoarchean Kromberg-type section, Barberton Greenstone Belt, South Africa. Journal of Petrology 53, 513–545.
Grove, T.L., Parman, S.W., 2004. Thermal evolution of the Earth as recorded by komatiites. Earth and Planetary Science Letters 219, 173–187.
Grove, T.L., de Wit, M.J., Dann, J., 1997. Komatiites from the Komatii type section, Barberton, South Africa. In: de Wit, M.J., Ashwal, L.D. (Eds.), Greenstone Belts. Oxford University Press, Oxford, pp. 436–450.
Guillaume, B., Husson, L., Funiciello, F., Faccenna, C., 2013. The dynamics of laterally variable subductions: laboratory models applied to the Hellenides. Solid Earth 4, 179–200.
Guitreau, M., Blichert-Toft, J., Mojzsis, S., Roth, A.S.G., Bourdon, B., 2013. A legacy of Hadean silicate differentiation from Hf isotopes in Eoarchean rocks of the Nuvvuagittuq supracrustal belt (Quebec, Canada). Earth and Planetary Science Letters 362, 171–181.
Gvirtzman, Z., Stern, R.J., 2004. Bathymetry of Mariana trench-arc system and formation of the Challenger Deep as a consequence of weak plate coupling. Tectonics 23, TC2011,. https://doi.org/10.1029/2003TC001581.
Hacker, B.R., Mosenfelder, J.L., Gnos, E., 1996. Rapid emplacement of the Oman ophiolite: thermal and geochronologic constraints. Tectonics 15 (6), 1230–1247.
Hall, A.L., 1918. The Geology of the Barberton Gold Mining District. Geological Survey Memoir 9, 347 pp (with maps). Department of Mines and Industry, Union of South Africa.
Halla, J., Whitehouse, M.J., Ahmad, T., Bagai, Z., 2017. Archaean granitoids: an overview and significance from a tectonic perspective. In: Halla, J., Whitehouse, M.J., Ahmad, T., Bagai, Z. (Eds.), Crust–mantle Interactions and Granitoid Diversification: Insights from Archaean Cratons, vol. 449. Geological Society, London, Special Publications, pp. 1–18.
Hanor, J.S., Duchač, K.C., 1987. Isovolumetric silicification of early Archean komatiites: geochemical mass balances and constraints on origin. Journal of Geology 98, 863–877.
Hamilton, W.B., 1998. Archean magmatism and deformation were not products of plate tectonics. Precambrian Research 91 (1), 143–179.
Hamilton, W.B., 2011. Plate tectonics began in Neoproterozoic time, and plumes from deep mantle have never operated. Lithos 123, 1–20.
Harper, G.D., Saleeby, J.B., Heizler, M., 1994. Formation and emplacement of the Josephine ophiolite and the Nevada orogeny in the Klamath Mountains, California-Oregon: U/Pb zircon and $^{40}Ar/^{39}Ar$ geochronology. Journal of Geophysical Research 99 (B3), 4293–4321.
Hawkesworth, C.J., Kemp, A.I.S., 2006. Evolution of the continental crust. Nature 443, 811–817.
Hawkesworth, C.J., Cawood, P.A., Dhuime, B., 2016. Tectonics and crustal evolution. GSA Today 264, 4–11.
Heubeck, C., Lowe, D., 1994. Late syndepositional deformation and detachment tectonics in the Barberton Greenstone Belt, South Africa. Tectonics 13, 1514–1536.
Heubeck, C., Blassing, S., Grund, M., Drabon, N., Homann, M., Nabban, S., 2016. Geological constrains on archean (3.22 Ga) coastal-zone processes from the Dycedale Syncline, Barberton Greenstone Belt. South African Journal of Geology 119, 495–518.
Hodges, K., 2017. Subduction undone. Nature 543, 44–45.
Hoffman, S.E., 1985. Alteration Mineralogy and Geochemistry of the Archaean Onverwacht Group Barberton Mountain Land, South Africa. Unpublished MSc. Thesis. Oregon State University.
Hoffman, S.E., Wilson, M., Stakes, D.S., 1986. An inferred oxygen isotope profile of Archaean Oceanic crust. Onverwacht Group. South Africa. Nature 321, 55–58.
Hofmann, A., Wilson, A.H., 2007. Silicified basalts, bedded cherts and other sea floor alteration phenomena of the 3.4 Ga Nondweni greenstone belt, South Africa. In: Van Kranendonk, M.J., Smithies, R.H., Bennett, V.C. (Eds.), Earth's Oldest Rocks. Developments in Precambrian Geology, vol. 15. Elsevier, Amsterdam, pp. 571–605.
Hofmann, A., Harris, C., 2008. Silica alteration zones in the Barberton Greenstone Belt: a window into subseafloor processes 3.5-3.3 Ga ago. Chemical Geology 257, 221–239.
Hofmann, A., Bolhar, R., Orbergen, B., Foucher, F., 2013. Cherts of the Barberton Greenstone Belt, South Africa: Petrology and trace-element geochemistry of 3.5–3.3 Ga old silicified volcaniclastic sediments. South African Journal of Geology 116, 297–322.
Hynes, A., 2014. How feasible was subduction in the Archean? Canadian Journal of Earth Sciences 51, 286–296. https://doi.org/10.1139/cjes-2013-0111.
Ishizuka, O., Tani, K., Reagan, M.K., 2014. Izu-Bonin-Mariana forearc crust as a modern ophiolite analogue. Elements 10, 115–120.
Jackson, M.P.A., Robertson, D.I., 1983. Regional implications of early precambrian strains in the Onverwacht group adjacent to the Lochiel granite, North-West Swaziland. Special Publication of the Geological Society of South Africa 9, 45–62.
Jahn, B.M., Gruau, G., Glikson, A.Y., 1982. Komatiities of the Onverwacht Group, S. Africa: REE geochemistry, Sm/Nd age, and mantle evolution. Contributions to Mineralogy and Petrology 80, 25–40.
Johnson, T.E., Brown, M., Gardiner, N.J., Christopher, L., Kirkland, C.L., Smithies, H.R., 2017. Earth's first stable continents did not form by subduction. Nature 545, 232–239. https://doi.org/10.1038/nature21383.
Jones, J.G., 1969. Pillow lavas as depth indicators. American Journal of Science 267, 181–195.
Kamo, S.L., 1992. Archean Crustal Evolution in the Barberton Mountain Land, South Africa: U-pb and Nd Isotope Constraints. MSc thesis, Unpublished. McMaster University, Canada, 113 pp.
Kamo, S.L., Davis, D.W., 1994. Reassessment of archean crustal development in the barberton mountain land, South-africa, based on U–Pb dating. Tectonics 13, 167–192.
Kareem, K., 2005. Komatiites of the Weltevreden Formation, Barberton Greenstone Belts, South Africa: Implications for the Chemistry and Temperature of the Archean Mantle. PhD thesis. Louisiana State University and Agricultural and Mechanical College, 227 pp.
Karson, J.A., Früh-Green, G.L., Kelley, D.D., Williams, E.A., Yoerger, D.R., Jakuba, M., 2005. Detachment shear zone of the atlantis massif core complex, mid-atlantic Ridge, 30°N. Geochemistry Geophysics Geosystems 7, Q06016. https://doi.org/10.1029/2005GC001109.
Kelbert, A., Meqbel, N., Egbert, G.D., Tandon, K., 2014. ModEM: a modular system for inversion of electromagnetic geophysical data. Computers & Geosciences 66, 40–53.
Keller, C.B., Schoene, B., 2012. Statistical geochemistry reveals disruption in secular lithospheric evolution about 2.5 Gyr ago. Nature 485, 490–493.
Kisters, A.F.M., Anhaeusser, C.R., 1995. Emplacement features of Archean TTG plutons along the southern margin of the Barberton Greenstone Belt, South Africa. Precambrian Research 75, 1–15.
Kisters, A., Stevens, G., Dziggel, A., Armstrong, R., 2003. Extensional detachment faulting and core-complex form in the south Barberton granite-greenstone terrain, South Africa: evidence for a 3.2 Ga orogenic collapse. Precambrian Research 127, 355–378.
Kisters, A., Belchers, R.W., Poujol, M., Dziggel, A., 2010. Continental growth and convergent related arc plutonism in the Mesoarchaean: evidence from the Barberton granite-greenstone terrain, South Africa. Precambrian Research 178, 15–26.
Kleinhanns, I.C., Kramers, J.D., Kamber, B.S., 2003. Importance of water for Archaen granitoid petrology: a comparative study of TTG and potassic granitoids from Barberton Mountain Land, South Africa. Contributions to Mineralogy and Petrology 145, 377–389.
Knauth, L.P., Lowe, D.R., 2003. High Archean climatic temperature inferred from oxygen isotope geochemistry of cherts in the 3.5 Ga Swaziland Supergroup, South Africa. Geological Society of America Bulletin 115, 566–580.
Koepke, J., Feig, S.T., Snow, J., Freise, M., 2004. Petrogenesis of oceanic plagiogranites by partial melting of gabbros: an experimental study. Contributions to Mineralogy and Petrology 146, 414–432.
Komiya, T., Maruyama, S., Masuda, T., Nohda, S., Hayashi, M., Okamoto, K., 1999. Plate tectonics at 3.8–3.7 Ga: field evidence from the Isua accretionary complex, Southern West Greenland. Journal of Geology 107, 515–554.
Komiya, T., Hayashi, M., Maruyama, S., Yurimoto, H., 2002. Intermediate-P/T type Archean metamorphism of the Isua supracrustal belt: implications for secular change of geothermal gradients at subduction zones and for Archean plate tectonics. American Journal of Science 302 (9), 806–826.
Komiya, T., Maruyama, S., Hirata, T., Yurimoto, H., Nohda, S., 2004. Geochemistry of the oldest MORB and OIB in the Isua Supracrustal Belt, southern West Greenland: implications for the composition and temperature of early Archean upper mantle. Island Arc 13 (1), 47–72.
Komiya, T., Yamamoto, S., Aoki, S., Sawaki, Y., Ishikawa, A., Tashiro, T., Koshida, K., Shimojo, M., Aoki, K., Collerson, K.D., 2015. Geology of the Eoarchean, > 3.95 Ga, Nulliak supracrustal rocks in the Saglek Block, northern Labrador, Canada: the oldest geological evidence for plate tectonics. Tectonophysics 662, 40–66.
Korenaga, J., 2013. Initiation and evolution of plate tectonics on Earth: theories and observations. Annual Reviews of Earth and Planetary Sciences 41, 117–151.
Kröner, A., Hegner, E., Wendt, J.L., Byerly, G.R., 1996. The oldest part of the Barberton granitoid-greenstone terrain, South Africa: evidence for crust formation between 3.5 and 3.7 Ga. Precambrian Research 78, 105–124.
Kröner, A., Hoffmann, J.E., Xie, H., Wu, F., Münker, C., Hegner, E., Wong, J., Wan, Y., Liu, D., 2013. Generation of early Archaean felsic greenstone volcanic rocks through crustal melting in the Kaapvaal, craton, southern Africa. Earth and Planetary Science Letters 381, 188–197.
Kröner, A., Anhaeusser, C.R., Hoffmann, J.E., Wong, J., Geng, H., Hegner, E., Xie, H., Yang, J., Liu, D., 2016. Chronology of the oldest supracrustal sequences in the paleoarchean Barberton Greenstone Belt, South Africa and Swaziland. Precambrian Research 279, 123–143.
Kuetter, S., Weckmann, U., de Wit, M., 2016. A deep electrical conductivity structure of the southern Barberton Greenstone Belt, South Africa, derived from magnetotelluric measurements. South African Journal of Geology 119 (1), 273–290. https://doi.org/10.2113/gssajg.119.1.273.
Kusky, T.M., Windley, B.F., Safonova, I., Wakita, K., Wakabayashi, J., Polat, A., Santosh, M., 2013. Recognition of ocean plate stratigraphy in accretionary orogens through Earth history: a record of 3.8 billion years of sea floor spreading, subduction, and accretion. Gondwana Research 24, 501–547.

Lahaye, Y., Arndt, N., Byerly, G., Chauvel, C., Fourcade, S., Gruau, G., 1995. The influence of alteration on the trace-element and Nd isotopic compositions of komatiites. Chemical Geology 126, 43–64.
Lallemand, S., Heuret, A., Boutelier, D., 2005. On the relationships between dip, back-arc stress, upper plate absolute motion, and crustal nature in subduction zones. Geochemistry Geophysics Geosystems 6 (9), Q09006. https://doi.org/10.1029/2005GC000917.
Lamb, S.H., 1984a. Geology of the Eastern Margin of the Barberton Greenstone Belt, North West Swaziland. PhD thesis, unpublished. Cambridge University, U.K, 178 pp.
Lamb, S., 1984b. Structures on the eastern margin of the Archean Barberton greenstone belt, Northwest Swaziland. In: Kröner, A., Greiling, R. (Eds.), Precambrian Tectonics Illustrated. E. Schweizerbart'sche Verlagsbuchhandlung, Stuttgart, pp. 19–41.
Lamb, S.H., 1987. Archean synsedimentary tectonic deformation- a comparison with the Quaternary. Geology 15, 565–568.
Lana, C., Kisters, A., Stevens, G., 2010a. Exhumation of Mesoarchean TTG gneisses from the middle crust: insights from the Steynsdorp core complex, Barberton granitoid-greenstone terrain, South Africa. Geological Society of America Bulletin 122, 183–197. https://doi.org/10.1130/B26580.1.
Lana, C., Tohver, E., Cawood, P., 2010b. Quantifying rates of dome-and-keel formation in the Barberton granitoid-greenstone belt, South Africa. Precambrian Research 177, 199–211.
Ledevin, M., Arndt, N., Sinionovici, A., 2015. The rheological behaviour of fracture-filling cherts: example of Barite Valley dikes, Barberton Greenstone Belt, South Africa. Solid Earth Discussions 6, 1227–1264.
Ling, M.-X., Li, Y., Ding, X., Teng, F.-Z., Yang, X.-Y., Fan, W.-M., Xu, Y.-G., Sun, W., 2013. Destruction of the North China Craton induced by ridge subduction. Journal of Geology 121, 197–213. https://doi.org/10.1086/669248.
Louzada, K.L., 2003. The Magmatic Evolution of the Upper ca.3450 Ma Hooggenoeg Formation, Barberton Greenstone Belt, Kaapvaal Craton, South Africa. Master of Science thesis. Utrecht University, p. 86.
Lowe, D., 1994. Accretionary history of the Archean Barberton Greenstone Belt (3.55-3.22 Ga) southern Africa. Geology 22, 1099–1102.
Lowe, D., Byerly, G., 1986. Archaean flow-top alteration zones formed initially in a low temperature sulphate-rich environment. Nature 324, 245–248.
Lowe, D., Byerly, G., 1999. Stratigraphy of the West-central part of the Barberton Greenstone Belt, South Africa. In: Lowe, D., Byerly, G. (Eds.), Geological Evolution of the Barberton Greenstone Belt, South Africa, vol. 329. Geological Society of America, pp. 1–36. Special Volume.
Lowe, D., Byerly, G., 2007. An overview of the geology of the Barberton Greenstone Belt: implications for early crustal development. In: Van Kranendonk, M., Smithies, R., Bennet, V.C. (Eds.), Developments in Precambrian Geology, vol. 15. Elsevier, B.V, Amsterdam, pp. 481–526.
Lowe, D., Byerly, G., Huebeck, C., 2012. Geological Map of the West-central Barberton Greenstone Belt, South Africa, Scale 1:25,000. Geological Society of America Map and Chart Series no.103.
MacLeod, C.J., Searle, R.C., Murton, B.J., Casey, J.F., Mallows, C., Unsworth, S.C., Achenbach, K.L., Harris, M., 2009. Life cycle of oceanic core complexes. Earth and Planetary Science Letters 287, 333–344.
MacLennan, S.A., 2012. Structural, Geophysical and Geochemical Characterisation of a Mesoarchean Paleosuture Zone, Barberton Greenstone Belt, South Africa. Unpublished Thesis. University of Cape Town, 224 pp.
Maier, W.D., Roelofse, F., Barnes, S.-J., 2003. The concentration of the platinum-group elements in South African komatiites: implications for mantle sources, melting regime and PGE fractionation during crystallization. Journal of Petrology 44 (10), 1787–1804. https://doi.org/10.1093/petrology/egg059.
Maré, L.P., Fourie, C.J.S., 2012. New geochemical and palaeomagnetic results from Neoarchaean dyke swarms in the Badplaas-Barberton area, South Africa. South African Journal of Geology 115.2, 145–170.
Martin, H., 1986. Effect of steeper Archean geothermal gradient on subduction-zone magmas. Geology 14, 753–756.
Martin, H., 1994. The Archean grey gneisses and the genesis of the continental crust. In: Condie, K.C. (Ed.), Archean Crustal Evolution. Elsevier, Amsterdam, pp. 205–259.
Martin, H., 1999. Adakitic magmas: modern analogues of Archean granitoids. Lithos 46, 411–429.
Martin, H., Smithies, R.H., Rapp, R., Moyen, J.-F., Champion, D., 2005. An overview of adakite, tonalite-trondhjemite-granodiorite (TTG), sanukitoid: relationships and some implications for crustal evolution. Lithos 79, 1–24.
Martin, H., Moyen, J.-F., Guitreau, M., Blichert-Toft, J., Le Pennec, J.L., 2014. Why Archaean TTG cannot be generated by MORB melting in subduction zones. Lithos 198–199, 1–13.
Maruyama, S., Ebisuzaki, T., 2017. Origin of the Earth: a proposal of new model called ABEL. Geoscience Frontiers 8, 253–274.
Maruyama, S., Komiya, T., 2011. The oldest pillow lavas, 3.8-3.7 Ga from the Isua supercrustal belt, SW Greenland: Plate tectonics had already begun by 3.8 Ga. Journal of Geography 120, 869–876.
Maruyama, S., Santosh, M., Azuma, S., 2016. Initiation of plate tectonics in the Hadean: Eclogitization triggered ABEL bombardment. Geoscience Frontiers 7, 1–17. https://doi.org/10.1016/j.gsf.2016.11.009.
McDonough, W.F., McCulloch, M.T., Sun, S.S., 1985. Isotopic and geochemical systematics of Tertiary-Recent basalts from southeastern Australia and implications for the evolution of the sub-continental lithosphere. Geochimica et Cosmochimica Acta 49, 2051–2067.
Menell, R.P., Brewer, T.H., Delve, J.R., Anhaeusser, C.R., 1981. The Geology of the Kalkkloof Chrysotile Asbestos Deposit and Surrounding Area, Barberton Mountain Land. Economic Geology Research Unit, University of the Witwatersrand. Information Circular 154.
Meqbel, N., 2009. The Electrical Conductivity Structure of the Dead Sea Basin Derived from 2D and 3D Inversion of Magnetotelluric Data. PhD thesis. Freie Universität Berlin, Germany, 215pp.
Mints, M.V., Belousova, E.A., Konilov, A.N., Natapov, L.M., Shchipansky, A.A., Griffin, W.L., O'Reilly, S.Y., Dokukina, K.A., Kaulina, T.V., 2010. Mesoarchean subduction processes: 2.87 Ga eclogites from the Kola Peninsula, Russia. Geology 38, 739–742. https://doi.org/10.1130/G31219.1.
Moore, J.G., 1965. Petrology of deep-sea basalts near Hawaii. American Journal of Science 263, 40–52.
Moore, J.G., 1970. Water content of basalts erupted on the ocean floor. Contributions to Mineralogy and Petrology 28, 272–279.
Moyen, J.-F., 2009. High Sr/Y and La/Yb ratios: the meaning of the "adakitic signature". Lithos 112, 556–574.
Moyen, J.-F., 2011. The composite Archaean grey gneisses: petrological significance, and evidence for a non-unique tectonic setting for Archaean crustal growth. Lithos 123, 21–36.
Moyen, J.-F., Martin, H., 2012. Forty years of TTG research. Lithos 148, 312–336.
Moyen, J.-F., Stevens, G., Kisters, A.F.M., Belcher, R.W., 2006. Record of mid-Archean subduction from metamorphism in the Barberton terrain, South Africa. Nature 443, 559–562.
Moyen, J.-F., Stevens, G., Kisters, A.F.M., Belcher, R.W., 2007. TTG plutons of the Barberton granitoid-greenstone terrain, South Africa. In: Van Kranendonk, M.J., Smithies, R.H., Bennett, V.C. (Eds.), Earth's Oldest Rocks. Development in Precambrian Geology, pp. 607–667 v. 15 (K.C. Condie, Series Editor).
Munyai, M.R., Dirks, P.H.G.M., Charlesworth, E.G., 2011. Archaean gold mineralisation during post-orogenic extension in the New Consort Gold Mine, Barberton Greenstone Belt, South Africa. South African Journal of Geology 114, 121–144.
Naqvi, S.M., Khan, R.M.K., Manikyamba, C., Ram Mohan, M., Khanna, T.C., 2006. Geochemistry of the NeoArchaean high-Mg basalts, boninites and adakites from the Kushtagi-Hungund greenstone belt of the Eastern Dharwar Craton (EDC); implications for tectonic setting. Journal of Asian Earth Sciences 27, 25–44.
Nédélec, A., Chevrel, M.O., Moyen, J.F., Ganne, J., Fabre, S., 2012. TTGs in the making: natural evidence from Inyoni shear zone (Barberton, South Africa). Lithos 153, 25–38.
Neumann, E.-R., Abu El-Rus, M.A., Tiepolo, M., Ottolini, L., Vannucci, R., Whitehouse, M., 2015. Serpentinization and deserpentinization reactions in the upper mantle beneath Fuerteventura revealed by peridotite xenoliths. Journal of Petrology 56 (1), 3–31.
Nijman, W., de Vries, S.T., 2009. Geological Map of the Lower Archaean Buck Ridge Volcano-sedimentary Complex, Barberton Greenstone Belt, Republic of South Africa. 3 Map Sheets and Explanatory Notes, CD-ROM Edition. Faculty of Geosciences, Utrecht University, the Netherlands. ISBN: 978-90-5744-153-0 [available from: Sedimentology Group, Dept. of Earth Sciences, Utrecht University].
Paris, I.A., 1984. The Geology of the Farms Josefsdal, Dunbar and Part of Diepgezet in the Barberton Greenstone Belt. PhD thesis, unpublished. University of Witwatersrand, Johannesburg.
Paris, I., 1987. The 3.5 Ga Barberton greenstone successions, South Africa: implications for modelling the evolution of the Archaean crust. Geological Journal 22, 5–24.
Paris, I., Stanistreet, I.A., Hughes, M.J., 1983. Cherts of the Barberton Greenstone Belt interpreted as products of submarine exhalative activity. Journal of Geology 93, 111–129.
Parman, S.W., Grove, T.L., 2004a. Petrology and geochemistry of Barberton komatiites and basaltic komatiites: evidence of Archean fore-arc magmatism. In: Kusky, T.M. (Ed.), Precambrian Ophiolites and Related Rocks. Developments in Precambrian Geology, vol. 13, pp. 539–565.
Parman, S.W., Grove, T.L., 2004b. Harzburgite melting with and without H_2O: experimental data and predictive modelling. Journal of Geophysical Research 109, B02201. https://doi.org/10.1029/2003JB002566.
Parman, S.W., Dann, J.C., Grove, T.L., de Wit, M.J., 1997. Emplacement conditions of komatiitic magmas from the 3.49 Ga Komati formation, Barberton Greenstone Belt, South Africa. Earth and Planetary Science Letters 150, 303–323.
Parman, S.W., Grove, T.L., Dann, J.C., 2001. The production of Barberton komatiites in an Archean subduction zone. Geophysical Research Letters 28 (13), 2513–2516.
Parman, S.W., Grove, T.L., Dann, J.C., de Wit, M.J., 2004. A subduction origin for komatiites and cratonic lithopheric mantle. South African Journal of Geology 107, 107–118.
Paulick, H., Bach, W., Godard, M., De Hoog, J.C.M., Suhr, G., Harvey, J., 2006. Geochemistry of abyssal peridotites (Mid-Atlantic Ridge, 15°20′N, ODP Leg 209): implications for fluid/rock interaction in slow spreading environments. Chemical Geology 234, 179–210.
Pearce, J.A., 1983. Role of the sub-continental lithosphere in magma genesis at active continental margins. In: Hawkesworth, C.J., Norry, M.J. (Eds.), Continental Basalts and Mantle Xenoliths. Shiva, Nantwich, UK, pp. 230–249.
Pearce, J.A., 2008. Geochemical fingerprinting of oceanic basalts with applications to ophiolite classification and the search for Archean oceanic crust. Lithos 100, 14–48.
Pearce, J.A., 2014. Immobile element fingerprinting of ophiolites. Elements 10, 101–108.
Pearce, J.A., Norry, M.J., 1979. Petrogenetic implications of Ti, Zr, Y, and Nb variations in volcanic rocks. Contributions to Mineralogy and Petrology 69, 33–47.

Pearce, J.A., Parkinson, I.J., 1993. Trace element models for mantle melting: application to volcanic arc petrogenesis. In: Prichard, H.M., Alabaster, T., Harris, N.B.W., Neary, C.R. (Eds.), Magmatic Processes and Plate Tectonics, vol. 76. Geological Society London Special Publication, pp. 373–403.
Pearce, J.A., Harris, N.B.W., Tingle, A.G., 1984. Trace element discrimination diagrams for the tectonic interpretation of granitic rocks. Journal of Petrology 25, 956–983.
Pearce, J.A., Barker, P.F., Edwards, S.J., Parkinson, I.J., Leat, P.T., 2000. Geochemistry and tectonic significance of peridotites from the South Sandwich arc-basin system, South Atlantic. Contributions to Mineralogy and Petrology 139, 36–53.
Pearce, J.A., Stern, R.J., Bloomer, S.H., Fryer, P., 2005. Geochemical mapping of the Mariana arc-basin system: implications for the nature and distribution of subduction components. Geochemistry Geophysics Geosystems 6 (7), Q07006. https://doi.org/10.1029/2004GC000895.
Polat, A., Frei, R., Apple, P.W.U., Dilek, Y., Fryer, B., Ordóñez-Calderón, J.C., Yang, Z.l., 2008. The origin and compositions of Mesoarchean oceanic crust: evidence from the 3075 Ma Ivisaartoq greenstone belt, SW Greenland. Lithos 100, 293–321.
Rapp, R.P., Shimizu, N., Norman, M.D., 2003. Growth of early continental crust by partial melting of eclogite. Nature 425, 605–609.
Reagan, M.K., Ishizuka, O., Stern, R.J., Kelley, K.A., Ohara, Y., Blichert-Toft, J., Blomer, S.H., Cash, J., Fryer, J., Hanan, B.B., Hickey-Vargas, Ishii, T., Kimura, J.-I., Peate, D.W., Rowe, M.C., Woods, M., 2010. Fore-arc basalts and subduction initiation in the Izu-Bonin-Mariana system. Geochemistry Geophysics Geosystems 11 (3). https://doi.org/10.1029/2009GC002871.
Reimer, T.O., 1980. Archaean sedimentary barite deposits of the Swaziland Supergroup (Barberton Mountain Land, South Africa). Precambrian Research 12, 393–410.
Robin-Popieul, C.C.M., Arndt, N.T., Chauvel, C., Byerly, G.R., Sobolev, A.V., Wilson, A., 2012. A new model for Barberton komatiites: deep critical melting with high melt retention. Journal of Petrology 53 (11), 2191–2229.
Robins, B., Sandstå, N.R., Furnes, H., de Wit, M., 2011. Evidence for refilling of previously emptied basaltic pillows in the Hooggenoeg complex, Barberton Greenstone Belt. Geological Magazine 148 (3), 435–441.
Ross, P.-S., Bédard, J.H., 2009. Magmatic affinity of modern and ancient subalkaline volcanic rocks determined from trace-element discriminant diagrams. Canadian Journal of Earth Sciences 46, 823–839.
Saccani, E., 2015. A new method of discriminating different types of post-Archean ophiolitic basalts and their tectonic significance using Th-Nb and Ce-Dy-Yb systematics. Geoscience Frontiers 6, 581–501.
Sanchez-Garrido, C., Stevens, G., Armstrong, R.A., Moyen, J.F., Martin, H., Doucelance, R., 2011. Diversity in Earth's early felsic crust: Paleoarchean peraluminous granites of the Barberton Greenstone Belt. Geology 39, 963–966.
Sandstå, N.R., Robins, B., Furnes, H., de Wit, M., 2011. The origin of large varioles in flow-banded pillow lava from the Hooggenoeg Complex, Barberton Greenstone Belt, South Africa. Contributions to Mineralogy and Petrology 162, 365–377.
Savov, I.P., Ryan, J.G., D'Antonio, M., Kelley, K., Mattie, P., 2005. Geochemistry of serpentinized peridotites from the Mariana forearc Conical Seamount, ODP Leg 125: implications for the elemental recycling at subduction zones. Geochemistry Geophysics Geosystems 6 (4), Q04J15. https://doi.org/10.1029/2004GC000777.
Scharf, T.A., Codilean, A.T., de Wit, M.J., Jansen, J.D., Kubik, P.W., 2012. Strong rocks sustain ancient post-orogenic topography in southern Africa. Geology 41, 331–334.
Schoene, B., Bowring, S., 2010. Rates and mechanisms of Mesoarchean magmatic arc construction, eastern Kaapvaal craton, Swaziland. Geological Society of America Bulletin 122 (3/4), 408–429. https://doi.org/10.1130/B26501.1.
Schoene, B., de Wit, M.J., Bowring, S., 2008. Mesoarchean assembly and stabilization of the eastern Kaapvaal craton: a structural-thermochronological perspective. Tectonics 27, 1–27. https://doi.org/10.1029/2008TC002267. TC5010, 2008.
Schoene, B., Dudas, F.O.L., Bowring, S., de Wit, M.J., 2009. Sm-Nd isotopic mapping of lithospheric growth and stabilization in the eastern Kaapvaal craton. Terra Nova 21, 219–228. https://doi.org/10.1111/j.1365-3121.2009.00877.
Searle, M.P., 2007. Structural geometry and timing of deformation in the Hawasina window, Al Jabal al Akhdar and Saih Hatat culminations, Oman Mountians. GeoArabia 12, 99–130.
Searle, M.P., Warren, C.J., Waters, D.J., Parrish, R.R., 2004. Structural evolution, metamorphism and restoration of the Arabian continental margin, Saih Hatat region Oman Mountains. Journal of Structural Geology 26, 451–473.
Seyfried, W.E., Berndt, M.E., Seewald, J.S., 1988. Hydrothermal alteration processes at mid-ocean ridges: constraints from diabase alteration experiments, hot-spring fluids and composition of the oceanic crust. Canadian Mineralogist 26, 787–804.
Shervais, J.W., 1982. Ti–V plots and the petrogenesis of modern and ophiolitic lavas. Earth and Planetary Science Letters 32, 114–120.
Shirey, S.B., Richardson, S.H., 2011. Start of the Wilson cycle at 3 Ga shown by diamonds from subcontinental mantle. Science 333, 434–436. https://doi.org/10.1126/science.1206275.
Smart, K.A., Tappe, S., Stern, R.A., Webb, S.J., Ashwal, D.L., 2016. Early Archean tectonics and mantle redox recorded in the Witwatersrand diamonds. Nature Geoscience 9 (3), 255–259. https://doi.org/10.1038/ngeo2628.
Smith, A.C., 2006. Tethyan ophiolite emplacement, Africa to Europe motions, and Atlantic spreading. In: Robertson, A.H.F., Mountrakis, D. (Eds.), Tectonic Development of the Eastern Mediterranean Region, vol. 260. Geological Society, London, Special Publications, pp. 11–34.
Smithies, R.H., 2000. The Archaean tonalite-trondhjemite-granodiorite (TTG) series is not an analogue of Cenozoic adakite. Earth and Planetary Science Letters 182, 115–125.
Smithies, R., Van Kranendonk, M., Champion, D., 2007. The Mesoarchean emergence of modern-style subduction. Gondwana Research 11, 50–68. https://doi.org/10.1016/j.gr.2006.02.001.
Sobolev, A.V., Asafov, E.V., Andrey, A., Gurenko, A.A., Arndt, N.T., Batanova, V.G., Portnyagin, M.V., Garbe-Schönberg, D., Krasheninniko, S.P., 2016. Komatiites reveal a hydrous Archaean deep-mantle reservoir. Nature 531, 628–638.
Som, S.M., Catling, D.C., Harnmeijer, J.P., Polivka, P.M., Buick, R., 2012. Air density 2.7 billion years ago limited to less than twice modern levels by fossil raindrop imprints. Nature 484, 359–362.
St-Onge, M.R., Searle, M.P., Wodicka, N., 2006. Trans-hudson orogen of north America and Himalaya-Karakoram-Tibetan orogen of asia: structural and thermal characteristics of the lower and upper plates. Tectonics 25, TC4006,. https://doi.org/10.1029/2005TC001907.
Staudigel, H., Hart, R., 1983. Alteration of basaltic glass: mechanism and significance for the oceanic crust-seawater budget. Geochimica et Cosmochimica Acta 47, 37–50.
Staudigel, H., Furnes, H., McLoughlin, N., Banerjee, N., Connell, L.B., Templeton, A., 2008. 3.5 billion years of glass bioalteration: volcanic rocks as a basis for microbial life. Earth-Science Reviews 89, 156–176.
Staudigel, H., Furnes, H., de Wit, M., 2015. Paleoarchean trace fossils in altered volcanic glass. Proceedings of the National Academy of Science, USA. https://doi.org/10.1073/pnas.1421052112.
Stern, R.J., 2013. When Did Plate Tectonics Begin on Earth, and what Came before? GSA Blog. http://geosociety.wordpress.com/2013/04/28/when-did-plate-tectonics-begin-on-earth-and-what-came-before/.
Stevens, G., Moyen, J.-F., 2007. Metamorphism in the Barberton granite greenstone terrain: a record of Paleoarchean accretion. In: Van Kranendonk, M.J., Smithies, R.H., Bennett, V.C. (Eds.), Earth's Oldest Rocks, vol. 15. Development in Precambrian Geology, pp. 669–698 (K.C. Condie, Series Editor).
Strik, G., de Wit, M.J., Langereis, C.G., 2007. Palaeomagnetism of the neoarchaean Pongola and Ventersdorp supergroups and an appraisal of the 3.0–1.9 Ga apparent polar wander path of the Kaapvaal craton, Southern Africa. Precambrian Research 153 (1–2), 96–115.
Stüben, D., Neumann, T., Taibi, N.-E., Glasby, G.P., 1998. Segmentation of the southern Mariana back-arc spreading center. The Island Arc 7, 513–524.
Suganuma, Y., Hamano, Y., Niitsuma, S., Hoashi, M., Hisamitsu, T., Niitsuma, N., Kodama, K., Nedachi, M., 2006. Paleomagnetism of the marble bar chert member, Western Australia: implications for apparent polar wander path for Pilbara craton during archean time. Earth and Planetary Science Letters 252 (3–4), 360–371.
Tarduno, J.A., 8 other authors, 2010. Geodynamo, solar wind, and magnetopause 3.4–3.45 billion years ago. Science 327, 1238–1240.
Thompson Stiegler, M., Cooper, M., Byerly, G.R., Lowe, D.R., 2012. Geochemistry and petrology of komatiites of the pioneer ultramafic complex of the 3.3 Ga Weltevreden formation, Barberton Greenstone Belt, South Africa. Precambrian Research 212–213, 1–12.
Toulkeridis, T., Clauer, N., Kroner, A., Todt, W., 2015. A mineralogical, chemical and isotope investigation of shales from the Barberton Greenstone Belt, South Africa, to constrain source materials and post-depositional evolution. South African Journal of Geology 118.4, 389–410.
Turner, S., Rushmer, T., Reagan, M., Moyen, J.-F., 2014. Heads down early on? Start of subduction on Earth. Geology 42, 139–142.
Usui, Y., Tarduno, J.A., Watkeys, M., Hofmann, A., Cottrell, R.D., 2009. Evidence for a 3.45-billion-year-old magnetic remanence: hints of an ancient geodynamo from conglomerates of South Africa. Geochemistry Geophysics, Geochemistry, Geosystems 10. https://doi.org/10.1029/2009GC002496.
Van Kranendonk, M.J., 2011a. Onset of Plate tectonics. Science 333, 413–414.
Van Kranendonk, M.J., 2011b. Cool greenstone drips and the role of partial convective overturn in Barberton Greenstone Belt evolution. Journal of African Earth Sciences 60, 346–352.
Van Kranendonk, M.J., Hickman, A.H., Smithies, R.H., Champion, D.C., 2007. Paleoarchean development of a continental nucleus: the East Pilbara terrane of the Pilbara craton, Western Australia. In: Van Kranendonk, M.J., Smithies, R.H., Bennet, V. (Eds.), Earth's Oldest Rocks. Elsevier, pp. 307–337.
Van Kranendonk, M.J., Kröner, A., Hegner, E., Connelly, J., 2009. Age, lithology and structural evolution of the c. 3.53 Ga Theespruit Formation in the Tjakastad area, southwestern Barberton Greenstone Belt, South Africa, with implications for Archean tectonics. Chemical Geology 261, 115–139.
Van Kranendonk, M.J., Kröner, A., Hoffmann, J.E., Nagel, T., Anhaeusser, C.R., 2014. Just another drip: re-analysis of a proposed Mesoarchaean suture from the Barberton Mountain Land, South Africa. Precambrian Research 254, 19–35.
Van Kranendonk, M.J., Smithies, R.H., Griffin, W.L., Pirajno, F., 2015. Making it thick: a volcanic plateau origin of Paleaoarchean continental lithosphere of the Pilbara and Kaapvaal cratons. Geological Society Special Publication 389, 83–111.
Van Schijndel, V., Stevens, G., Zeh, A., Frei, D., Lana, C., 2017. Zircon geochronology and Hf isotopes of the Dwalile supracrustal suite, ancient gneiss complex, Swaziland: insights into the diversity of palaeoarchaean source rocks, depositional and metamorphic ages. Precambrian Research 295, 48–66.
Vermeesch, P., 2006. Tectonic discrimination revisited. Geochemistry, Geophysics. Geosystems 7. https://doi.org/10.1029/2005GC001092.
Viljoen, M.J., Viljoen, R.P., 1969a. An introduction to the geology of the Barberton granite-greenstone terrain. In: Upper Mantle Project, vol. 2. Special publication of the Geological Society of South Africa, pp. 9–28.

Viljoen, M.J., Viljoen, R.P., 1969b. The geology and geochemistry of the Lower ultramafic unit of the Onverwacht group and a proposed new class of igneous rocks. In: Upper Mantle Project, vol. 2. Special publication of the Geological Society of South Africa, pp. 55–85.
Viljoen, R.P., Saager, R., Viljoen, M.J., 1969. Metallogenesis and ore control in the Steynsdorp goldfield, Barberton Mountain land, South Africa. Economic Geology 64, 778–797.
Visser, D.J.L. (compiler), Van Eeden, O.R., Joubert, G.K., Sohnge, A.P.G., van Zyl, J.S., Rossow, P.J., Taljaard, J.J., 1956. The geology of the Barberton area. Special Publication Geological Survey of South Africa 15, 242 pp.
Vroon, P.Z., van Bergen, M.J., Klaver, G.J., White, W.M., 1995. Strontium, neodymium, and lead isotopic trace-element signatures of the East Indonesian sediments: provenance and implication for Banda Arc magma genesis. Geochimica et Cosmochimica Acta 59, 2573–2598.
Ward, J.H.W., 1999. The metallogeny of the Barberton Greenstone Belt, South Africa and Swaziland. Council for Geoscience, pretoria. Memoir 86, 108 pp.
Ward, J.H.W., 2000. Metallogenic Map of the Barberton Greenstone Belt, South Africa and Swaziland (1:1000 000). Council for Geoscience, Pretoria.
Weller, O.M., St-Onge, M.R., 2017. Record of modern-style plate tectonics in the Palaeoproterozoic Trans-Hudson orogen. Nature Geoscience 10, 305–311.
Whitney, J.A., 1988. The origin of granite: the role and source of water in the evolution of granitic magmas. The Geological Society of America Bulletin 100 (12), 1886–1892.
Willbold, M., Hegner, E., Stracke, A., Rocholl, A., 2009. Continental geochemical signatures in dacites from Iceland and implications for models of early Archean crust formation. Earth and Planetary Science Letters 279, 44–52.
Winchester, J.A., Floyd, P.A., 1977. Geochemical discrimination of different magma series and their differentiation products using immobile elements. Chemical Geology 20, 325–343.
Witze, A., 2006. The start of the world as we know it. Nature 442, 128–131.
Yamaguchi, T., Iizuka, T., Hokanishi, N., Nakai, S., de Wit, M.J., Furnes, H., 2015. Lu-Hf Isotope Systematics of 3.47 Ga Barberton Basalts: Constraints on Early Crust-mantle Evolution. Goldschmidt 2015 (Abstract). Czech Republic, Prague. August 16–21.
Yamato, P., Brun, J.P., 2017. Metamorphic record of catastrophic pressure drops in subduction zones. Nature Geoscience 10, 46–50.
Yearron, L.M., 2003. Archaean Granite Petrogenesis and Implications for the Evolution of the Barberton Mountain Land, South Africa. PhD thesis. Kingston University, UK, 342 pp.
Zegers, T.E., Van Keeken, P.E., 2001. Middle Archean continent formation by crustal delamination. Geology 29, 1083–1086.
Zeh, A., Gerdes, A., Barton, J.M., 2009. Archean accretion and crustal evolution of the Kalahari Craton—the zircon age and Hf isotope record of granitic rocks from Barberton/Swaziland to the Francistown Arc. Journal of Petrology 50, 933–966.
Zeh, A., Gerdes, A., Millonig, L., 2011. Hafnium isotope record of the Ancient Gneiss Complex, Swaziland, southern Africa: evidence for Archaean crust–mantle formation and crust reworking between 3.66 and 2.73 Ga. Journal of the Geological Society 168, 953–964.